Hole No. MJOB-G37 (From 0.00 m to -270.15 m)

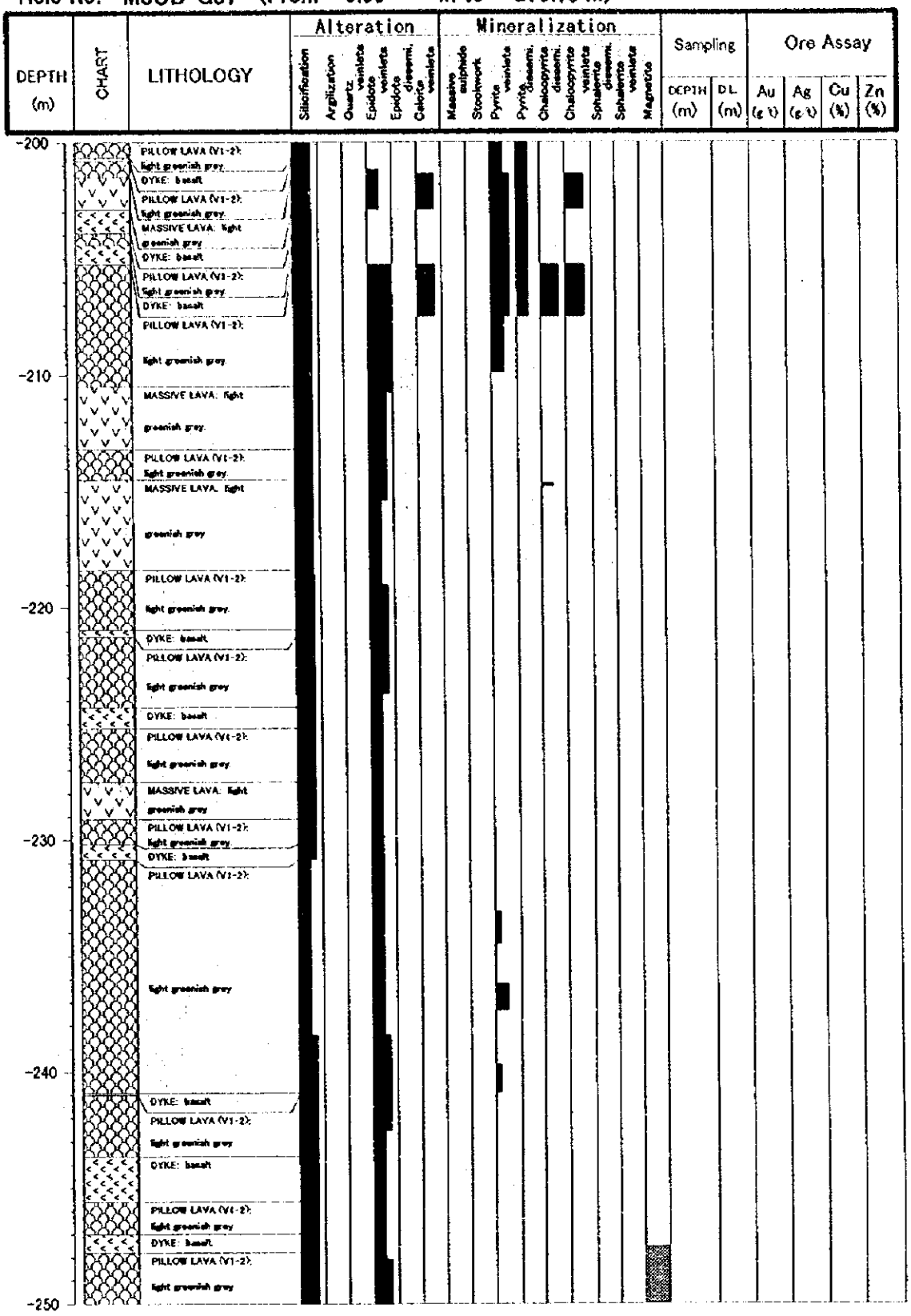

Hole No. MJOB-G37 (From 0.00 m to -270.15 m)

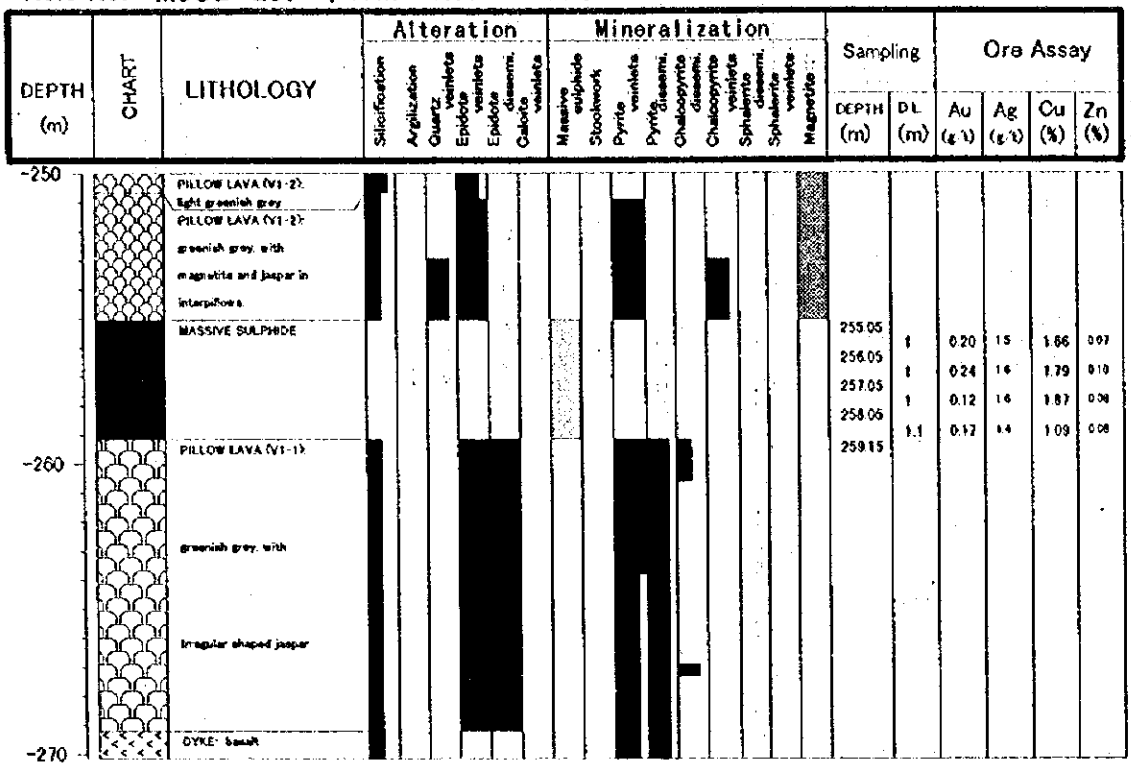

Hole No. MJOB-G38 (From 0.00 m to -300.60 m)

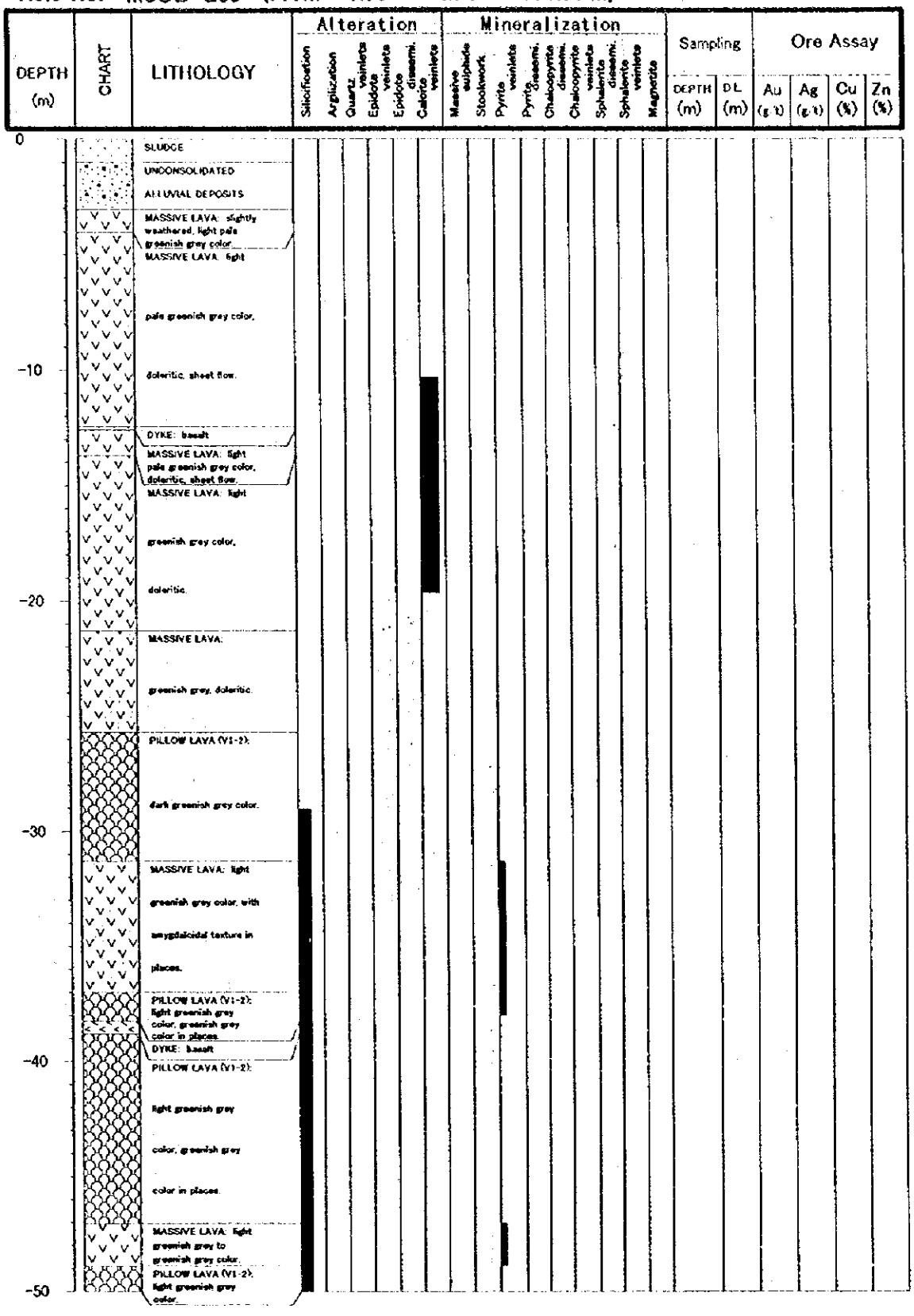

Hole No. MJOB-G38 (From 0.00 m to -300.60 m)

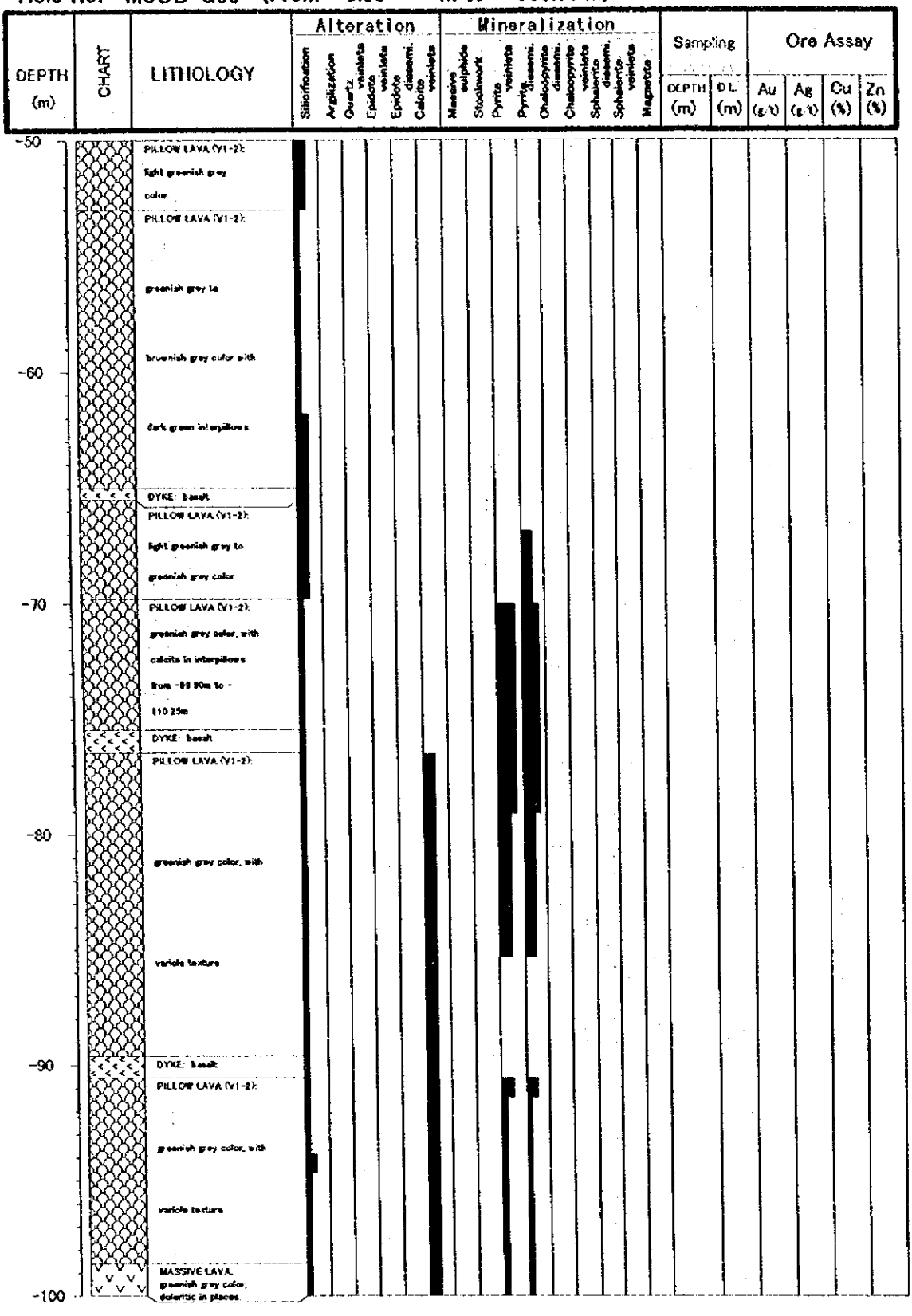

Hole No. MJOB-G38 (From 0.00 m to -300.60 m)

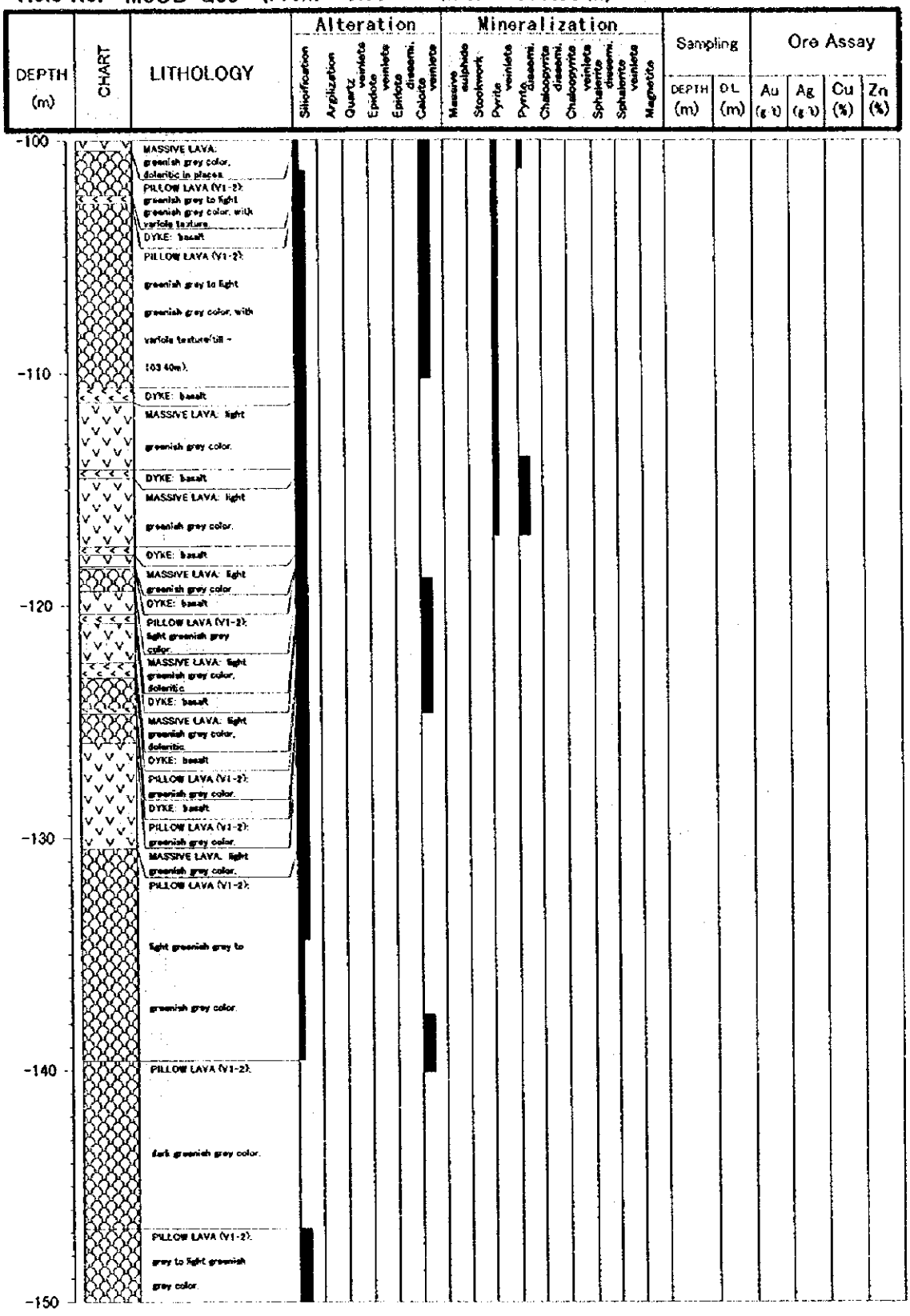

Hole No. MJOB-G38 (From 0.00 m to -300.60 m)

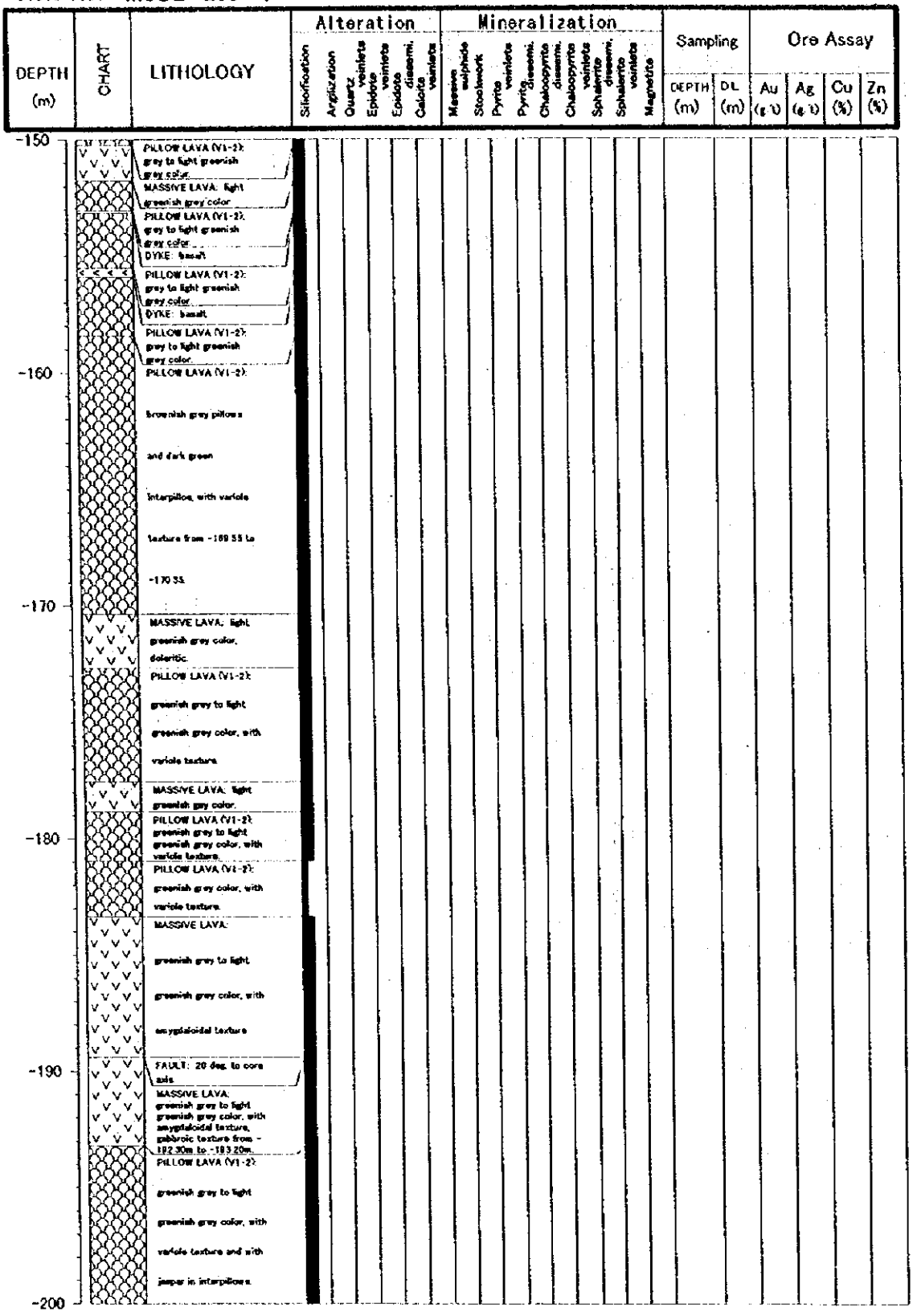

Hole No. MJOB-G38 (From 0.00 m to -300.60 m)

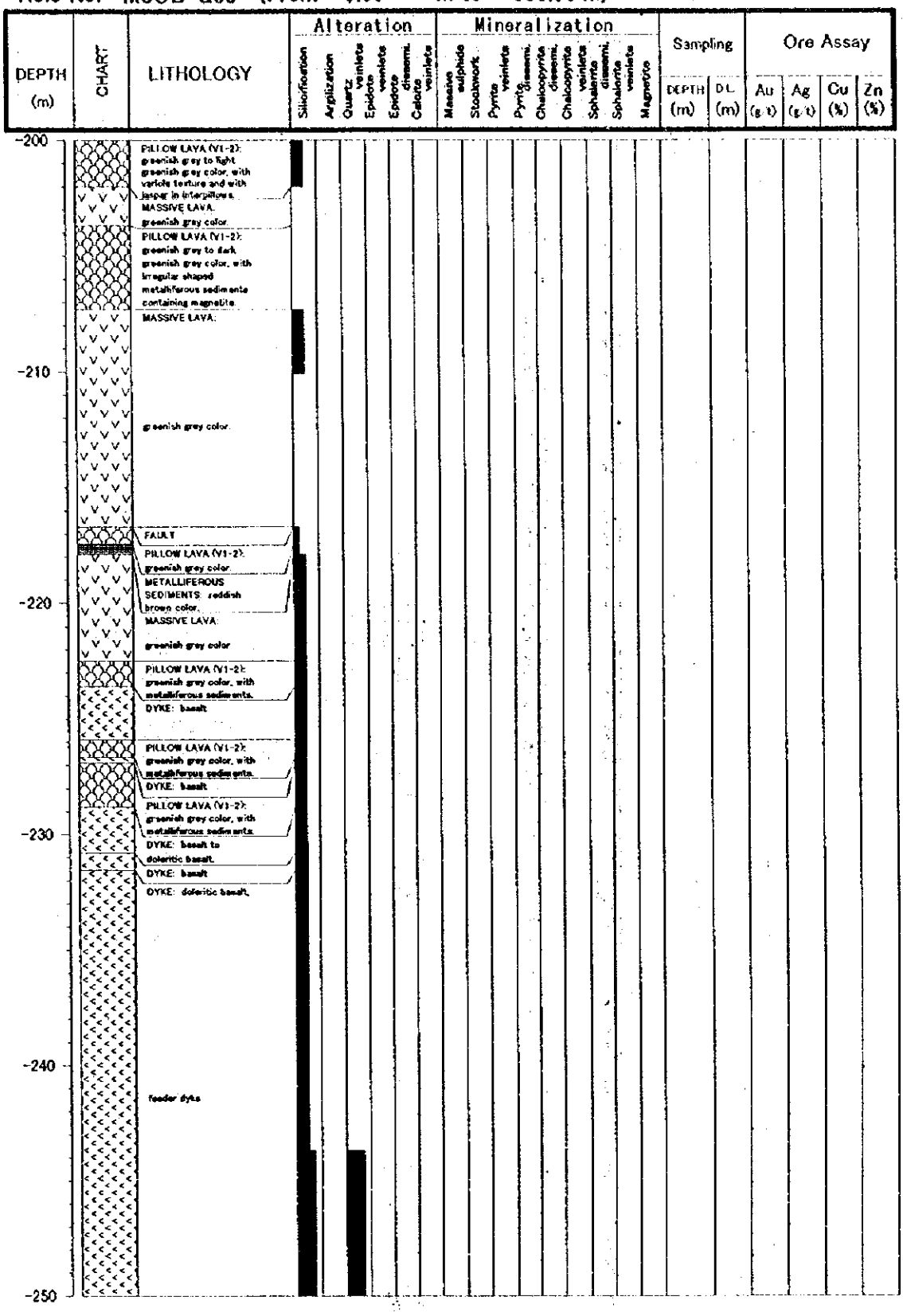

Hole No. MJOB-G38 (From 0.00 m to -300.60 m)

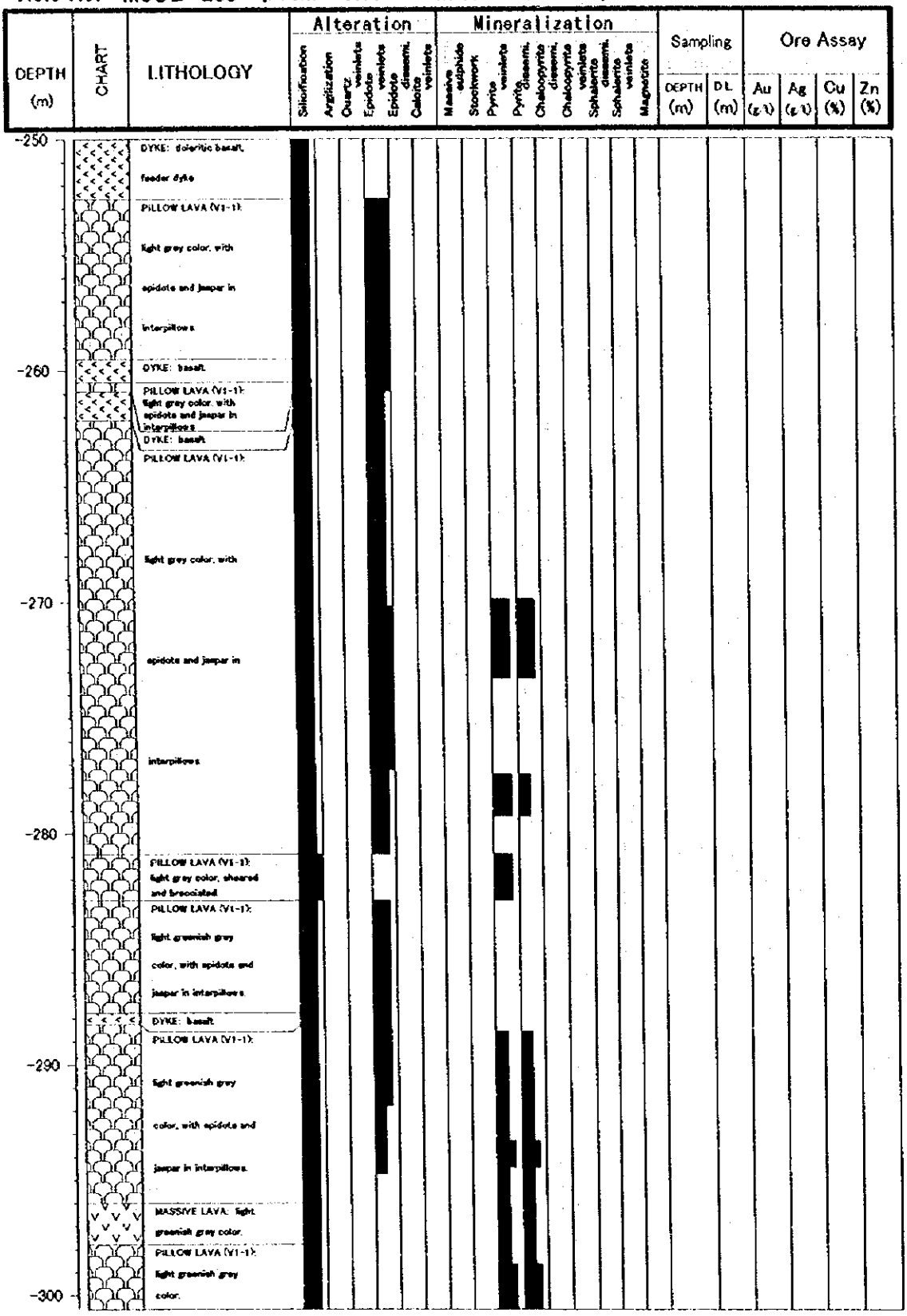

Hole No. MJOB-G39 (From 0.00 m to -201.90 m)

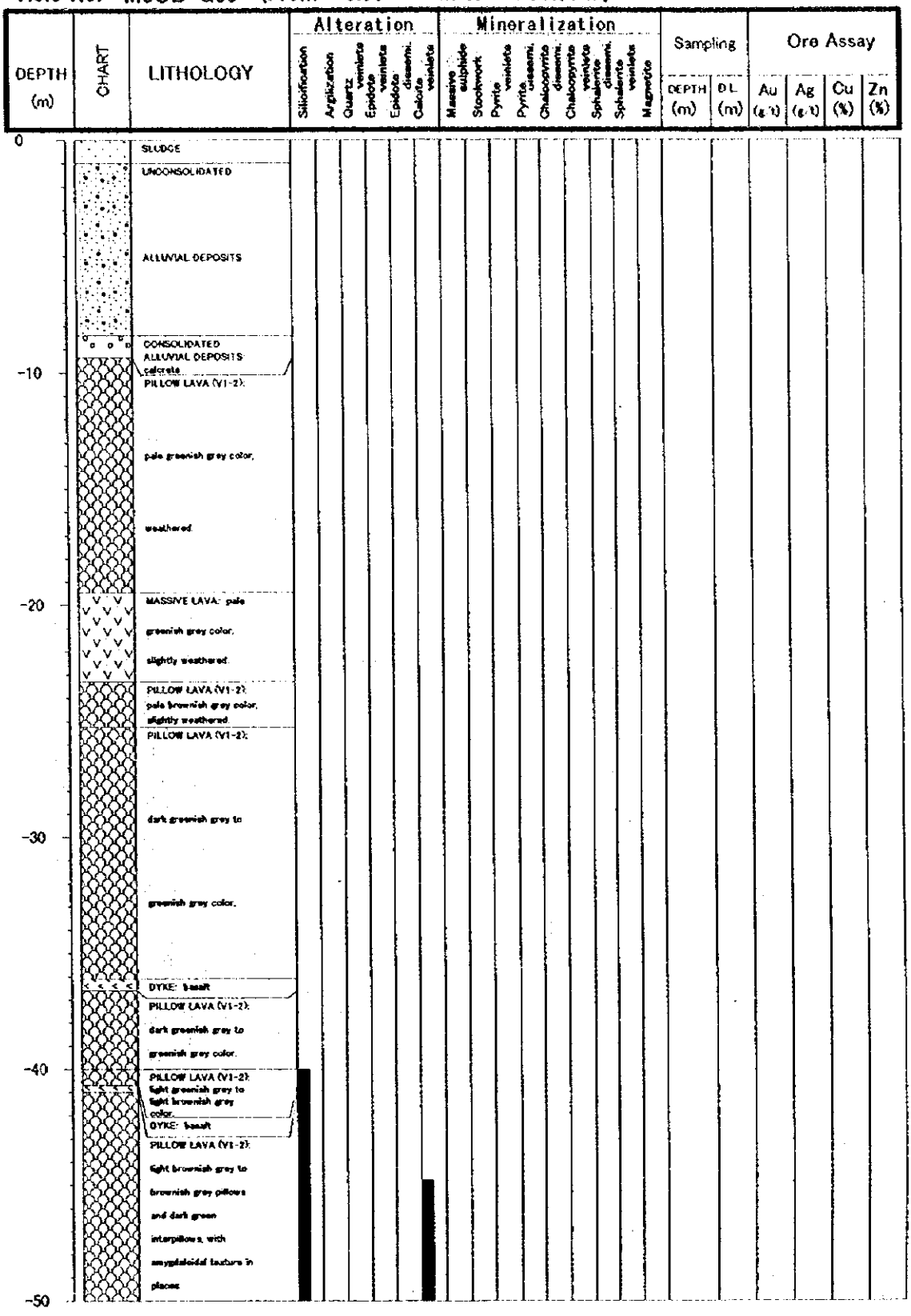

Hole No. MJOB-G39 (From 0.00 m to -201.90 m)

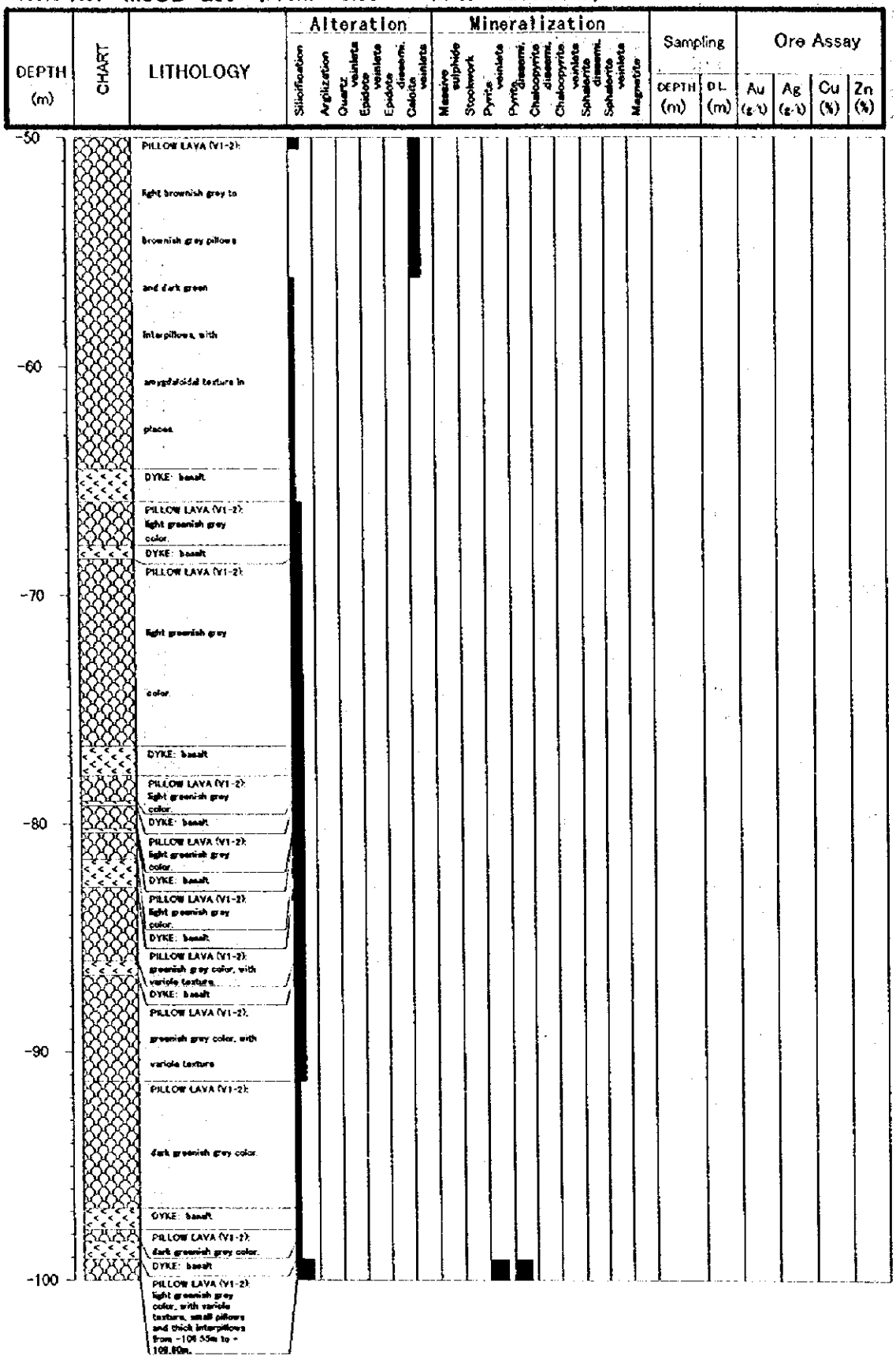

Hole No. MJOB-G39 (From 0.00 m to -201.90 m)

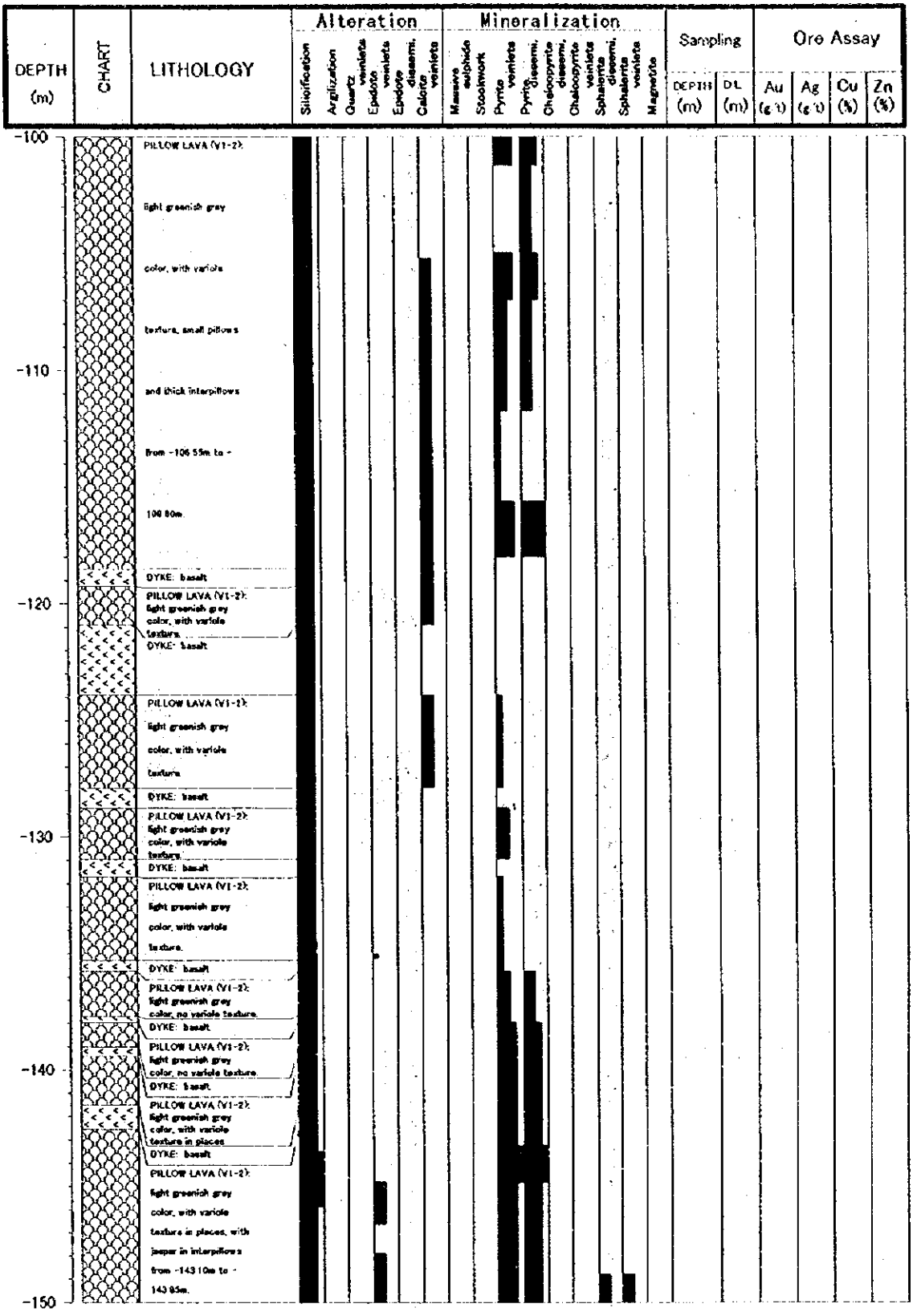

Hole No. MJOB-G39 (From 0.00 m to -201.90 m)

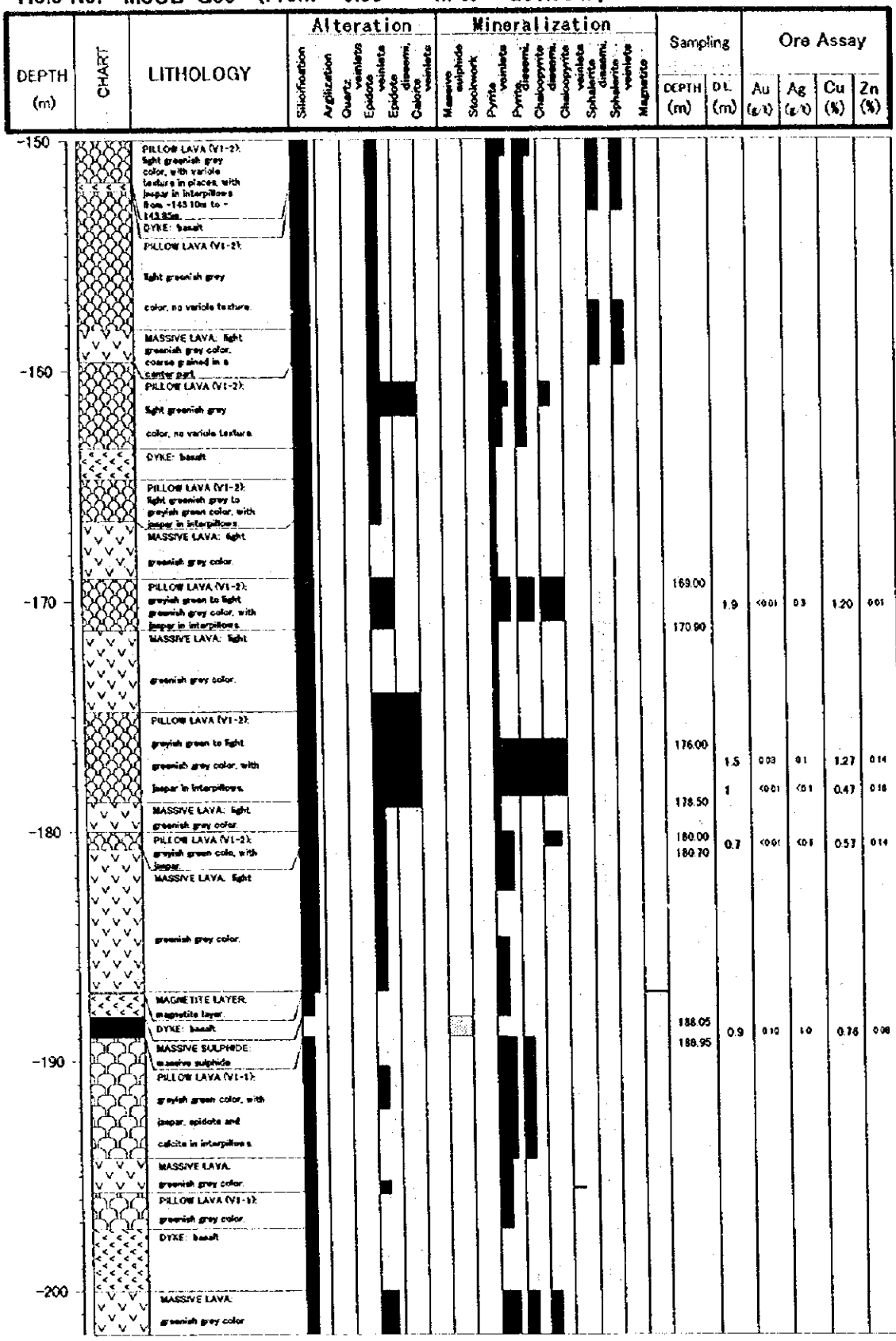

Hole No. MJOB-H1 (From 0.00 m to -350.70 m)

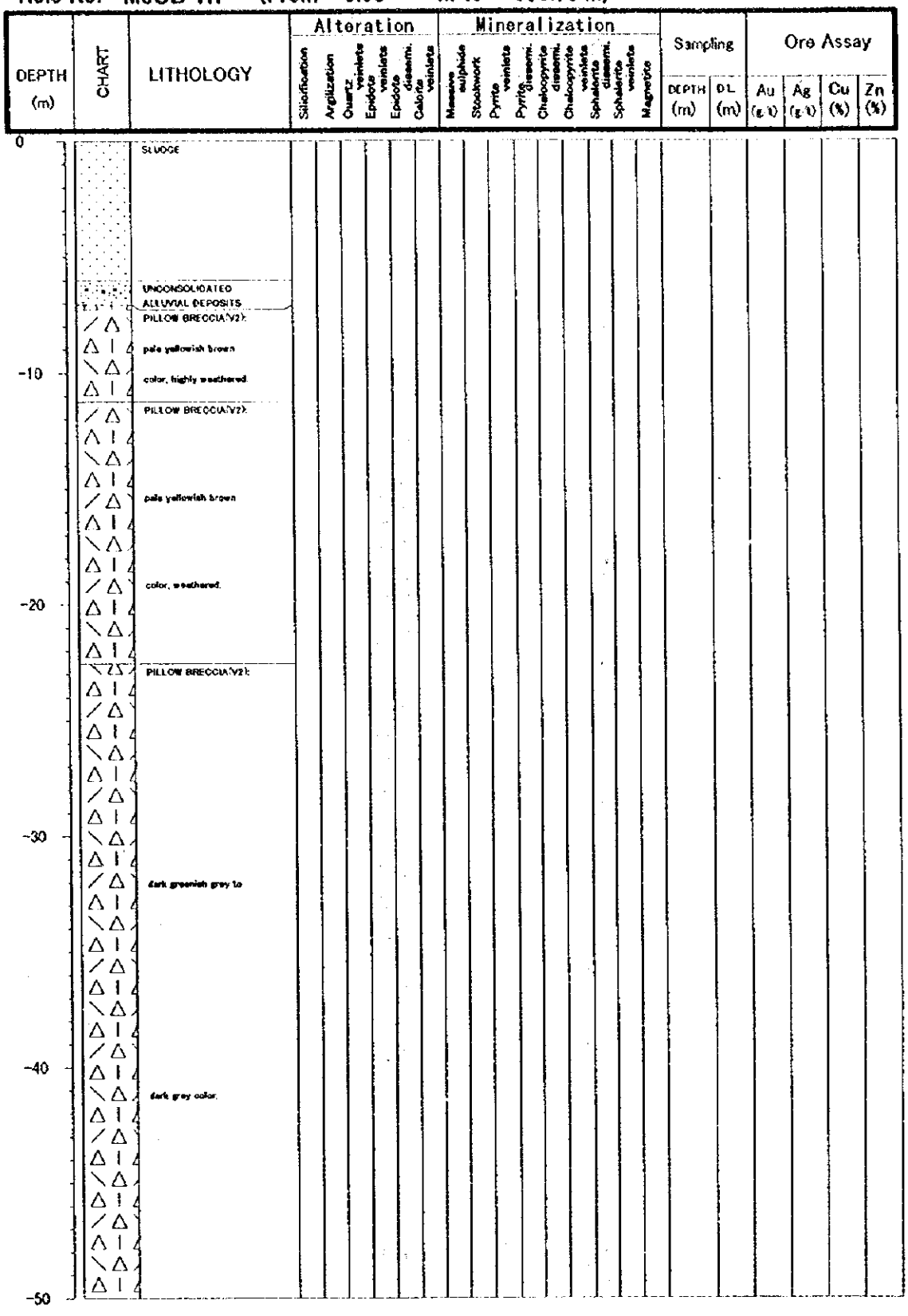

Hole No. MJOB-H1 (From 0.00 m to -350.70 m)

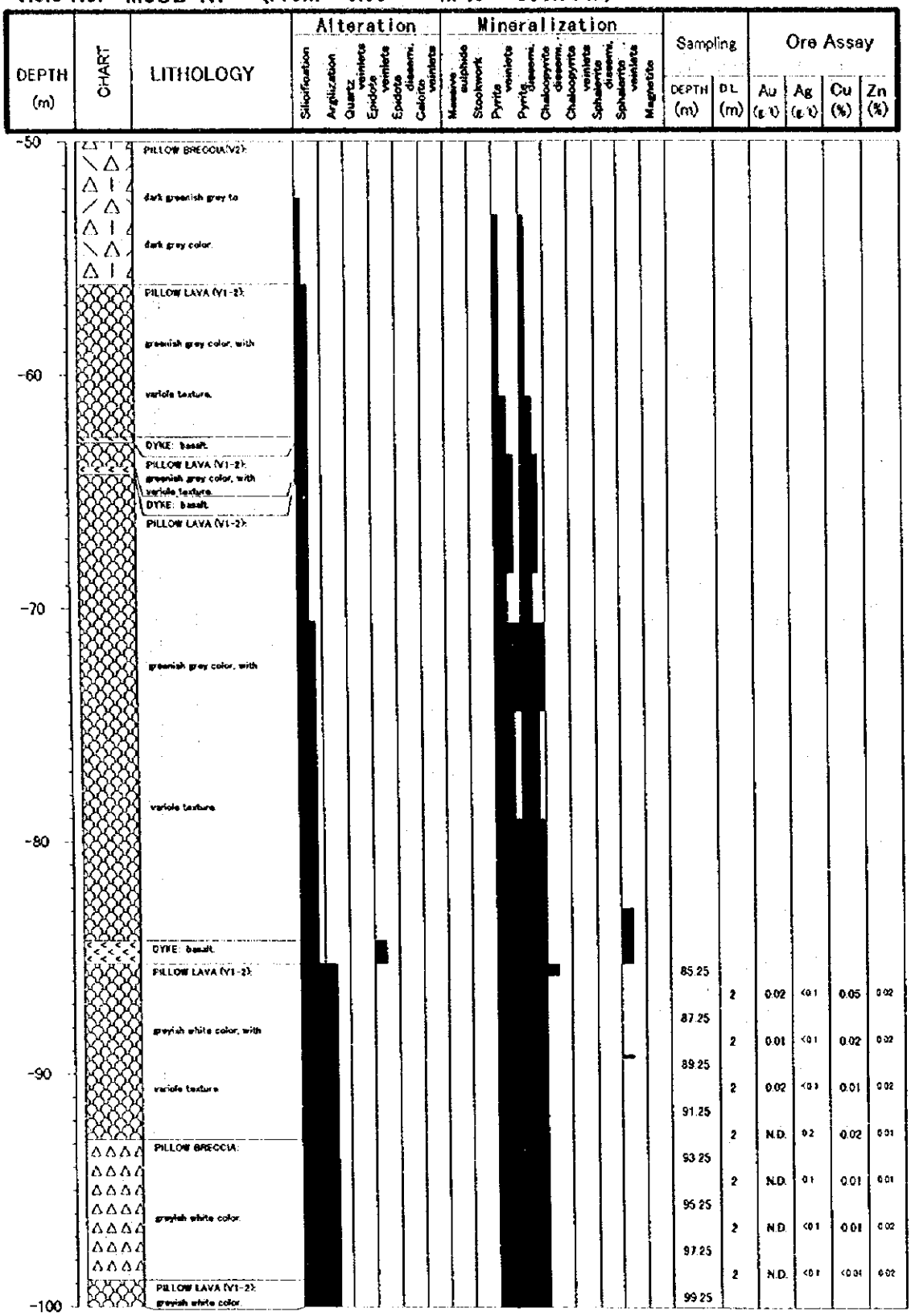

Hole No. MJOB-H1 (From 0.00 m to -350.70 m)

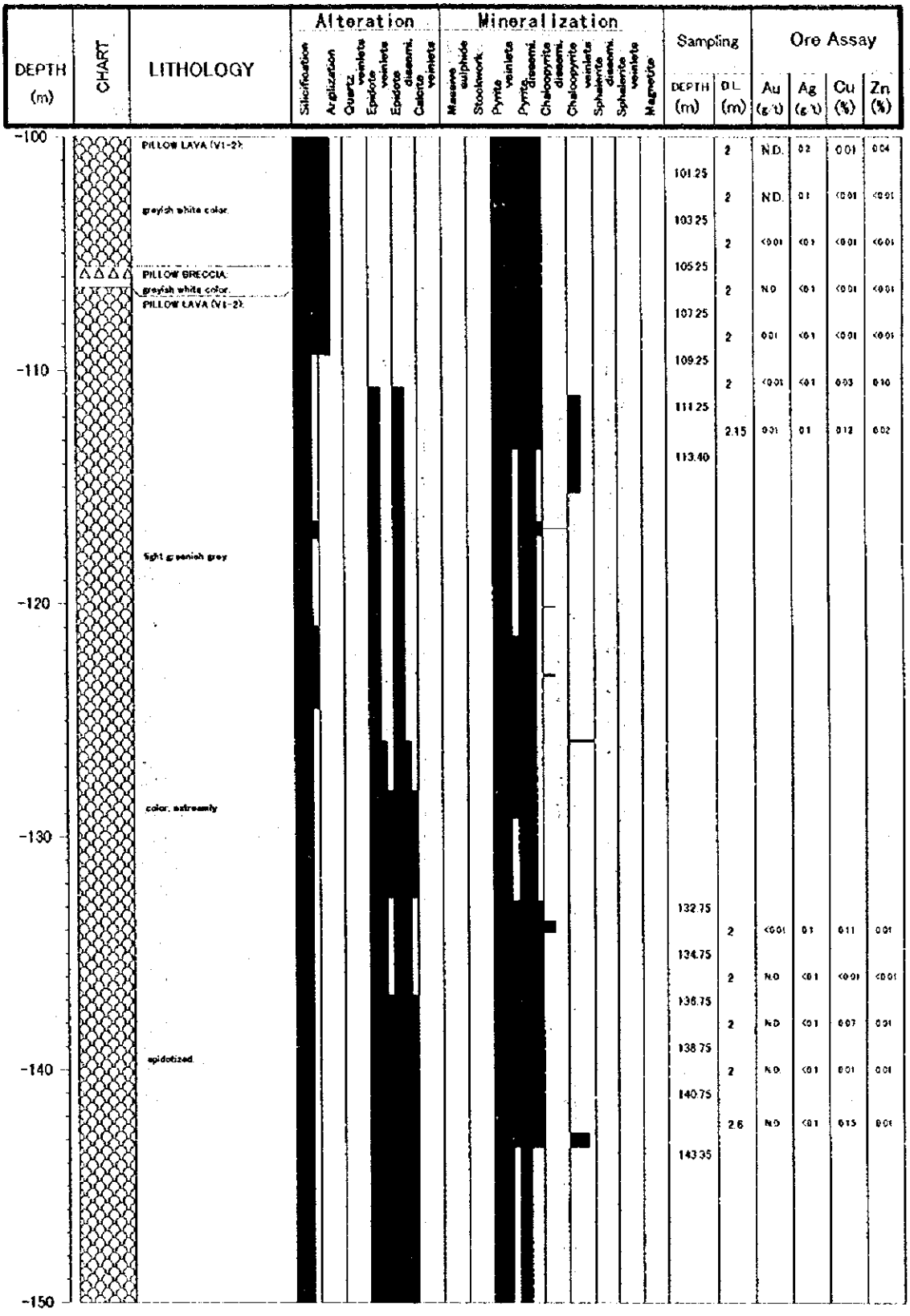

Hole No. MJOB-H1 (From 0.00 m to -350.70 m)

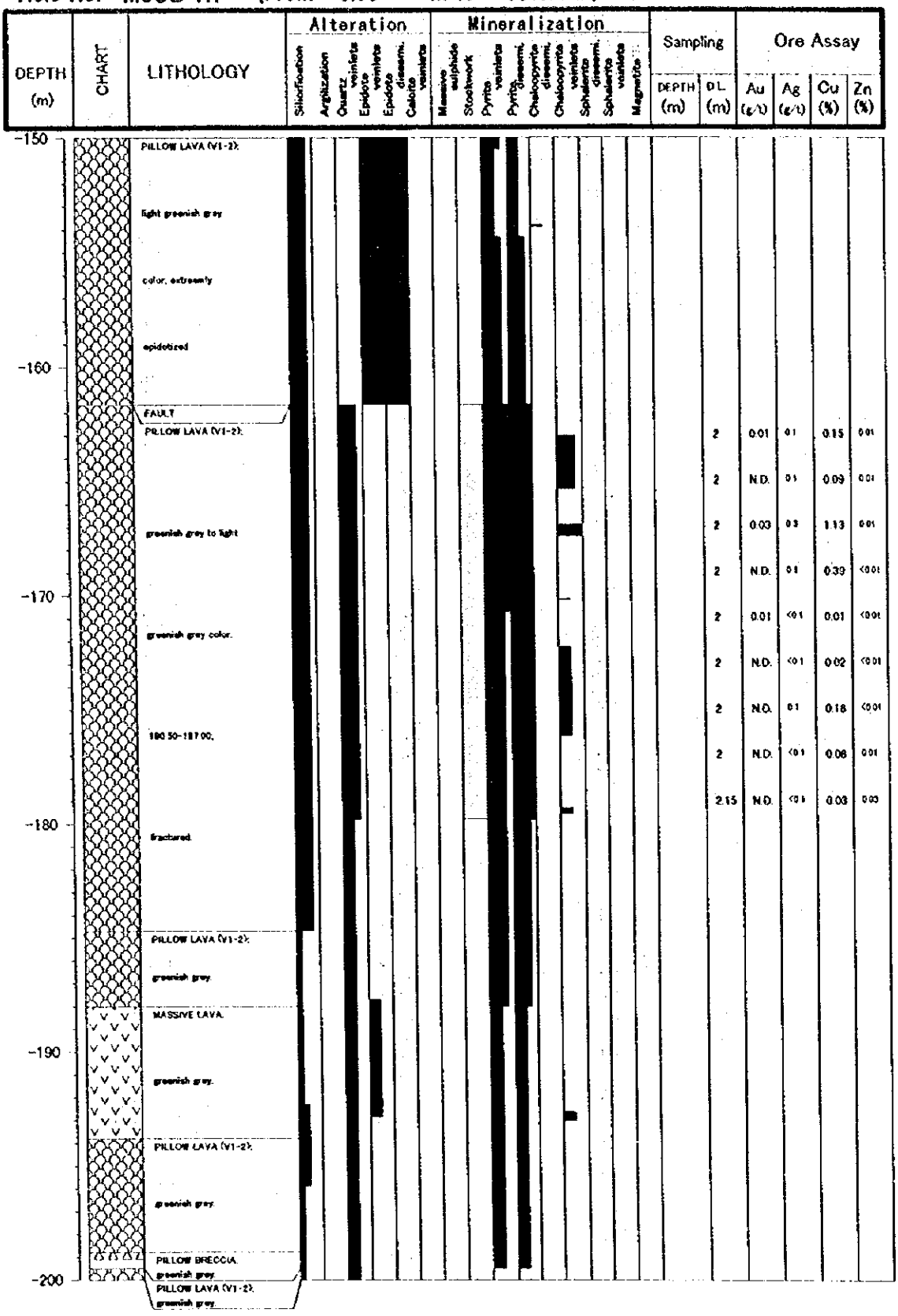

Hole No. MJOB-H1 (From 0.00 m to -350.70 m)

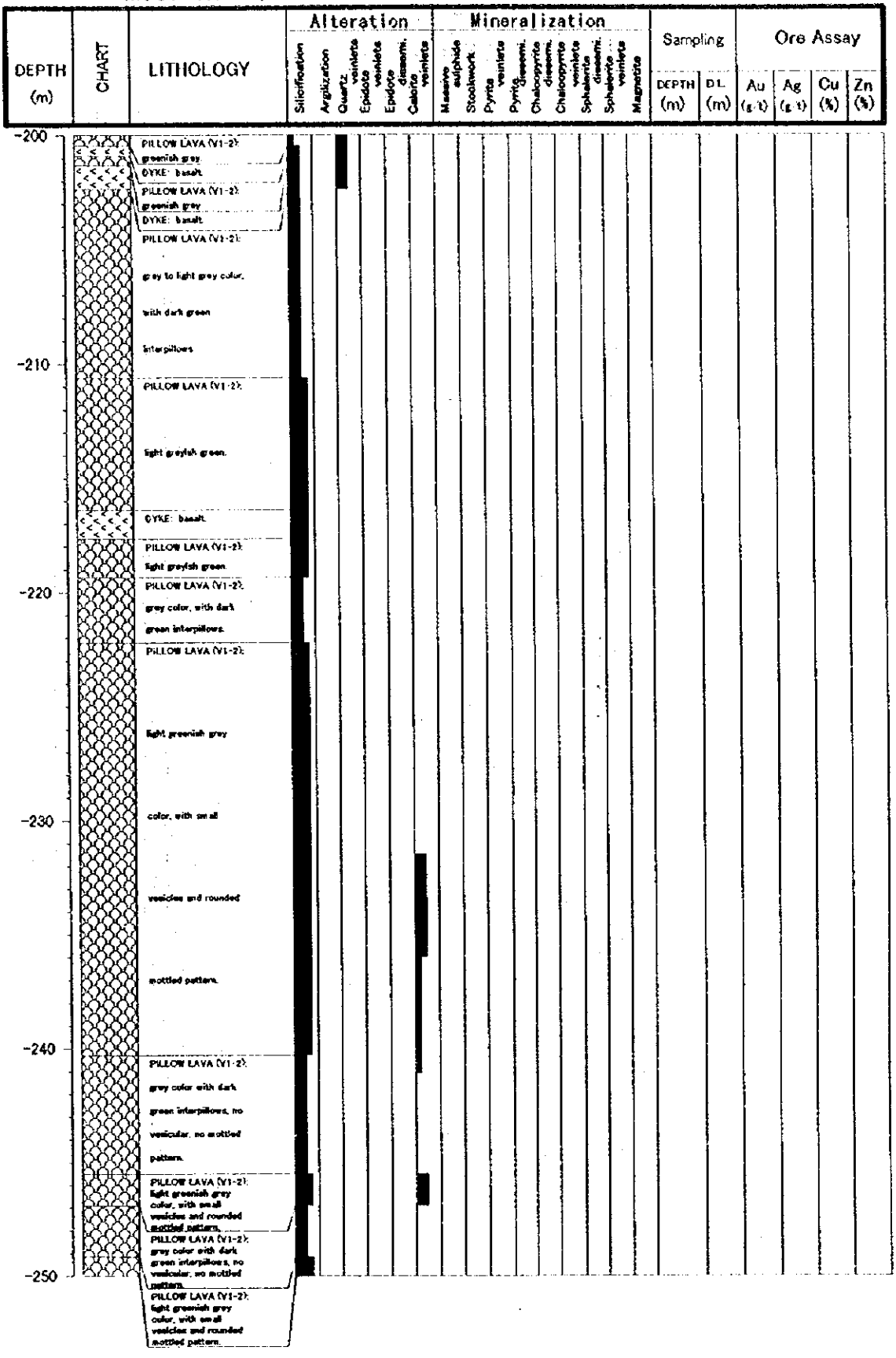

Hole No. MJOB-H1 (From 0.00 m to -350.70 m)

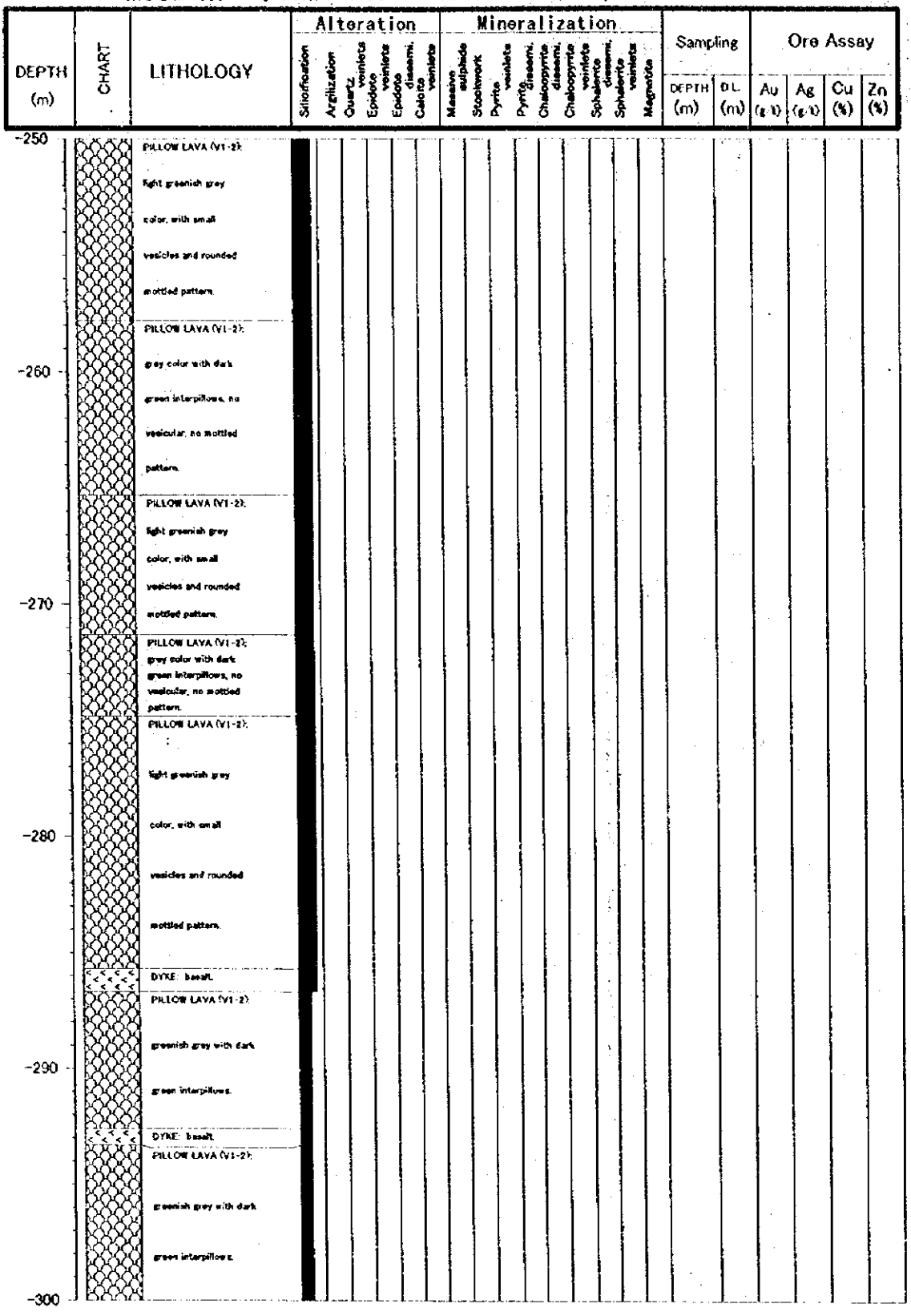

Hole No. MJOB-H1 (From 0.00 m to -350.70 m)

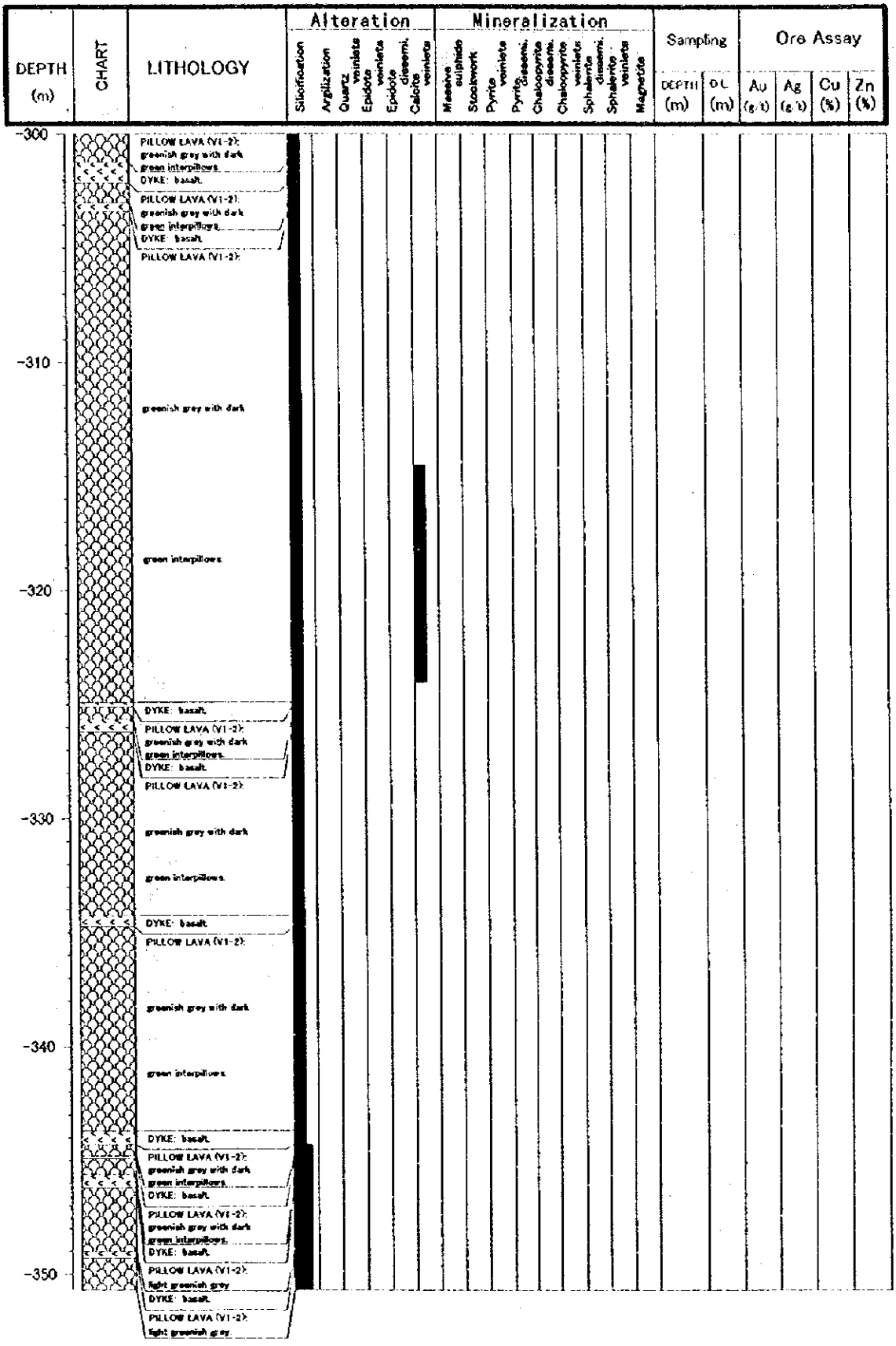

Hole No. MLOB-H2 (From 0.00 m to -251.30 m)

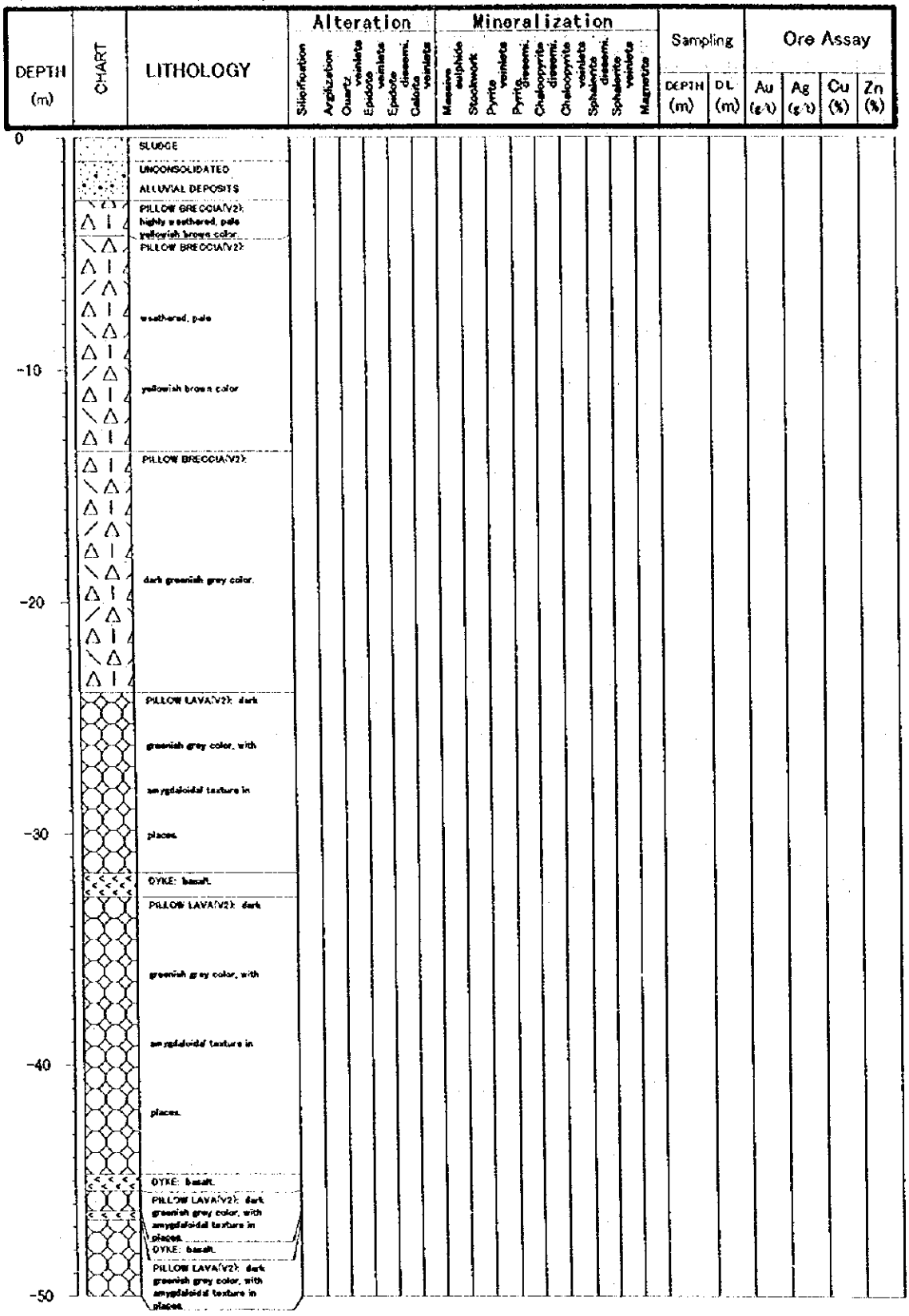

Hole No. MLOB-H2 (From 0.00 m to -251.30 m)

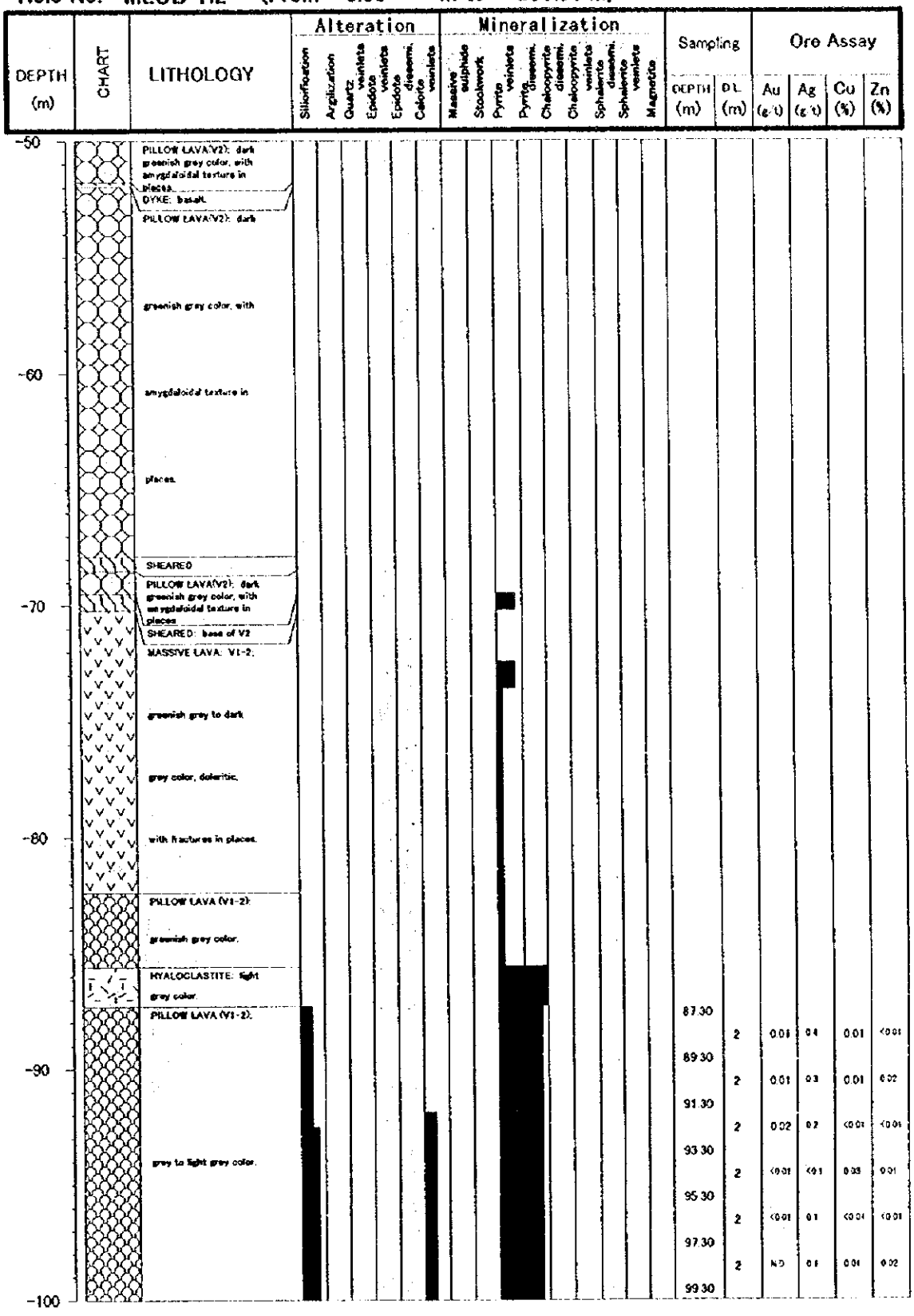

Hole No. MLOB-H2 (From 0.00 m to -251.30 m)

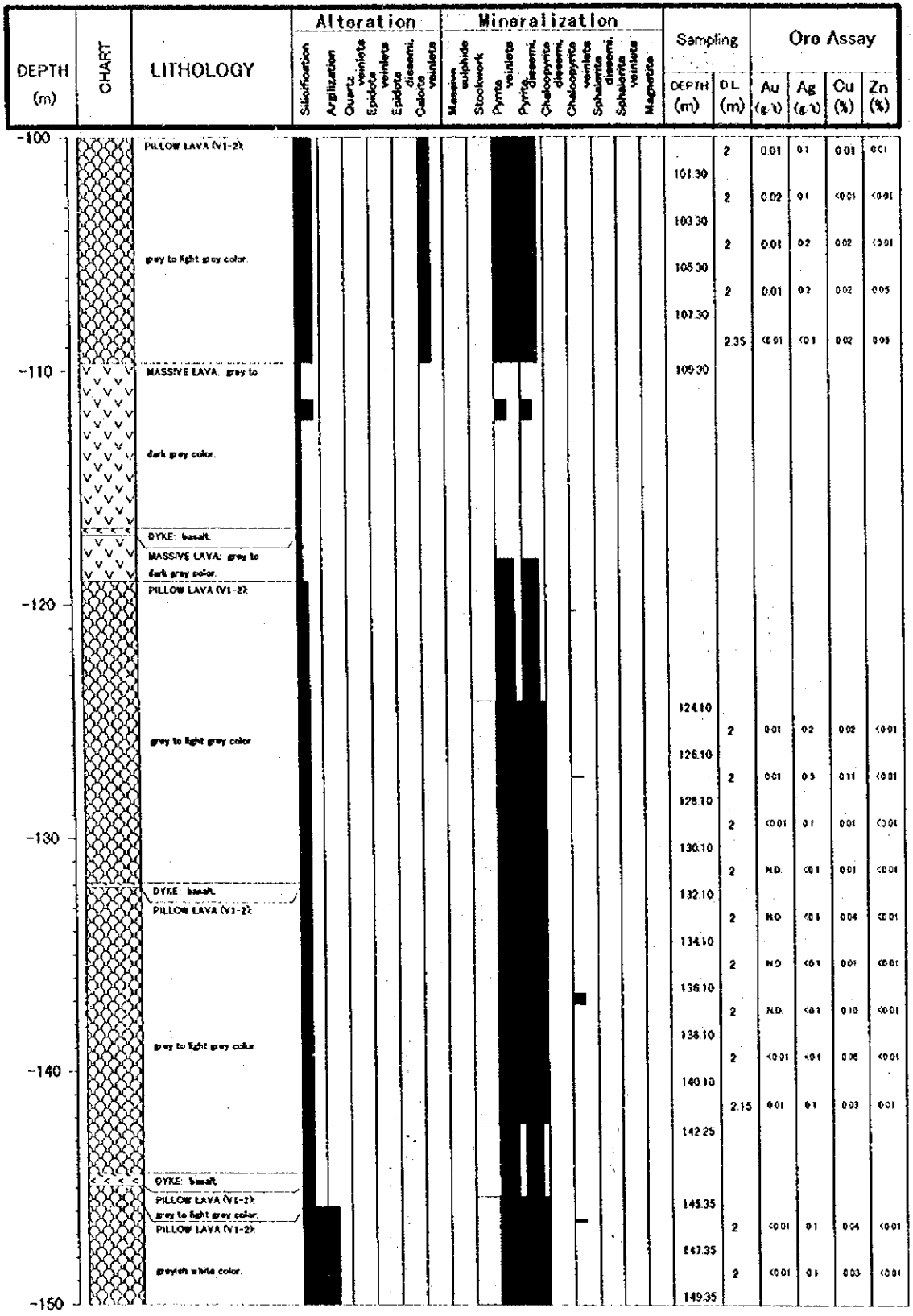

Hole No. MLOB-H2 (From 0.00 m to -251.30 m)

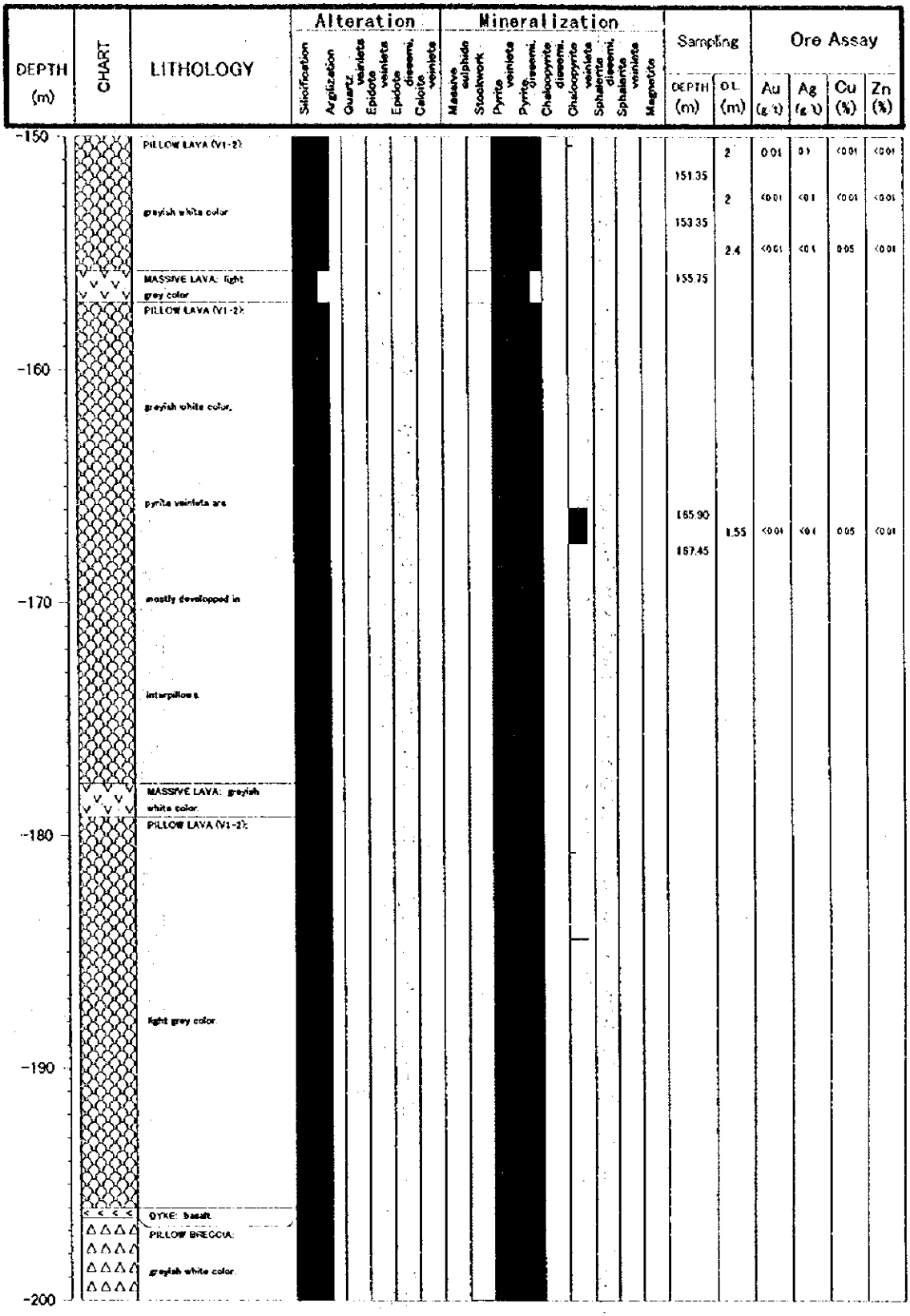

Hole No. MLOB-H2 (From 0.00 m to -251.30 m)

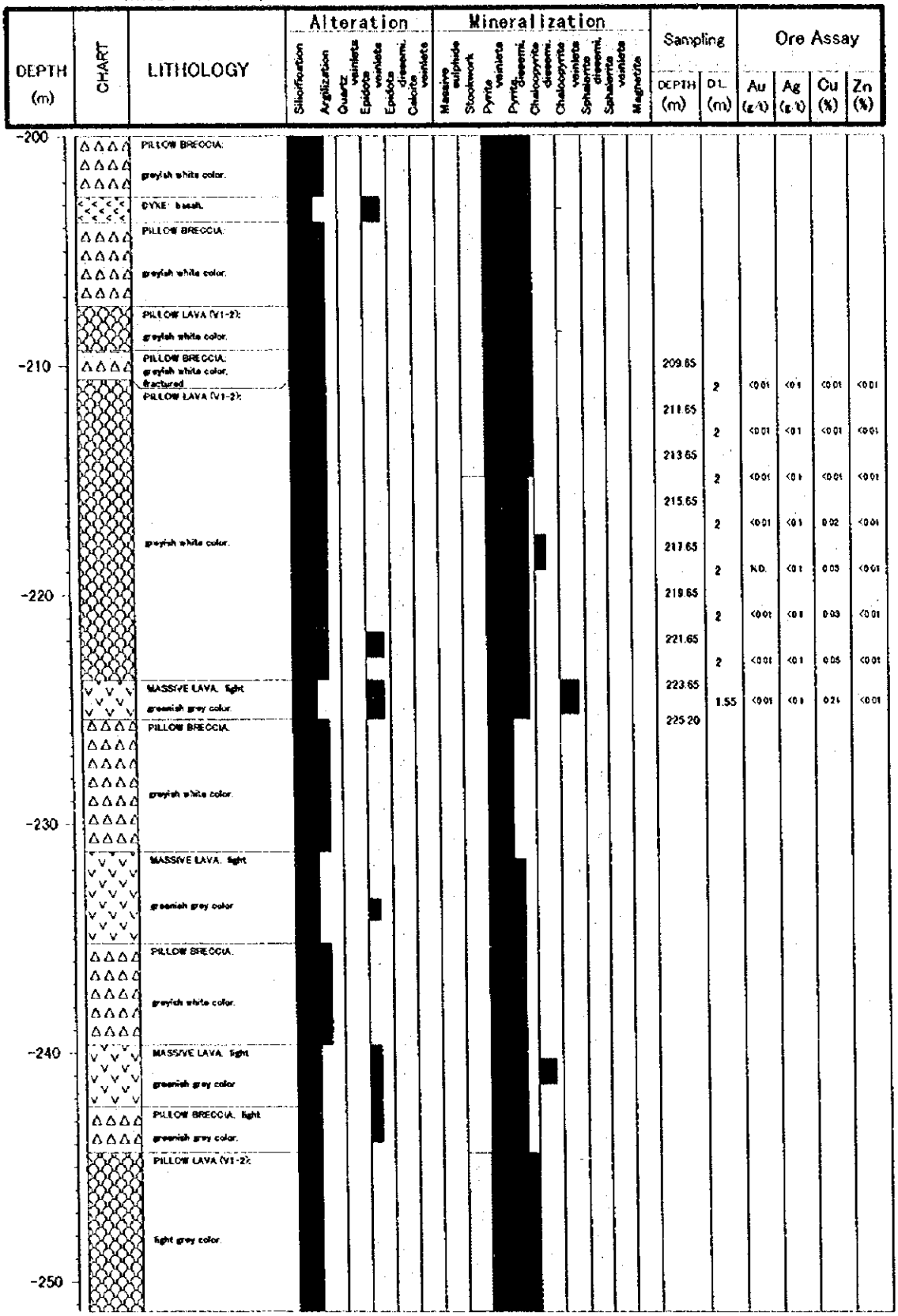

Hole No. MJOB-S1 (From 0.00 m to -250.40 m)

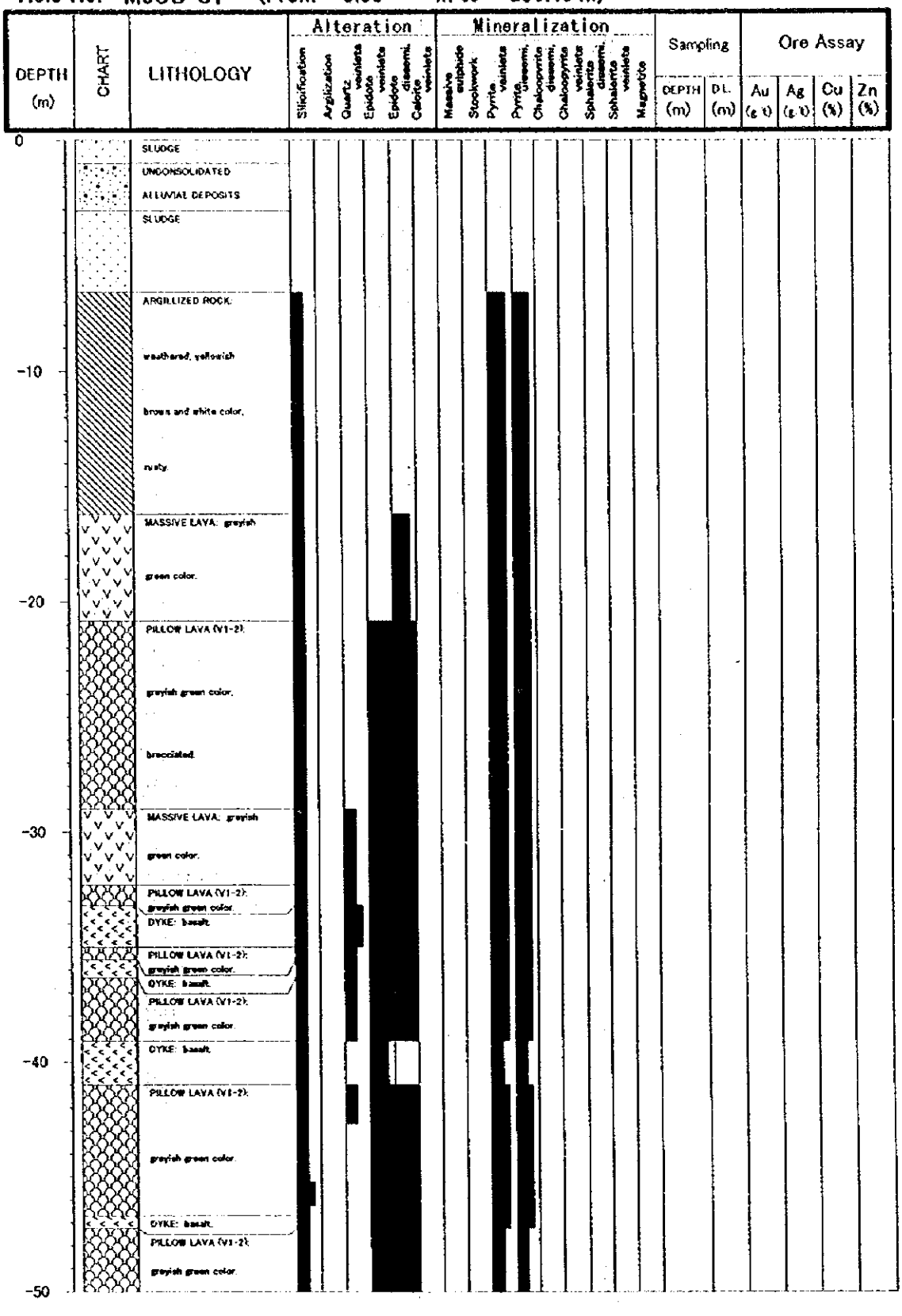

Hole No. MJOB-S1 (From 0.00 m to -250.40 m)

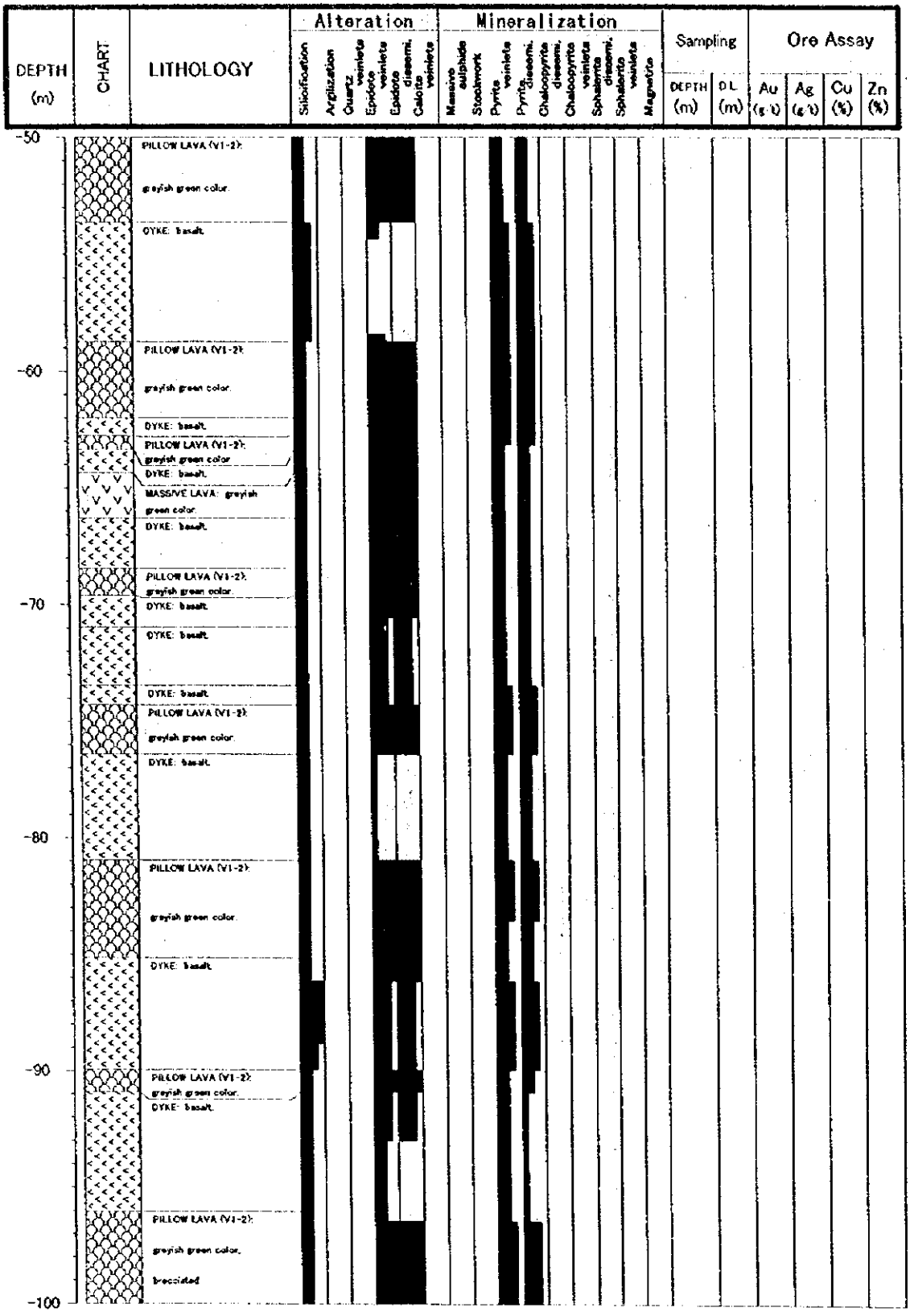

Hole No. MJOB-S1 (From 0.00 m to -250.40 m)

DEPTH (m)	CHART	LITHOLOGY
-100		PILLOW LAVA (V1-2): greyish green color, brecciated.
		DYKE: basalt.
		PILLOW LAVA (V1-2): greyish green color, with intense silicification and epidotization in interpillows
-110		
		MASSIVE LAVA: greyish green color.
		PILLOW LAVA (V1-2): greyish green color.
-120		DYKE: basalt.
		PILLOW LAVA (V1-2): greenish grey color, brecciated in places.
-130		PILLOW LAVA (V1-2): light greenish grey color.
		DYKE: basalt.
		DYKE: basalt.
		DYKE: basalt.
-140		PILLOW LAVA (V1-2): greenish grey color, brecciated in places.
		MASSIVE LAVA: greenish grey color.
		PILLOW LAVA (V1-2): greenish grey color.
-150		DYKE: basalt.

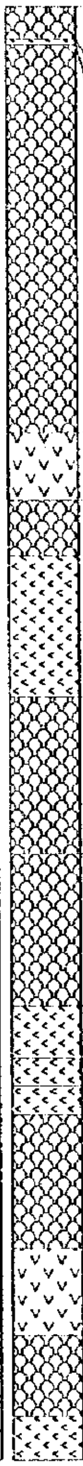

Alteration: Silicification, Argilization, Quartz veinlets, Epidote veinlets, Epidote dissemi., Calcite veinlets

Mineralization: Massive sulphide, Stockwork, Pyrite veinlets, Pyrite dissemi., Chalcopyrite dissemi., Chalcopyrite veinlets, Sphalerite dissemi., Sphalerite veinlets, Magnetite

Sampling DEPTH (m)	Sampling OL (m)	Ore Assay Au (g/t)	Ore Assay Ag (g/t)	Ore Assay Cu (%)	Ore Assay Zn (%)
108.50 - 110.50	2	<0.01	<0.1	0.02	0.06
110.50 - 112.50	2	<0.01	0.1	0.01	0.02
112.50 - 114.60	2.1	<0.01	<0.1	0.02	0.02
123.70 - 125.70	2	<0.01	0.1	<0.01	0.01
125.70 - 127.70	2	<0.01	<0.1	<0.01	0.01
127.70 - 129.70	2	<0.01	<0.1	0.01	<0.01
129.70 - 131.70	2	<0.01	<0.1	<0.01	0.01
131.70 - 133.70	2	<0.01	<0.1	<0.01	0.01
133.70 - 135.70	2	<0.01	0.2	0.04	<0.01
135.70 - 138.10	2.4	0.01	<0.1	<0.01	<0.01

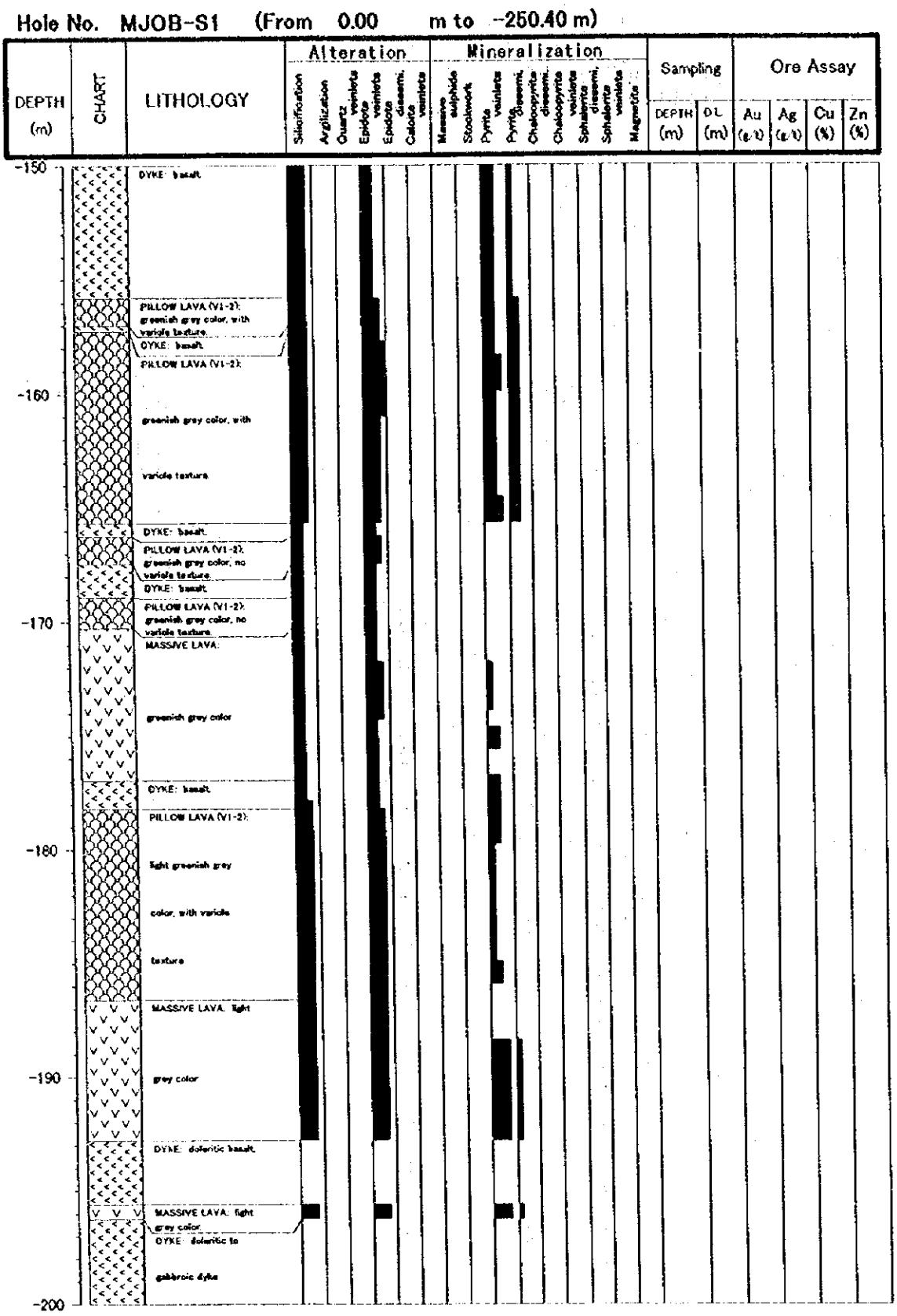
Hole No. MJOB-S1 (From 0.00 m to -250.40 m)
DEPTH (m)
CHART
LITHOLOGY
Alteration
Silicification
Argilization
Quartz veinlets
Epidote veinlets
Epidote disseminated
Calcite veinlets
Mineralization
Massive sulphide
Stockwork
Pyrite veinlets
Pyrite disseminated
Chalcopyrite disseminated
Chalcopyrite veinlets
Sphalerite disseminated
Sphalerite veinlets
Magnetite
Sampling
DEPTH (m)
D.L (m)
Ore Assay
Au (g/t)
Ag (g/t)
Cu (%)
Zn (%)
-150
-160
-170
-180
-190
-200
DYKE: basalt
PILLOW LAVA (V1-2): greenish grey color, with variole texture
DYKE: basalt
PILLOW LAVA (V1-2): greenish grey color, with variole texture
DYKE: basalt
PILLOW LAVA (V1-2): greenish grey color, no variole texture
DYKE: basalt
PILLOW LAVA (V1-2): greenish grey color, no variole texture
MASSIVE LAVA: greenish grey color
DYKE: basalt
PILLOW LAVA (V1-2): light greenish grey color, with variole texture
MASSIVE LAVA: light grey color
DYKE: doleritic basalt
MASSIVE LAVA: light grey color
DYKE: doleritic to gabbroic dyke

Hole No. MJOB-S1 (From 0.00 m to -250.40 m)

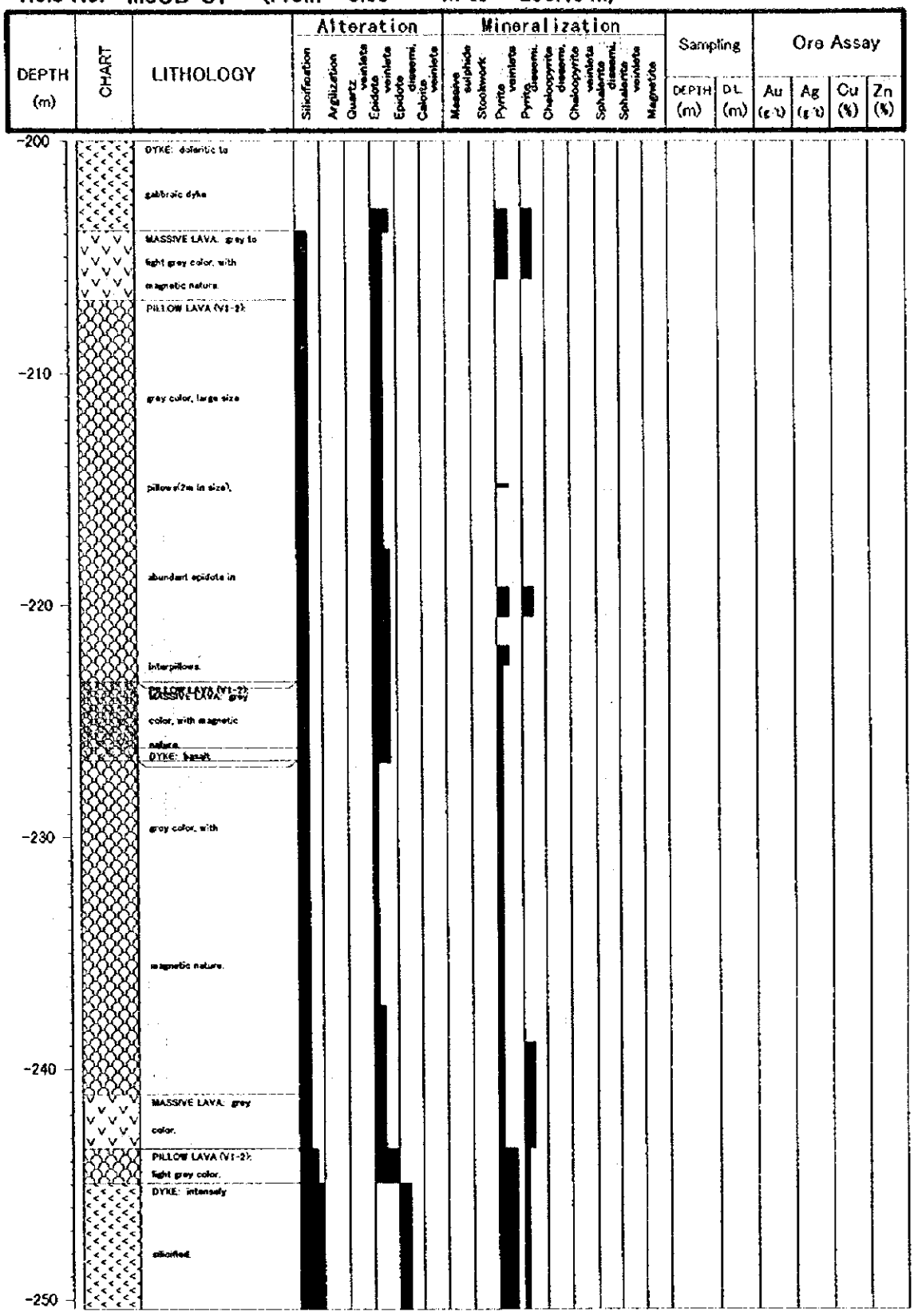

Hole No. MJOB-S2 (From 0.00 m to -253.85 m)

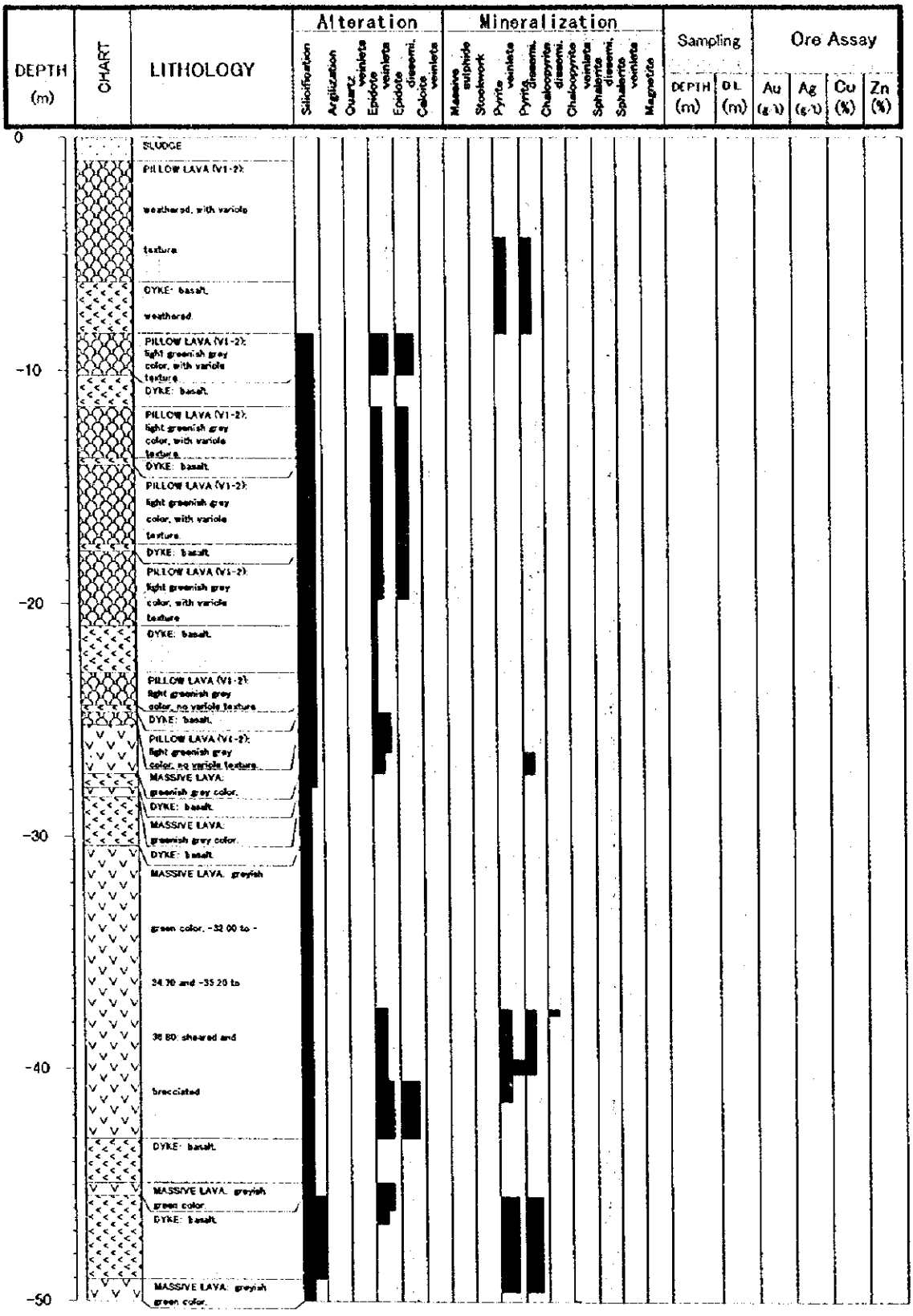

Hole No. MJOB-S2 (From 0.00 m to -253.85 m)

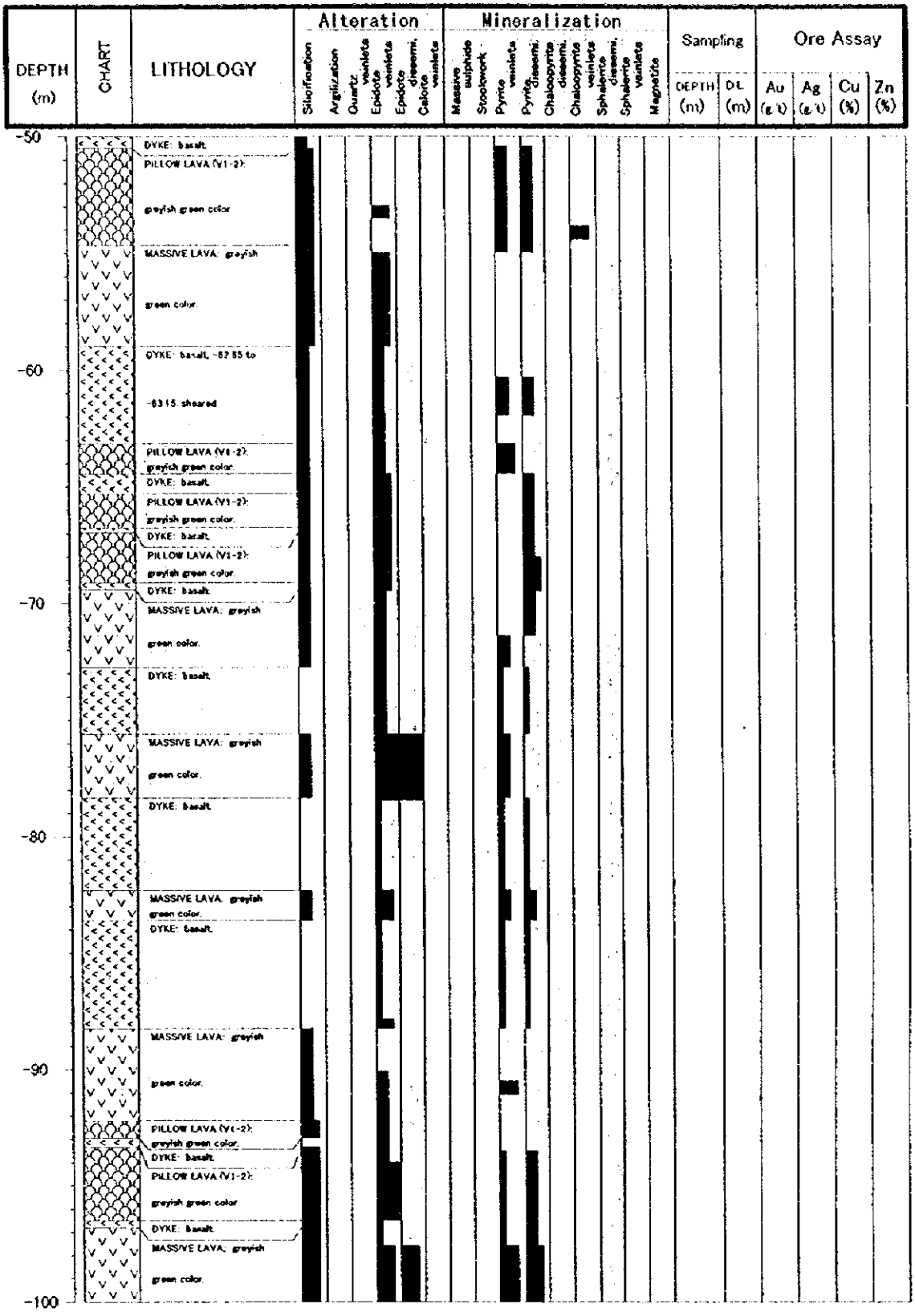

Hole No. MJOB-S2 (From 0.00 m to -253.85 m)

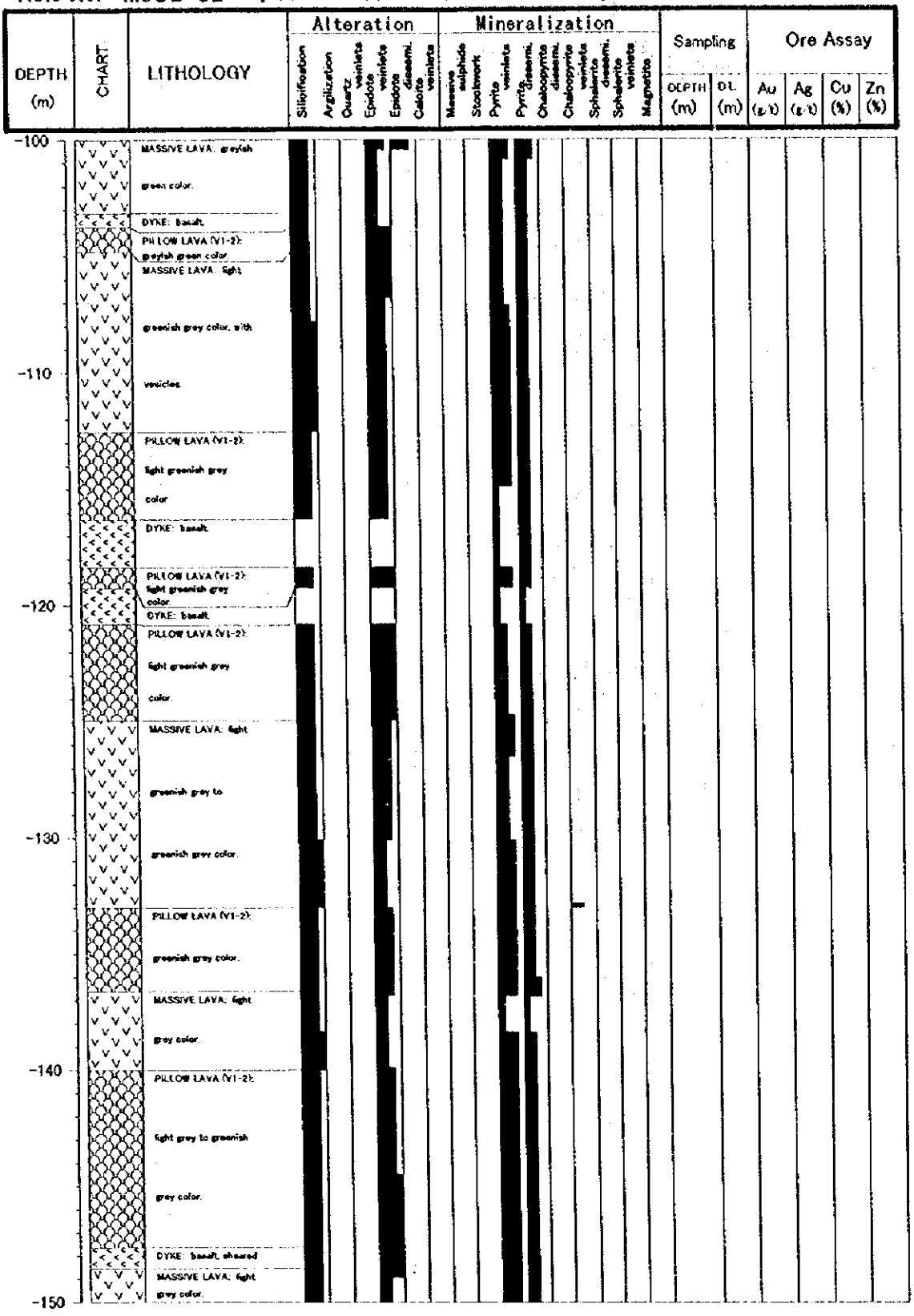

Hole No. MJOB-S2 (From 0.00 m to -253.85 m)

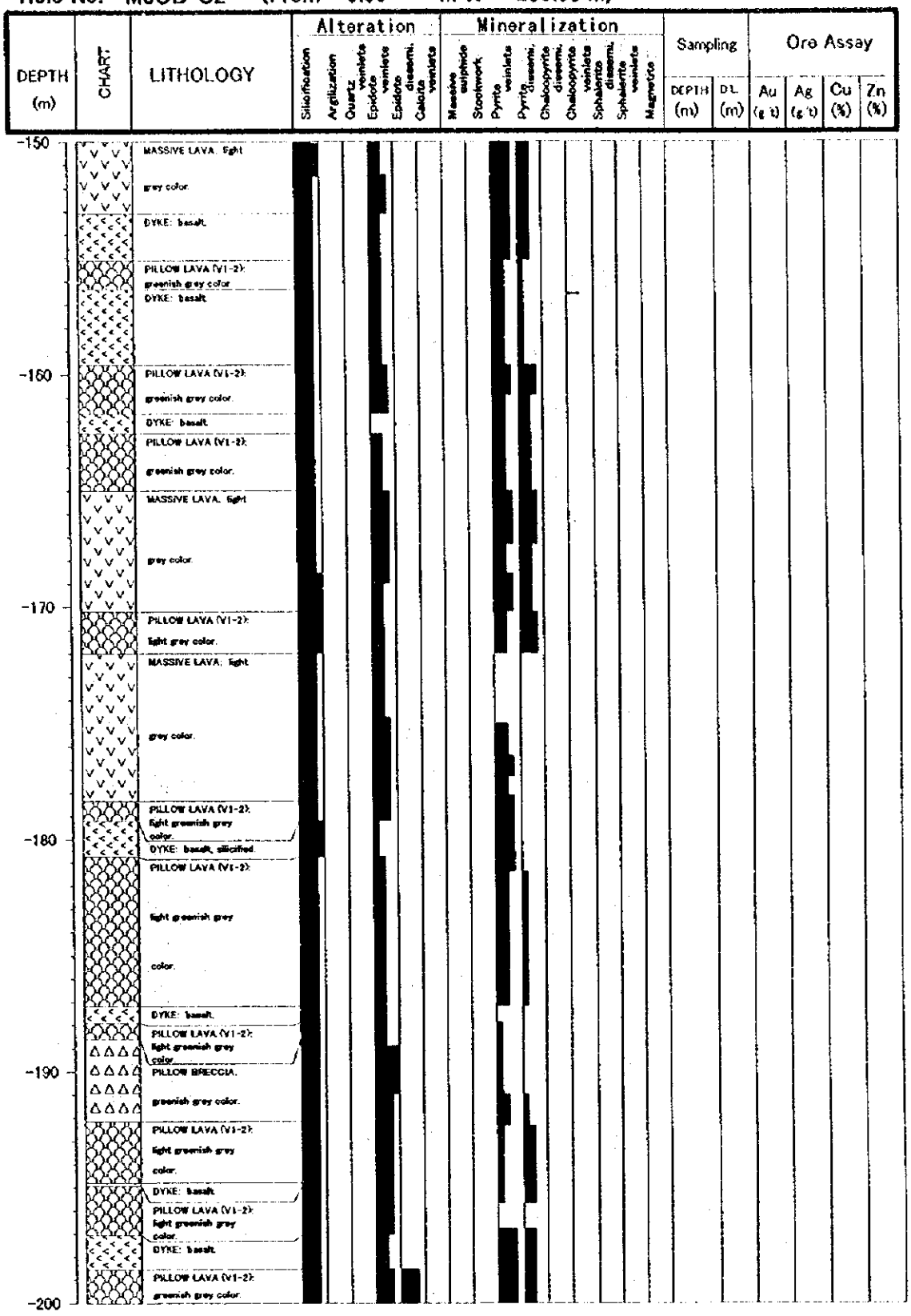

Hole No. MJOB-S2 (From 0.00 m to -253.85 m)

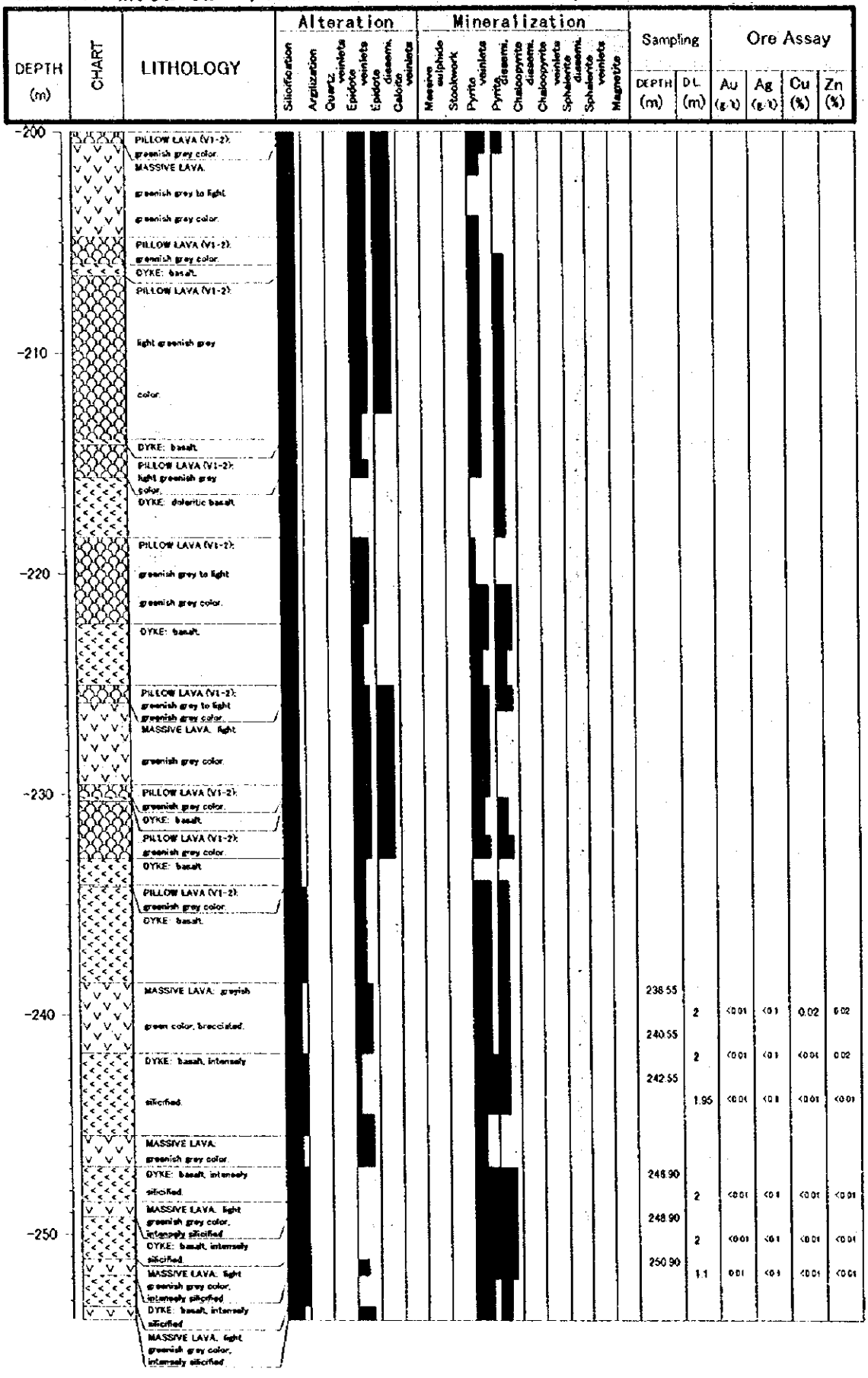

Appendix 4

Assay results of drilling cores

MJOB-G35

Sample No.	Depth(m)		Length (m)	Au(g/t)	Ag(g/t)	Cu(%)	Pb(ppm)	Zn(%)	Fe2O3 (%)
	From	To							
G35- 1	127.25	127.70	0.45	<0.01	<0.1	0.04	16	0.01	21.30
G35- 2	127.70	128.10	0.4	<0.01	<0.1	<0.01	21	0.02	23.50
G35- 3	128.10	129.10	1	0.10	0.6	1.04	64	0.04	51.60
G35- 4	129.10	130.10	1	0.15	0.9	0.98	84	0.05	55.30
G35- 5	130.10	131.10	1	0.18	1.2	0.86	101	0.05	58.10
G35- 6	131.10	132.10	1	0.13	1.0	0.84	88	0.05	54.30
G35- 7	132.10	132.70	0.6	<0.01	<0.1	0.13	23	0.02	16.40
G35- 8	132.70	133.35	0.65	0.03	0.4	1.67	39	0.01	60.50

Mineral Laboratory, Directorate of Minerals, Ministry of Commerce & Industry, Oman

AVERAGE		Length(m)	Cu(%)	Zn(%)
massive sulphide	127.25-133.35	6.1	0.80	0.04

MJOB-G36

Sample No.	Depth(m)		Length (m)	Au(g/t)	Ag(g/t)	Cu(%)	Pb(ppm)	Zn(%)	Fe2O3 (%)
	From	To							
G36- 1	177.00	178.00	1	0.13	1.0	2.26	55	0.05	55.30
G36- 2	178.00	179.00	1	0.16	1.2	2.17	76	0.05	58.40
G36- 3	179.00	180.20	1.2	0.10	1.1	0.81	80	0.05	60.50
G36- 4	180.20	180.75	0.55	N.D.	0.1	0.30	27	0.01	21.30
G36- 5	180.75	182.30	1.55	0.13	1.2	0.70	82	0.05	57.00
G36- 6	182.30	182.95	0.65	N.D.	0.2	0.12	20	0.01	22.40
G36- 7	182.95	183.95	1	0.11	1.2	0.83	66	0.04	57.90
G36- 8	183.95	184.95	1	0.10	1.1	0.77	60	0.08	57.20
G36- 9	184.95	185.95	1	0.10	0.9	0.75	56	0.08	60.00
G36- 10	185.95	186.95	1	0.09	1.1	1.14	68	0.04	58.40
G36- 11	186.95	187.95	1	0.10	1.0	0.82	70	0.04	57.50
G36- 12	187.95	188.95	1	0.10	1.4	1.71	70	0.03	58.70
G36- 13	188.95	189.95	1	0.08	1.2	1.17	74	0.03	59.20
G36- 14	189.95	190.95	1	0.10	1.1	1.78	70	0.03	56.70
G36- 15	190.95	191.95	1	0.04	0.9	0.93	62	0.04	58.30
G36- 16	191.95	192.95	1	0.08	1.0	0.93	68	0.04	59.10
G36- 17	192.95	193.95	1	0.06	0.8	0.84	58	0.05	59.20
G36- 18	193.95	194.95	1	0.07	0.8	1.03	68	0.06	57.90
G36- 19	194.95	195.95	1	0.09	1.0	1.29	70	0.05	57.00
G36- 20	195.95	196.95	1	0.06	0.9	0.82	56	0.07	58.60
G36- 21	196.95	197.95	1	0.04	1.1	1.51	60	0.08	57.50
G36- 22	197.95	198.95	1	0.08	1.2	0.76	60	0.08	58.90
G36- 23	198.95	199.95	1	0.08	0.8	1.05	50	0.08	57.20
G36- 24	199.95	200.95	1	0.07	1.0	1.42	52	0.07	57.50
G36- 25	200.95	201.95	1	0.13	1.2	1.28	50	0.06	55.20
G36- 26	201.95	202.95	1	0.11	3.1	1.34	58	0.06	58.50
G36- 27	202.95	203.95	1	0.10	5.1	1.00	54	0.07	58.60
G36- 28	203.95	204.95	1	0.13	1.7	2.13	72	0.09	58.50
G36- 29	204.95	205.95	1	0.12	1.5	1.04	60	0.07	59.40
G36- 30	205.95	206.95	1	0.09	1.1	1.08	46	0.05	60.20
G36- 31	206.95	207.95	1	0.11	0.9	0.86	48	0.06	56.60
G36- 32	207.95	208.95	1	0.12	0.9	1.18	48	0.06	58.90
G36- 33	208.95	209.95	1	0.11	1.1	0.92	48	0.05	59.40
G36- 34	209.95	210.95	1	0.05	1.2	1.73	60	0.05	60.90
G36- 35	210.95	211.95	1	0.09	1.8	1.41	58	0.05	60.30
G36- 36	211.95	212.95	1	0.05	0.7	1.13	54	0.04	60.80
G36- 37	212.95	213.95	1	0.05	0.7	1.55	56	0.05	60.20
G36- 38	213.95	214.95	1	0.10	1.1	2.13	66	0.04	58.00
G36- 39	214.95	215.95	1	0.10	1.1	2.42	54	0.05	60.40
G36- 40	215.95	216.95	1	0.07	0.6	1.15	40	0.02	60.50
G36- 41	216.95	217.95	1	0.07	0.6	1.70	40	0.02	53.90
G36- 42	217.95	218.95	1	0.07	1.0	0.99	46	0.03	60.90
G36- 43	218.95	219.95	1	0.07	0.9	1.17	48	0.02	58.20
G36- 44	219.95	220.95	1	0.07	1.0	0.57	54	0.04	56.60
G36- 45	220.95	221.95	1	0.11	1.8	1.22	84	0.06	53.90
G36- 46	221.95	222.95	1	0.09	1.6	0.99	72	0.06	55.90
G36- 47	222.95	223.95	1	0.06	1.6	1.16	80	0.06	57.20
G36- 48	223.95	224.95	1	0.09	1.5	0.66	69	0.06	53.90
G36- 49	224.95	225.75	0.8	0.11	1.5	0.35	73	0.05	57.80
G36- 50	225.75	226.65	0.9	N.D.	0.2	0.12	28	0.02	23.50

MJOB-G36

Sample No.	Depth(m)		Length (m)	Au(g/t)	Ag(g/t)	Cu(%)	Pb(ppm)	Zn(%)	Fe2O3 (%)
	From	To							
G36- 51	226.65	227.65	1	0.10	1.1	0.79	65	0.05	58.60
G36- 52	227.65	228.70	1.05	0.10	1.2	1.13	67	0.05	58.40
G36- 53	228.70	229.95	1.25	N.D.	<0.1	0.43	24	0.01	18.00
G36- 54	229.95	231.25	1.3	0.06	1.1	1.52	44	0.02	39.00

Mineral Laboratory, Directorate of Minerals, Ministry of Commerce & Industry, Oman

AVERAGE		Length(m)	Cu(%)	Zn(%)
massive sulphide	177.00-231.25	54.25	1.14	0.05

MJOB-G37

Sample No.	Depth(m)		Length	Au(g/t)	Ag(g/t)	Cu(%)	Pb(ppm)	Zn(%)	Fe2O3
	From	To	(m)						(%)
G37- 1	255.05	256.05	1	0.20	1.5	1.66	83	0.07	58.90
G37- 2	256.05	257.05	1	0.24	1.6	1.79	94	0.10	60.10
G37- 3	257.05	258.05	1	0.12	1.6	1.87	105	0.08	57.60
G37- 4	258.05	259.15	1.1	0.17	1.4	1.09	101	0.06	61.00

Mineral Laboratory, Directorate of Minerals, Ministry of Commerce & Industry, Oman

AVERAGE		Length(m)	Cu(%)	Zn(%)
massive sulphide	255.05-259.15	4.1	1.59	0.08

MJOB-G39

Sample No.	Depth(m)		Length	Au(g/t)	Ag(g/t)	Cu(%)	Pb(ppm)	Zn(%)	Fe2O3
	From	To	(m)						(%)
G39- 1	169.00	170.90	1.9	<0.01	0.3	1.20	23	0.01	23.30
G39- 2	176.00	177.00	1	0.03	0.1	1.27	21	0.14	18.40
G39- 3	177.00	178.50	1.5	<0.01	<0.1	0.47	23	0.16	19.80
G39- 4	180.00	180.70	0.7	<0.01	<0.1	0.57	25	0.14	24.10
G39- 5	188.05	188.95	0.9	0.10	1.0	0.76	84	0.08	56.70

Mineral Laboratory, Directorate of Minerals, Ministry of Commerce & Industry, Oman

AVERAGE		Length(m)	Cu(%)	Zn(%)
massive sulphide	188.05-188.95	0.9	0.84	0.09

MJOB-H1

Sample No.	Depth(m)		Length	Au(g/t)	Ag(g/t)	Cu(%)	Pb(ppm)	Zn(%)	Fe2O3
	From	To	(m)						(%)
H1- 1	85.25	87.25	2	0.02	<0.1	0.05	<10	0.02	7.92
H1- 2	87.25	89.25	2	0.01	<0.1	0.02	<10	0.02	8.54
H1- 3	89.25	91.25	2	0.02	<0.1	0.01	<10	0.02	8.23
H1- 4	91.25	93.25	2	N.D.	0.2	0.02	<10	0.01	8.23
H1- 5	93.25	95.25	2	N.D.	0.1	0.01	<10	0.01	9.32
H1- 6	95.25	97.25	2	N.D.	<0.1	0.01	<10	0.02	8.85
H1- 7	97.25	99.25	2	N.D.	<0.1	<0.01	<10	0.02	8.85
H1- 8	99.25	101.25	2	N.D.	0.2	0.01	<10	0.04	9.47
H1- 9	101.25	103.25	2	N.D.	0.1	<0.01	<10	<0.01	8.54
H1- 10	103.25	105.25	2	<0.01	<0.1	<0.01	<10	<0.01	8.54
H1- 11	105.25	107.25	2	N.D.	<0.1	<0.01	<10	<0.01	9.32
H1- 12	107.25	109.25	2	0.01	<0.1	<0.01	<10	<0.01	9.63
H1- 13	109.25	111.25	2	<0.01	<0.1	0.03	<10	0.10	12.11
H1- 14	111.25	113.40	2.15	0.01	0.1	0.12	<10	0.02	12.58
H1- 15	132.75	134.75	2	<0.01	0.1	0.11	<10	0.01	13.35
H1- 16	134.75	136.75	2	N.D.	<0.1	<0.01	<10	<0.01	12.11
H1- 17	136.75	138.75	2	N.D.	<0.1	0.07	<10	0.01	11.49
H1- 18	138.75	140.75	2	N.D.	<0.1	0.01	<10	0.01	13.04
H1- 19	140.75	143.35	2.6	N.D.	<0.1	0.15	<10	0.01	12.73
H1- 20	161.65	163.65	2	0.01	0.1	0.15	<10	0.01	15.37
H1- 21	163.65	165.65	2	N.D.	0.1	0.09	<10	0.01	16.46
H1- 22	165.65	167.65	2	0.03	0.3	1.13	25	0.01	23.76
H1- 23	167.65	169.65	2	N.D.	0.1	0.39	<10	<0.01	19.88
H1- 24	169.65	171.65	2	0.01	<0.1	0.01	<10	<0.01	15.84
H1- 25	171.65	173.65	2	N.D.	<0.1	0.02	<10	<0.01	15.37
H1- 26	173.65	175.65	2	N.D.	0.1	0.18	<10	<0.01	18.94
H1- 27	175.65	177.65	2	N.D.	<0.1	0.08	<10	0.01	13.82
H1- 28	177.65	179.80	2.15	N.D.	<0.1	0.03	<10	0.03	14.75

Mineral Laboratory, Directorate of Minerals, Ministry of Commerce & Industry, Oman

AVERAGE	Length(m)	Cu(%)	Zn(%)
	56.9	0.10	0.02

MJOB-H2

Sample No.	Depth(m)		Length (m)	Au(g/t)	Ag(g/t)	Cu(%)	Pb(ppm)	Zn(%)	Fe2O3 (%)
	From	To							
H2- 1	87.30	89.30	2	0.01	0.4	0.01	N.D.	<0.01	12.58
H2- 2	89.30	91.30	2	0.01	0.3	0.01	N.D.	0.02	12.89
H2- 3	91.30	93.30	2	0.02	0.2	<0.01	N.D.	<0.01	11.65
H2- 4	93.30	95.30	2	<0.01	<0.1	0.03	N.D.	0.01	11.20
H2- 5	95.30	97.30	2	<0.01	0.1	<0.01	N.D.	<0.01	10.28
H2- 6	97.30	99.30	2	N.D.	0.1	0.01	N.D.	0.02	11.20
H2- 7	99.30	101.30	2	0.01	0.1	0.01	N.D.	0.01	10.42
H2- 8	101.30	103.30	2	0.02	0.1	<0.01	N.D.	<0.01	11.50
H2- 9	103.30	105.30	2	0.01	0.2	0.02	N.D.	<0.01	13.34
H2- 10	105.30	107.30	2	0.01	0.2	0.02	N.D.	0.05	14.42
H2- 11	107.30	109.65	2.35	<0.01	<0.1	0.02	N.D.	0.05	10.28
H2- 12	124.10	126.10	2	0.01	0.2	0.02	N.D.	<0.01	15.79
H2- 13	126.10	128.10	2	0.01	0.3	0.11	N.D.	<0.01	19.01
H2- 14	128.10	130.10	2	<0.01	0.1	0.01	N.D.	<0.01	13.80
H2- 15	130.10	132.10	2	N.D.	<0.1	0.01	N.D.	<0.01	8.89
H2- 16	132.10	134.10	2	N.D.	<0.1	0.04	N.D.	<0.01	10.28
H2- 17	134.10	136.10	2	N.D.	<0.1	0.01	N.D.	<0.01	10.42
H2- 18	136.10	138.10	2	N.D.	<0.1	0.10	N.D.	<0.01	10.42
H2- 19	138.10	140.10	2	<0.01	<0.1	0.06	N.D.	<0.01	11.35
H2- 20	140.10	142.25	2.15	0.01	0.1	0.03	N.D.	0.01	11.35
H2- 21	145.35	147.35	2	<0.01	0.1	0.04	N.D.	<0.01	12.73
H2- 22	147.35	149.35	2	<0.01	0.1	0.03	N.D.	<0.01	11.20
H2- 23	149.35	151.35	2	0.01	0.1	<0.01	N.D.	<0.01	14.12
H2- 24	151.35	153.35	2	<0.01	<0.1	<0.01	N.D.	<0.01	14.72
H2- 25	153.35	155.75	2.4	<0.01	<0.1	0.05	N.D.	<0.01	17.48
H2- 26	165.90	167.45	1.55	<0.01	<0.1	0.05	N.D.	<0.01	13.80
H2- 27	209.65	211.65	2	<0.01	<0.1	<0.01	N.D.	<0.01	13.03
H2- 28	211.65	213.65	2	<0.01	<0.1	<0.01	N.D.	<0.01	13.80
H2- 29	213.65	215.65	2	<0.01	<0.1	<0.01	N.D.	<0.01	15.18
H2- 30	215.65	217.65	2	<0.01	<0.1	0.02	N.D.	<0.01	10.74
H2- 31	217.65	219.65	2	N.D.	<0.1	0.03	N.D.	<0.01	11.81
H2- 32	219.65	221.65	2	<0.01	<0.1	0.03	N.D.	<0.01	11.66
H2- 33	221.65	223.65	2	<0.01	<0.1	0.05	N.D.	<0.01	10.74
H2- 34	223.65	225.20	1.55	<0.01	<0.1	0.21	N.D.	<0.01	12.43

Mineral Laboratory, Directorate of Minerals, Ministry of Commerce & Industry, Oman

AVERAGE	Length(m)	Cu(%)	Zn(%)
	68	0.03	0.01

MJOB-S1

Sample No.	Depth(m)		Length (m)	Au(g/t)	Ag(g/t)	Cu(%)	Pb(ppm)	Zn(%)	Fe2O3 (%)
	From	To							
S1- 1	108.50	110.50	2	<0.01	<0.1	0.02	<10	0.06	12.75
S1- 2	110.50	112.50	2	<0.01	0.1	0.01	<10	0.02	9.02
S1- 3	112.50	114.60	2.1	<0.01	<0.1	0.02	<10	0.02	9.95
S1- 4	123.70	125.70	2	<0.01	0.1	<0.01	<10	0.01	10.26
S1- 5	125.70	127.70	2	<0.01	<0.1	<0.01	<10	0.01	8.40
S1- 6	127.70	129.70	2	<0.01	<0.1	0.01	<10	<0.01	8.40
S1- 7	129.70	131.70	2	<0.01	<0.1	<0.01	<10	0.01	8.55
S1- 8	131.70	133.70	2	<0.01	<0.1	<0.01	<10	0.01	12.28
S1- 9	133.70	135.70	2	<0.01	0.2	0.04	<10	<0.01	13.22
S1- 10	135.70	138.10	2.4	0.01	<0.1	<0.01	<10	<0.01	11.66

Mineral Laboratory, Directorate of Minerals, Ministry of Commerce & Industry, Oman

AVERAGE	Length(m)	Cu(%)	Zn(%)
	20.50	0.01	0.02

MJOB-S2

Sample No.	Depth(m)		Length (m)	Au(g/t)	Ag(g/t)	Cu(%)	Pb(ppm)	Zn(%)	Fe2O3 (%)
	From	To							
S2- 1	238.55	240.55	2	<0.01	<0.1	0.02	<10	0.02	10.88
S2- 2	240.55	242.55	2	<0.01	<0.1	<0.01	<10	0.02	10.88
S2- 3	242.55	244.50	1.95	<0.01	<0.1	<0.01	<10	<0.01	6.53
S2- 4	246.90	248.90	2	<0.01	<0.1	<0.01	<10	<0.01	8.08
S2- 5	248.90	250.90	2	<0.01	<0.1	<0.01	<10	<0.01	8.40
S2- 6	250.90	252.00	1.1	0.01	<0.1	<0.01	<10	<0.01	11.66

Mineral Laboratory, Directorate of Minerals, Ministry of Commerce & Industry, Oman

AVERAGE	Length(m)	Cu(%)	Zn(%)
	11.05	0.01	0.01

Appendix 5

Assay results of surface samples

Ser. No.	Area Name	Sample No.	Coordinate		Au(g/t)	Ag(g/t)	Cu(%)	Pb(ppm)	Zn(%)	Fe2O3 (%)
			N(km)	E(km)						
1	Ghuzayn	GW-100	2636.12	495.64	<0.01	<0.1	0.86	25	0.30	7.40
2	Ghuzayn	GW-101	2636.12	495.64	<0.01	N.D.	0.31	16	0.46	9.30
3	Ghuzayn	GW-102	2636.12	495.64	<0.01	N.D.	0.14	14	0.18	7.70
4	Ghuzayn	GW-103	2636.12	495.64	<0.01	0.2	3.02	16	0.02	6.50
5	Sarami	SM-4	2650.75	478.88	<0.01	<0.1	0.57	19	<0.01	24.40
6	Sarami	SM-5	2650.14	478.64	0.01	<0.1	0.76	18	<0.01	50.00
7	Sarami	SM-6	2650.43	479.10	<0.01	<0.1	0.21	35	0.01	45.20
8	Sarami	SM-7	2648.86	481.36	<0.01	<0.1	2.11	21	0.02	12.70
9	Sarami	SM-8	2649.06	480.94	0.42	0.2	0.04	19	<0.01	19.60
10	Sarami	SM-9	2649.00	481.14	0.06	<0.1	1.54	39	<0.01	15.60
11	Sarami	SM-10	2650.66	478.62	0.05	<0.1	0.06	21	0.02	13.90
12	Sarami	SM-11	2650.66	478.62	0.07	<0.1	0.07	36	0.01	16.20
13	Mahab	MB-28	2658.60	468.45	<0.01	0.2	<0.01	<10	<0.01	21.46
14	Mahab	MB-29	2658.60	468.45	<0.01	<0.1	<0.01	<10	0.01	26.12
15	Mahab	MB-30	2658.60	468.45	<0.01	0.3	0.05	<10	0.02	61.88
16	Mahab	MB-31	2658.45	467.89	<0.01	0.3	<0.01	<10	<0.01	18.35
17	Maqail	MQ-13	2662.40	453.75	<0.01	1.4	1.12	<10	<0.01	7.21
18	Zuha	ZU-1	2675.97	452.16	<0.01	<0.1	0.58	<10	0.01	57.68
19	Zuha	ZU-2	2675.97	452.16	0.01	0.3	0.04	<10	<0.01	36.54
20	Zuha	ZU-3	2676.38	452.09	0.10	0.2	<0.01	<10	<0.01	18.66
21	Zuha	ZU-4	2679.16	452.20	<0.01	0.1	<0.01	<10	<0.01	19.60
22	Zuha	ZU-5	2679.42	452.55	<0.01	<0.1	<0.01	<10	<0.01	14.93
23	Zuha	ZU-6	2679.44	452.55	<0.01	<0.1	0.02	<10	0.01	21.61

Mineral Laboratory, Directorate of Minerals, Ministry of Commerce & Industry, Oman

Appendix 6

Description and photographs of polished sections of ore

Sample collected from drill cores: G35-131.00	
Ore type	Massive sulphide ore
Microscopic Observation	The ore consists of two parts of characteristic features. One part consists of fairly compact aggregates of pyrite grains, the grain size of which is larger than 200μm, although the aggregates are somehow porous and include quartz and a small amount of chalcopyrite. Some larger pyrite grains are moderately shattered. The other part consists of a matrix that fills the interstices of the compact pyrite masses. The matrix comprises fine-grained pyrite and a small amount of chalcopyrite in quartz basis. Pyrite grains in the matrix are subhedral or anhedral, and some parts have a feature of crystallized colloform textures. The size of individual grains ranges from 5μm to 500μm

Sample collected from drill cores: G36-179.80	
Ore type	Massive sulphide ore
Microscopic Observation	Although the general feature of ore texture is similar to those of the other G36 samples, wheel-like, skeleton-like or fine porous texture composed of minute pyrite grains in quartz is characteristic (Photo 1). The wheel-like texture consists of wheel tire, axle and several spokes with cavities among them. These textures are suggestive of the crystallization of colloidal iron sulphides. Chalcopyrite fills the interstices of pyrite and quartz grains. Small chalcopyrite and sphalerite inclusions are recognized in large pyrite crystals.

Sample collected from drill cores: G36-186.70	
Ore type	Massive sulphide ore
Microscopic Observation	Large anhedral pyrite grains, the size of which ranges from 1 to 2mm, distribute sporadically in the matrix consisting of small grains of pyrite, chalcopyrite and quartz. Pyrite grains in the matrix are subhedral or anhedral grains of the size 30-150μm, and irregular aggregates of minute pyrite grains of the size 2-10μm of colloform texture. Irregular patches of chalcopyrite fill the interstices of pyrite and quartz grains. Large pyrite grains have small cavities and the walls of these cavities and grain boundaries are lined with sharp crystal faces, suggesting that these large grains have been formed by the coalescence of smaller grains. Many small pyrite globules comprise minute subhedral or anhedral grains with cavities in the center. Chalcopyrite distributes sporadically in the interstices of pyrite and quartz grains.

Sample collected from drill cores: G36-193.60	
Ore type	Massive sulphide ore
Microscopic Observation	Pyrite occurs in some parts as euhedral grains of the size 100-500μm. Chalcopyrite fills the interstices of the euhedral pyrite grains (Photo 2). Some large anhedral pyrite grains are moderately fractured. Globular or irregular aggregates of minute pyrite grains occur in quartz basis. The texture is suggestive of the original colloform texture.

Sample collected from drill cores: G36-214.25	
Ore type	Massive sulphide ore
Microscopic Observation	Several euhedral or subhedral grains are healed to form large porous aggregates. The cavities are lined by crystal faces of pyrite. Some cavities are filled with chalcopyrite. The matrices of large aggregates consist of irregular aggregates of minute pyrite grains, ring-like arrangements of round pyrite grains, small patches of chalcopyrite and quartz basis (Photo 3). The textures suggest the original colloform textures.

Sample collected from drill cores: G36-227.80	
Ore type	Massive sulphide ore
Microscopic Observation	Small subhedral or anhedral pyrite crystals and small globular aggregates composed of minute pyrite grains predominate in quartz basis, although some large pyrite grains occur in some places. Large pyrite crystals are partly brecciated weakly and filled with quartz. Various shapes of aggregates of fine pyrite grains such as globular aggregates with small cavities, irregular mesh-like aggregates or ring-structured aggregates are suggestive of the colloidal origin. Chalcopyrite occurs sporadically in quartz and interstices of pyrite grains.

Sample collected from drill cores: G36-230.60	
Ore type	Massive sulphide ore
Microscopic Observation	Pyrite grains larger than 50μm are generally euhedral or subhedral, but those finer than 20μm are mostly anhedral. Pyrite grains of both categories distribute uniformly in quartz basis. Chalcopyrite fills irregularly the interstices of pyrite and quartz grains (Photo 4). Fine mixture of pyrite, chalcopyrite and quartz suggest the crystallization of the former colloidal deposits of iron sulphides. Ring arrangement of small subhedral pyrite grains surrounding the inner fine mixtures of pyrite and chalcopyrite, is also suggestive of the original colloform texture.

Sample collected from drill cores: G36-256.30	
Ore type	Massive sulphide ore
Microscopic Observation	Large sulphide aggregates comprise euhedral, subhedral or anhedral pyrite grains, cavities and quartz grains of various sizes. In some parts, the texture consisting of small pyrite grains and cavities are much finer than the other parts. In these fine textured parts, globular aggregates of minute pyrite grains with cavities in the center exist suggesting the original colloidal textures. Chalcopyrite occupies fairly large areas among large pyrite aggregates, while in fine-textured parts it fills only small cavities. Large patches of chalcopyrite are slightly fractured, and small lenticular voids develop along the cracks (Photo 5). Some parts are very porous and rich in small globular pyrite aggregates, suggesting the relict of colloform textures. A few minute inclusions of chalcopyrite and sphalerite, the size of which is 2-20μm, occur in large pyrite grains.

Sample collected from drill cores: G36-257.50	
Ore type	Massive sulphide ore
Microscopic Observation	Some amount of chalcopyrite and sphalerite occur in large pyrite grains, as minute inclusions of the size 2-25μm. Besides of these large pyrite grains, subhedral or anhedral small pyrite grains, globular aggregates of minute pyrite grains and mesh-like aggregates of pyrite and chalcopyrite distributed uniformly in quartz basis. Chalcopyrite replaces pyrite forming irregular patches in pyrite aggregates.

Sample collected from drill cores: H1-167.60	
Ore type	Pyrite-chalcopyrite-quartz vein
Microscopic Observation	Subhedral or anhedral pyrite crystals of coarse grain (300-1000μm) predominate followed by sporadically distributed small anhedral pyrite grains of the size 20-100μm. Some large pyrite crystals are quite clear, while some grains include small cavities. Some grains, especially those between large crystals are partly shattered (Photo 6). Chalcopyrite and quartz fill the interstices of pyrite grains. Rounded pyrite relicts are recognized in chalcopyrite. Inclusions in sulphide minerals are generally rare, although some small cavities are filled with chalcopyrite.

Sample collected from drill cores: H1-179.40	
Ore type	Disseminated sulphide ore
Microscopic Observation	Large subhedral or anhedral pyrite crystals of a size larger than 1mm, occur with rounded small pyrite grains of the size 20-150μm, which disseminate uniformly in gangue basis. Some pyrite grains are brecciated at the contact with larger pyrite grains. Chalcopyrite and sphalerite occur intimately associated each other (Photo 7). Chalcopyrite is mostly located in the center or inner parts of grain (Photo 8). In some parts, chalcopyrite is more porous than sphalerite. Chalcopyrite and sphalerite also occur in pyrite as fine inclusions.

Sample collected from drill cores: H2-146.30	
Ore type	Strongly disseminated sulphide ore
Microscopic Observation	Porous pyrite aggregates, the size of which ranges from 200μm to 2mm, distribute uniformly in gangue, with small pyrite crystals (50-150μm), fine pyrite globules (10-30μm) and chalcopyrite patches (10-500μm) (Photo 9). Some fine porous grains are suggestive of the original colloidal deposition of iron sulphides. Some pyrite grains between larger pyrite crystals are brecciated. A small amount of sphalerite and chalcopyrite inclusions are observed in large pyrite crystals.

Sample collected from drill cores: H2-223.70	
Ore type	Weakly disseminated sulphide ore
Microscopic Observation	Subhedral pyrite crystals, the size of which is 10-600μm, occur in an altered rock with chalcopyrite patches. Large subhedral crystals are porous in the center and include some pieces of gangue minerals. Chalcopyrite patches also include many gangue inclusions and accompany some amounts of sphalerite as small inclusions.

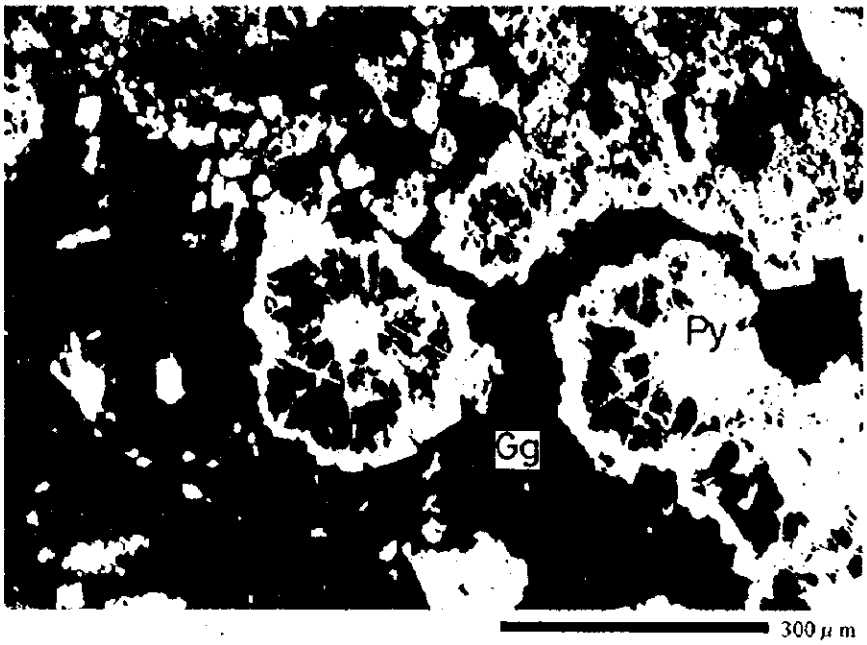

Photo. 1

Bore hole no.: G36
Depth: 179.80m

Massive sulphide ore

Py: Pyrite
Gg: Gangue mineral

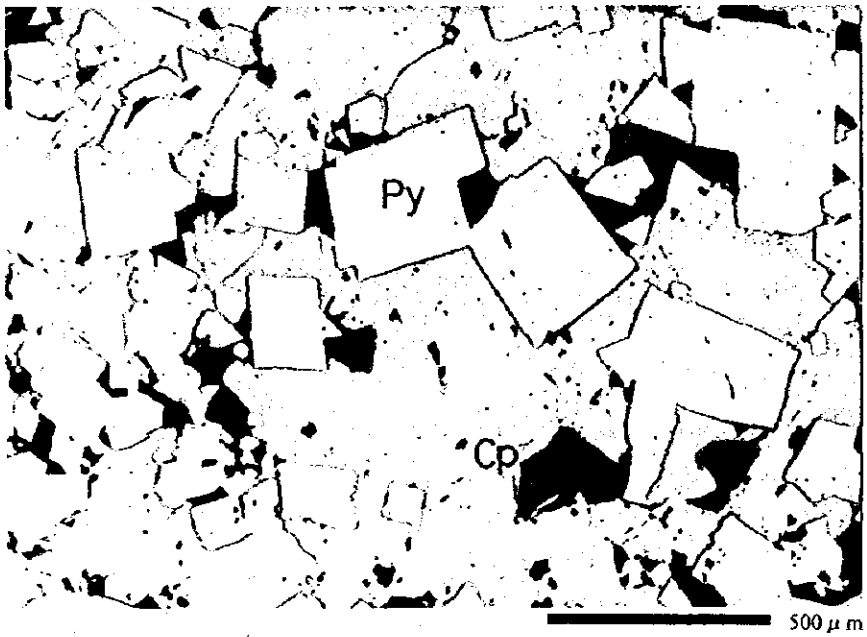

Photo. 2

Bore hole no.: G36
Depth: 193.60m

Massive sulphide ore

Py: Pyrite
Cp: Chalcopyrite

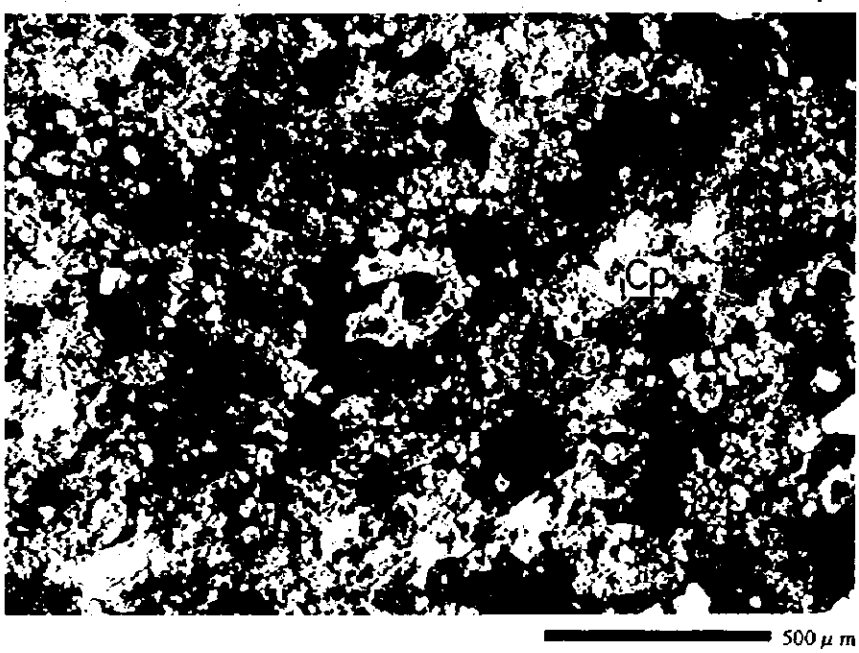

Photo. 3

Bore hole no.: G36
Depth: 214.25m

Massive sulphide ore

Cp: Chalcopyrite

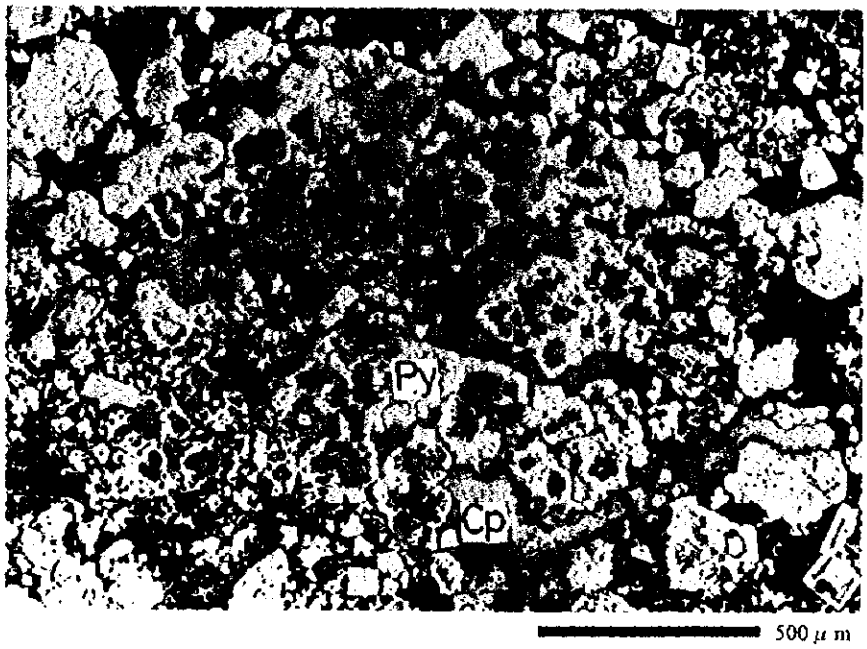

Photo. 4

Bore hole no.: G36
Depth: 230.60m

Massive sulphide ore

Py: Pyrite
Cp: Chalcopyrite

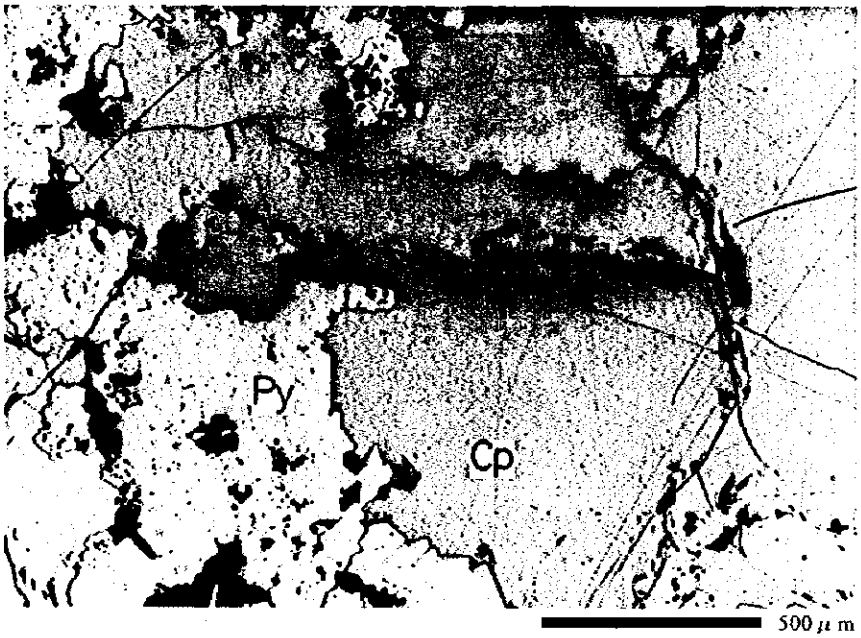

Photo. 5

Bore hole no.: G37
Depth: 256.30m

Massive sulphide ore

Py: Pyrite
Cp: Chalcopyrite

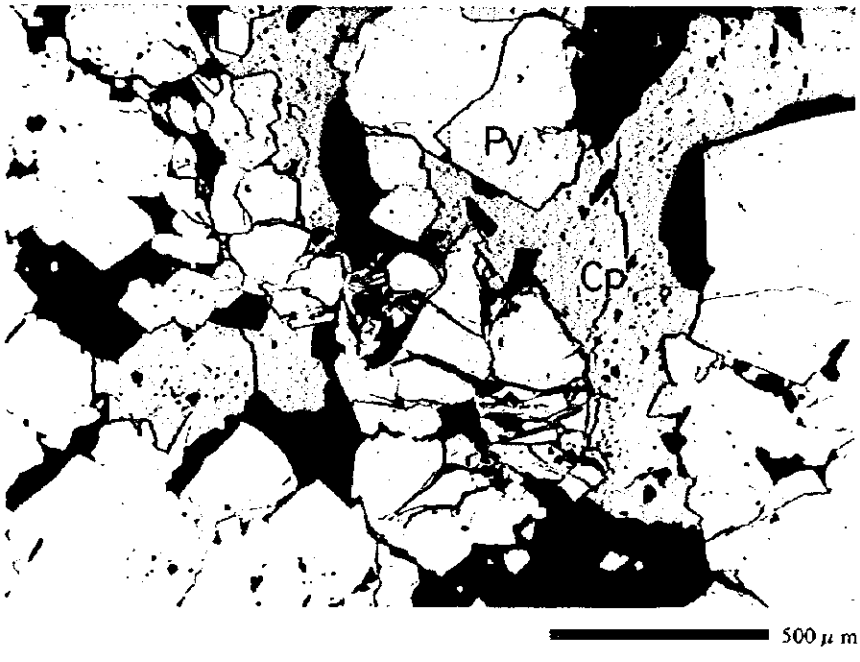

Photo.6

Bore hole no.: H1
Depth: 167.60m

Pyrite-Chalcopyrite
-quartz vein

Py: Pyrite
Cp: Chalcopyrite

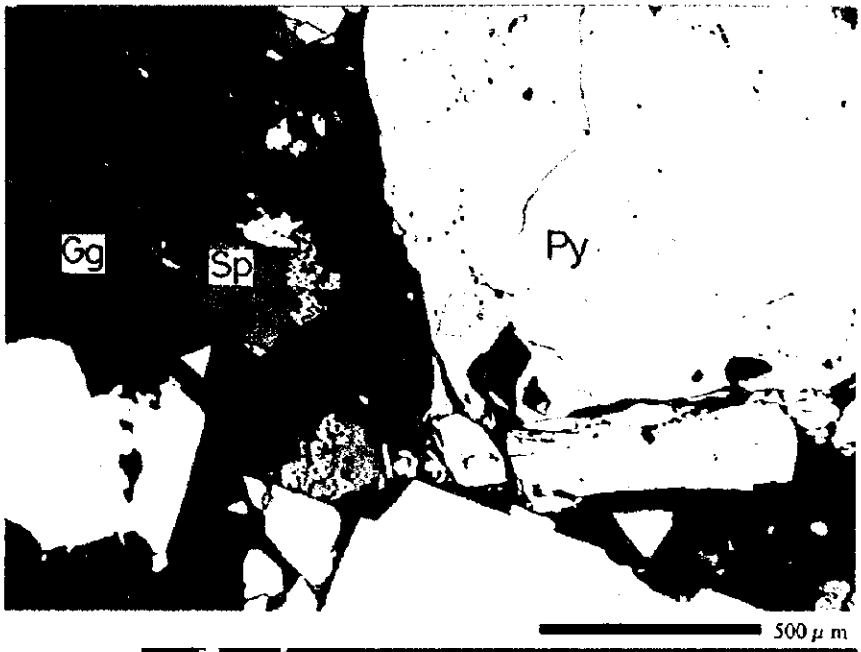

Photo.7
Bore hole no.: H1
Depth: 179.40m

Disseminated sulphide ore

Py: Pyrite
Sp: Sphalerite
Gg:Gangue minaral

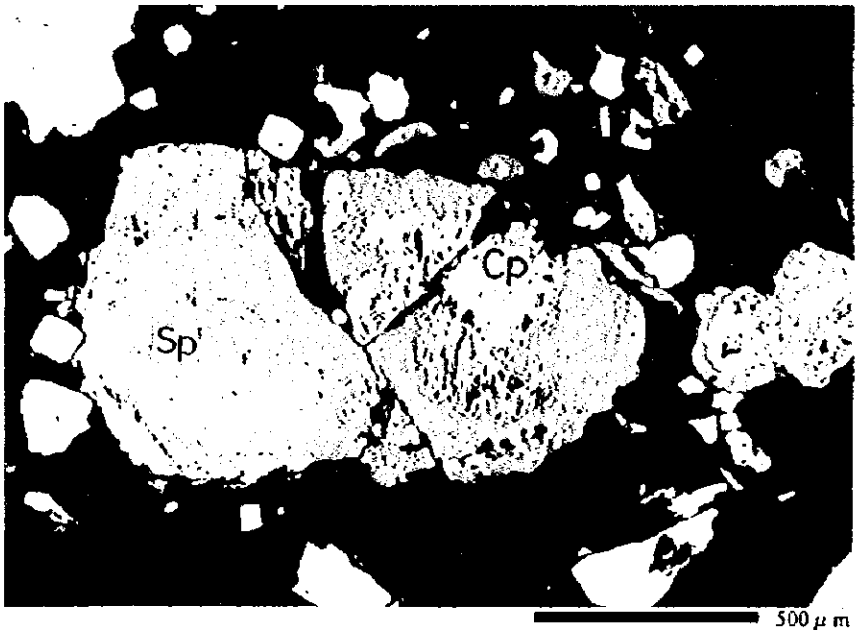

Photo.8
Bore hole no.: H1
Depth: 179.40m

Desseminated sulphide ore

Cp: Chalcopyrite
Sp: Sphalerite

Photo.9
Bore hole no.: H2
Depth: 146.30m

Disseminated sulphide ore

Py: Pyrite
Cp: Chalcopyrite

Appendix 7

IP Tomography survey results

IP Tomography in Ghuzayn Area

1 Objective of the survey

IP tomography survey, considered to be an effective technique for sulphide ore detection, was carried out in order to delineate the extension and shape of the ore bodies which were discovered in the South Batinah Coast area in Oman during 1996 and 1997.

2 Location of the survey

The survey was carried out over the ore bodies Nos. 2 and 3 discovered in Ghuzayn area during 1996 and 1997, respectively (Fig. 1).

As shown in Fig.2, two survey lines were set up over ore body No.3. One survey line has a length of 600m on the surface and set up along two boreholes in E-W direction, while the other line has a length of 400m on the surface and deployed along two boreholes in the N-S direction.

As indicated in Fig.3, one survey line of 400m in length on the surface was deployed over ore body No.2, along the boreholes MJOB-G5 and MJOB-G20 in the N-S direction.

3 Method of the survey

3-1 Measurement method

The Metal Mining Agency of Japan developed the IP tomography system employed in this survey and shown in the block diagram of Fig.4. This system adopts time-domain measurement and pole-dipole array. The remote current electrode was set on the wadi at about 2.5km to the north of ore body No.3 ore body, where 45 stainless electrodes of 30cm in length and 1cm in diameter were used.

Contact resistance resulted very large, because the survey area, especially in wadi, was covered with gravel. To decrease the contact resistance, two non-polarizable lead-lead chloride electrodes were saturated with water for a night within a large hole of a size of about 50cm containing bentonite. The current signal sent by the transmitter was an alternating rectangular wave with 8-second period. Stacking was 10 times and S/N was very good, however the very low resistivity of the ore body made it difficult to acquire enough potential data when the potential dipole was located near the ore body.

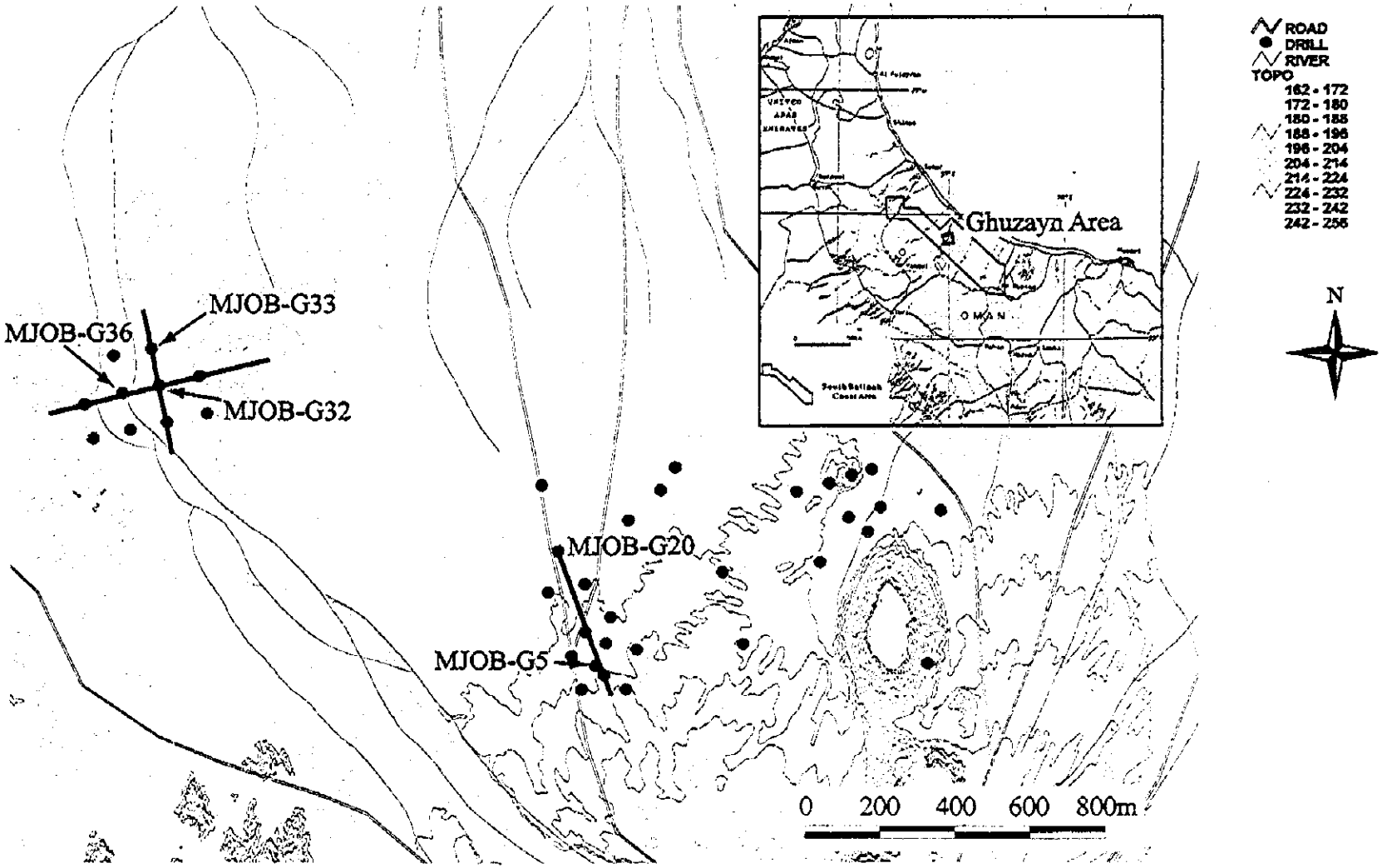

Fig.1 Location map of the IP tomography survey in Ghuzayn area

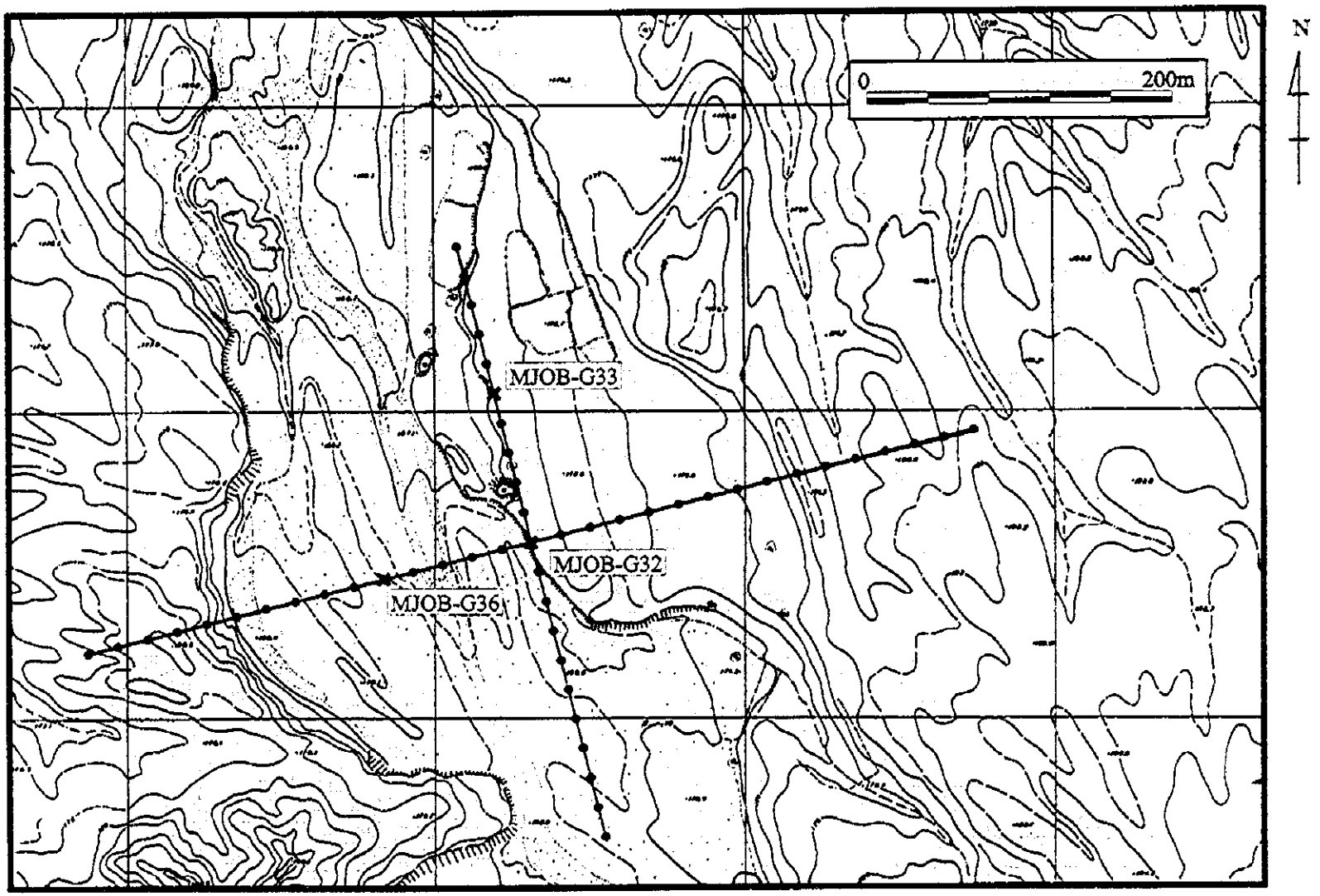

Fig. 2 Plan view of IP tomography survey lines over No.3 ore body, Ghuzayn area
(EW line and NS line)

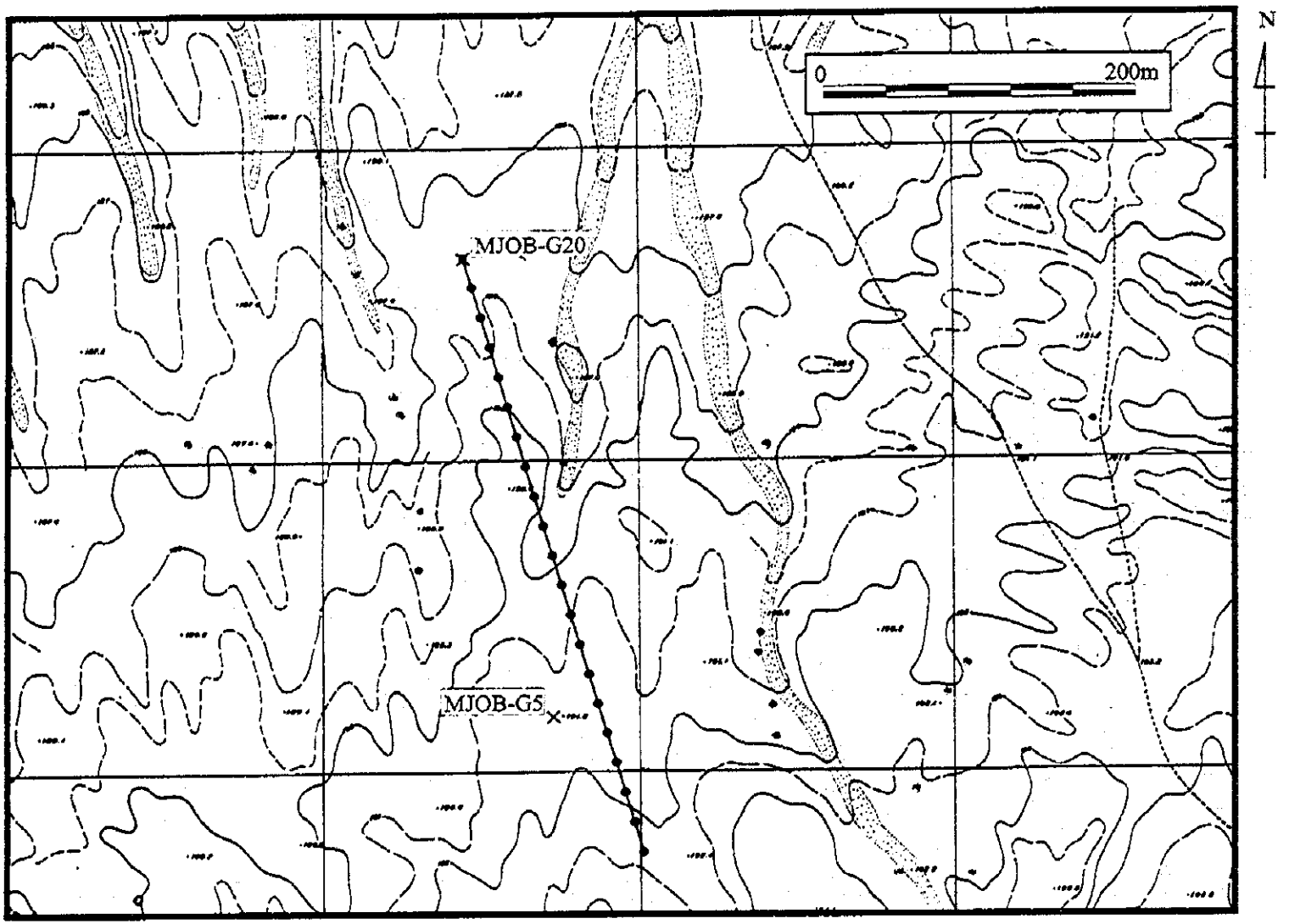

Fig. 3 Plan view of IP tomography survey line over No.2 ore body, Ghuzayn area (NS line)

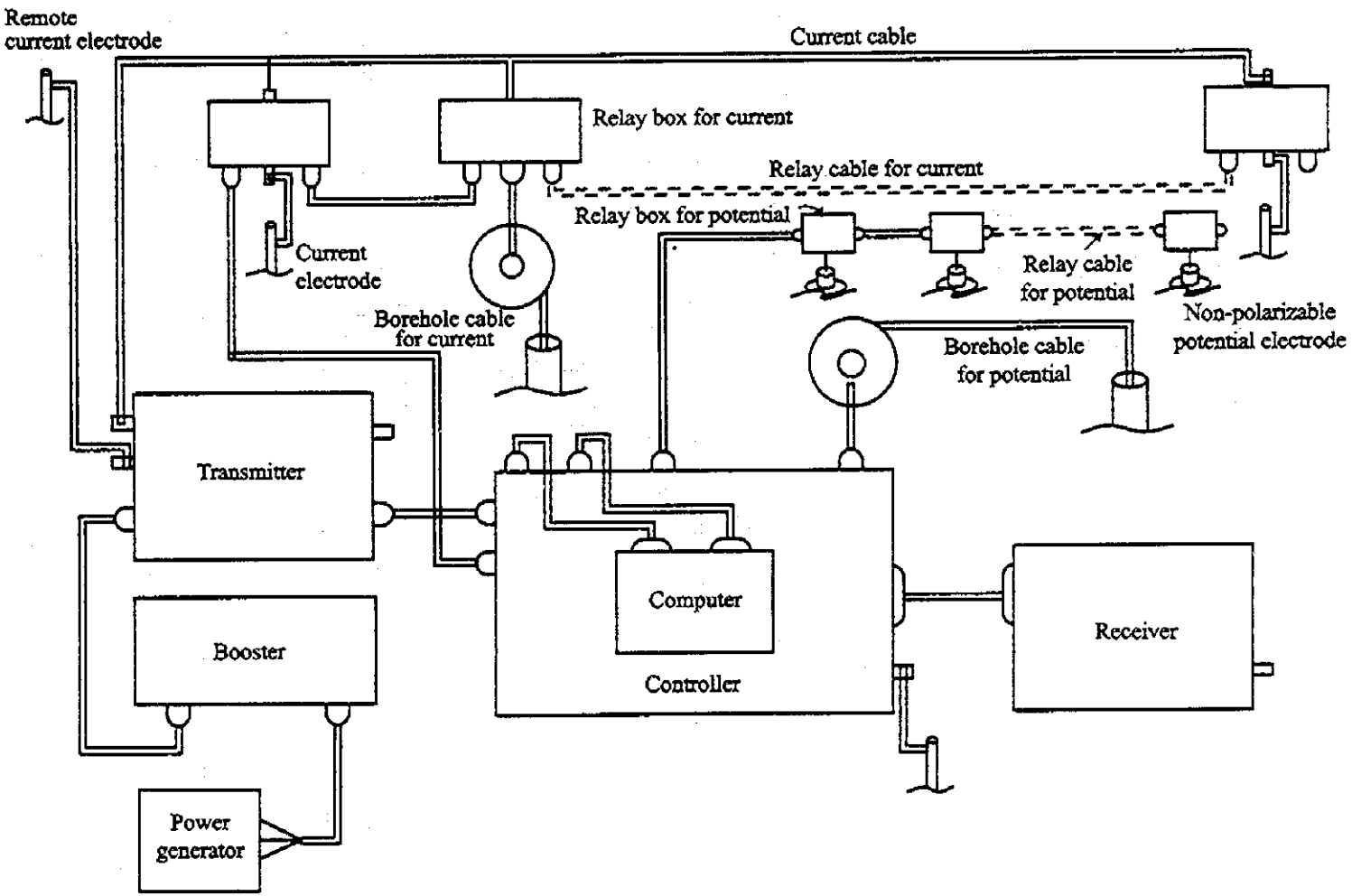

Fig.4 Block diagram of IP tomography system

3-2 Equipment

The outline of IP tomography system is described below.

(1) Transmitter

Output current:	10mA - 10A
Max. output voltage:	800V AC
Max. output power:	4.5kW
Accuracy of output current:	less than 0.1%
Current wave form:	rectangular (duty cycle 50%)
Period:	4, 8, 16, 32, 64, 128s

(2) Receiver

Input range:	3.1μV-10V
Resolution:	3.1μV
Input impedance:	2MΩ
Number of channel:	13
SP backing:	0 - 0.5V (automatic cancel)
Sampling time:	4 ms

4 Analysis

Acquired data was analyzed based on the flow chart shown in Fig. 5. At first, the acquired data underwent through a filtering process for secondary voltage data. Then chargeabilities of every window were calculated and wrong data were deleted. For the calculation of the chargeability, the delay time was set up in order to avoid the effect of EM coupling and the off time after delay time was divided into some windows. The mean value of the chargeabilities of every window was used for the data analysis.

Selected and calculated data were input into the analysis program. The program calculates forward modeling by finite element method (FEM) and inversion by Powell's hybrid method which is one of the non-linear least square methods. The results are visualized as resistivity and chargeability profiles.

The calculation flow is as follows:

(1) Calculation of compensation. This process compensates topography, remote electrode etc.

(2) Generation of initial resistivity model. This process generates initial resistivity model for 2D analysis using alpha-centers method by back projection technique.

(3) 2D resistivity analysis by alpha-centers method. This process calculates 2D resistivity structure by alpha-centers method.

(4) Generation of initial resistivity and chargeability models. This process generates initial resistivity and chargeability models for analysis by FEM. Initial resistivity model is the result of alpha-centers method. Initial chargeability model is selected from 3 models: mean value of apparent chargeability, calculated value by Seigel's equation, and manual value.

(5) Resistivity and chargeability analysis by FEM. This process calculates theoretical resistivity value using FEM and theoretical chargeability value using Seigel's equation. from initial model

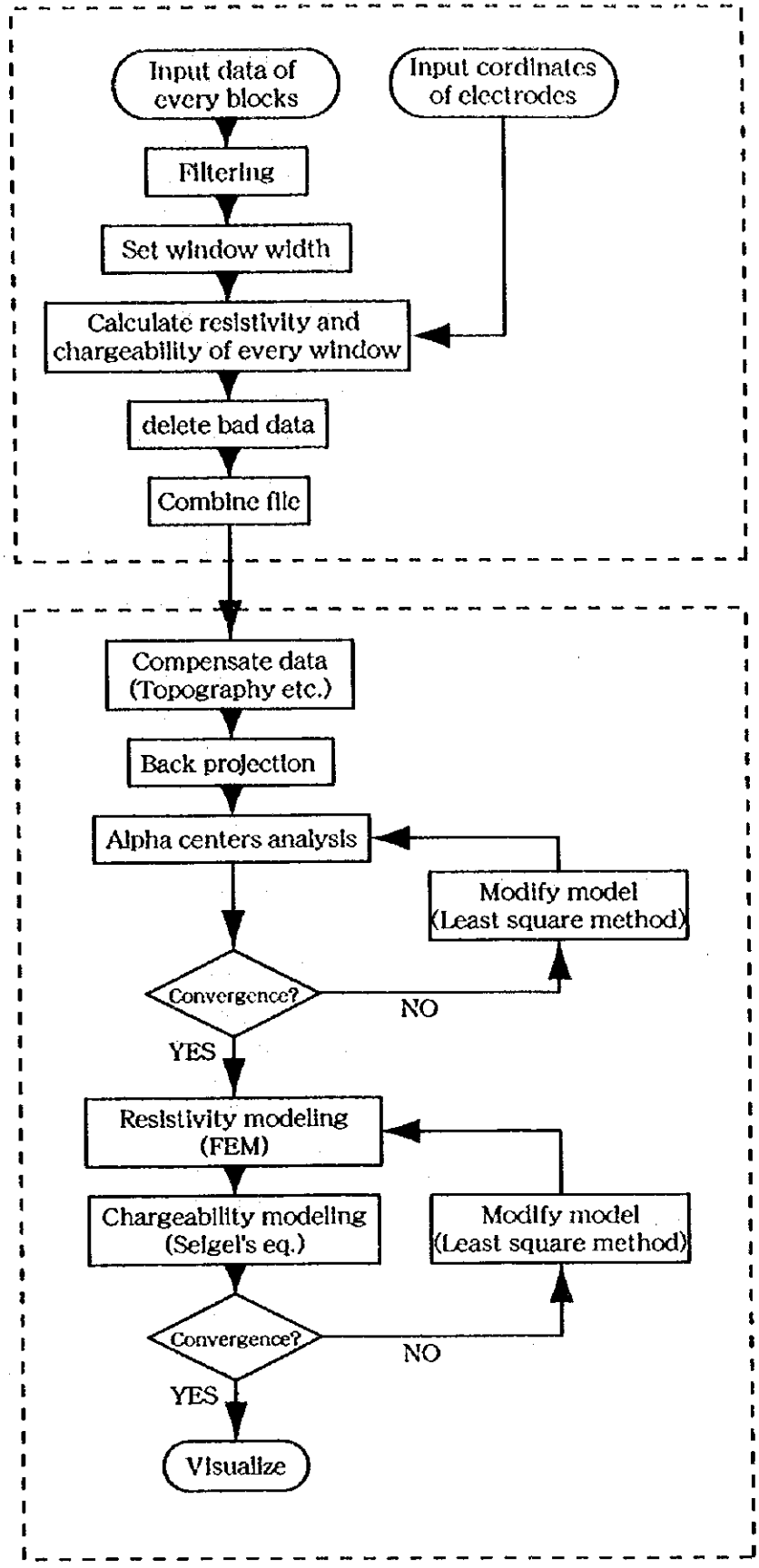

Fig.5 Flow chart of the data analysis

calculated by step (4). Then the resistivity and chargeability model are modified by Powell's hybrid technique until the difference between theoretical value and measured value become small enough.

(6) Visualization the results of resistivity and chargeability. This process visualizes the results of resistivity and chargeability section. This process goes through a filtering process.

Four parameters were important to consider during the analysis by alpha-centers method, i.e., horizontal alpha centers number (x direction), vertical alpha centers number (z direction), number of iterations, and number of rearrangement of alpha centers.

The block size in the analysis process of FEM is important for the accuracy of analysis. It is ideal that the block size be equal to the electrode spacing, but in this program the block size is set to be as twice as electrode spacing because of the limitation of computer memory and calculating time. To keep the accuracy of analysis, the analysis program make calculations by using 4 block patterns: (1) one block shifted upward, (2) one block shifted leftward, (3) one block shifted upward and leftward, and (4) no shifted block. The final result is calculated from the average of these 4 analysis sections.

5 Results of the Survey

5-1 E-W line over ore body No.3

5-1-1 Survey line

This survey line was designed to delineate the extension of the ore body No.3 that was discovered in 1997. Electrodes were deployed in the boreholes MJOB-G32 and MJOB-G36 that penetrated ore body No.3. Boreholes MJOB-G38 and MJOB-G39, that in the same section were not used for the survey because the boreholes were drilled after the survey. On the surface, this line had a length of 600m (maximum line length of this system) in order to delineate adequately the extension of the ore body (Fig. 6). The potential electrode spacing was 20m on the surface and 10m in the boreholes. The current electrode spacing was 40m both on the surface and in the boreholes.

5-1-2 Result of measurement

Almost all the data was good. However, in case of large current-potential spacings efficient data could not be acquired because of small potential differences.

The resistivity of the ore body No. 3 was supposed to be less than 1 Ω-m. Therefore efficient data could not be acquired and S/N ratio became worse when the potential electrode was located near the ore body. Negative apparent resistivity values due to the ore body appeared in some cases, but they were deleted because it was difficult to calculate effectively with the program algorithm.

The center of the line was located in wadi, and for this reason, the contact resistance around the potential electrodes was somewhat high for which the acquired data was not good due to the high S/N.

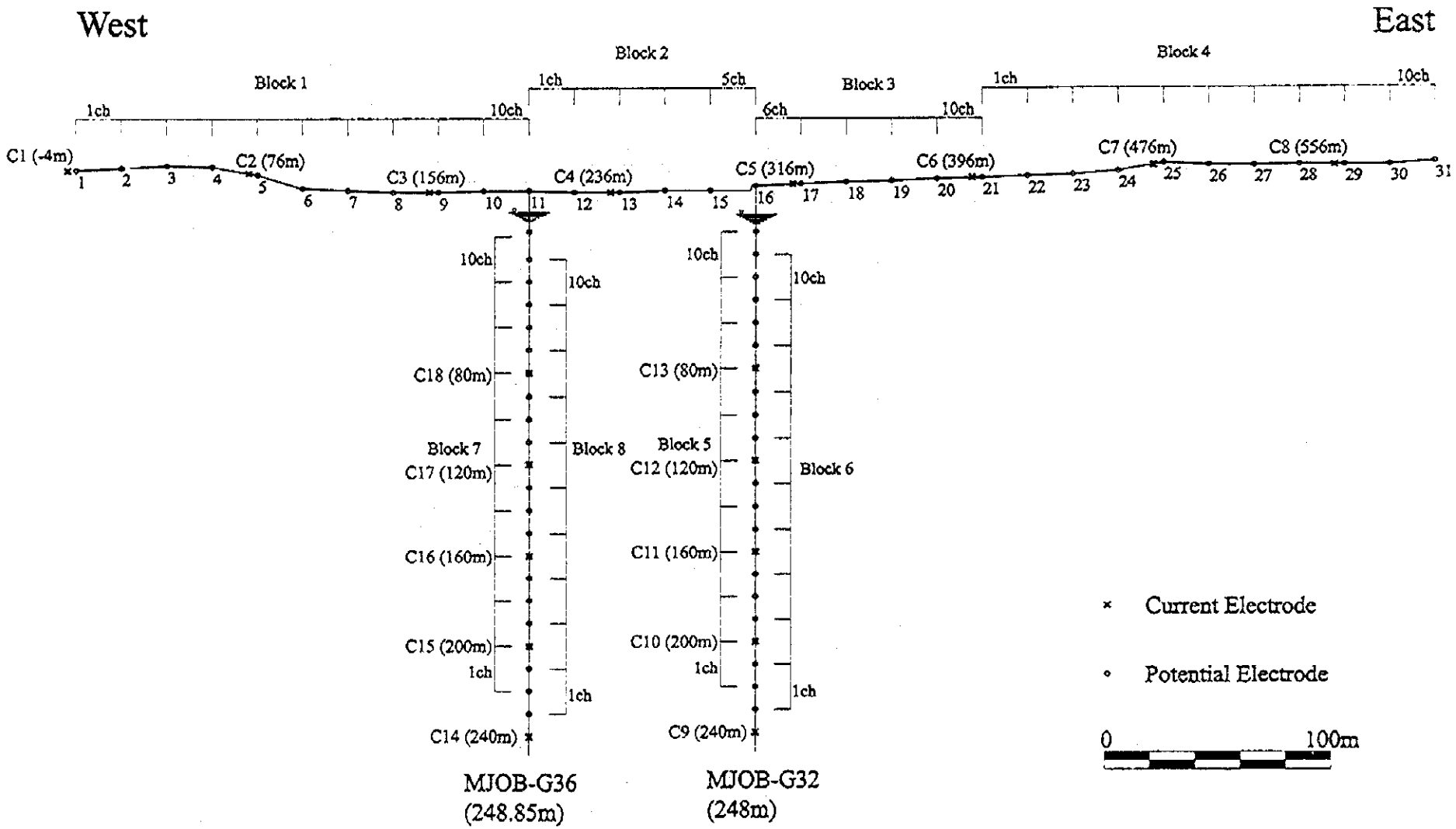

Fig.6 Profile of the IP tomography configuration along No.3 ore body EW line, Ghuzayn area

5-1-3 Results of analysis

The inverted resistivity is shown in Fig.7 (upper part), while the inverted chargeability is shown in Fig.7 (lower part).

The resistivity is analyzed generally low and the maximum resistivity is about 55 ohm-m. Resistivity near the surface is relatively high, especially at the eastern of the survey line. Because the center of the survey line is located within the wadi, groundwater level is assumed to be higher than the eastern side which is outside of the wadi. Low resistivity zone of less than 10 Ω-m are recognized around the bottom of the boreholes MJOB-G32 and MJOB-G36. In MJOB-G32 massive sulphide ore body was intersected at depth between 169.35m (0m level) and 209m (-39m level), and in MJOB-G36 ore body was intersected from 177.65m depth (-8m level) to 231.25m depth (-61m level). This low resistivity zone corresponds to this ore body intersection, but the location is analyzed a little deeper than the ore body location. The resistivity boundary of bedrock and ore body is not clear. The reasons are as follows:

1) In MJOB-G32, pyrite dissemination whose resistivity shows about one tenth of that of the bedrock exists below 70m depth (100m level). Pyrite dissemination affects the results of analysis.

2) The apparent resistivity related to the ore body results negative. These values were deleted during the analysis process, because the algorithm can not deal with negative values.

3) Primary potential data became extremely small around the ore body. These values were also deleted.

Two additional boreholes were carried out along this line after the survey. One hole is MJOB-G39 whose drilling length is 300m and located at 100m west from MJOB-G36. The other hole is MJOB-G38 whose length is 200m and is located at 100m east from MJOB-G32 site. MJOB-G38 did not intersect the ore body, but MJOB-G39 intersected only a thin part of the ore body at 188.05m depth (-18m level). Low resistivity zone appears as massive around the bottom of MJOB-G36, but the resistivity zone from 10 to 20 Ω-m tends to become wide. It is difficult to conclude only from the resistivity profile that the ore body does not extend outside.

In chargeability section, over 90mV/V chargeable zone corresponds to pyrite dissemination, which occurs around 80m depth (90m level) in MJOB-G32 and 120m depth (50m level) in MJOB-G36. Apart from resistivity section, the high chargeability zone looks massive, but the ore body cannot be recognized under pyrite dissemination, because almost every data which related to the ore body were deleted.

Two high chargeability zones occur near the surface. These zones are considered to be false images by interaction between the surface and high chargeability of pyrite dissemination, because raw potential data does not show high chargeability around here and high and low chargeability zones are shown alternately along the surface.

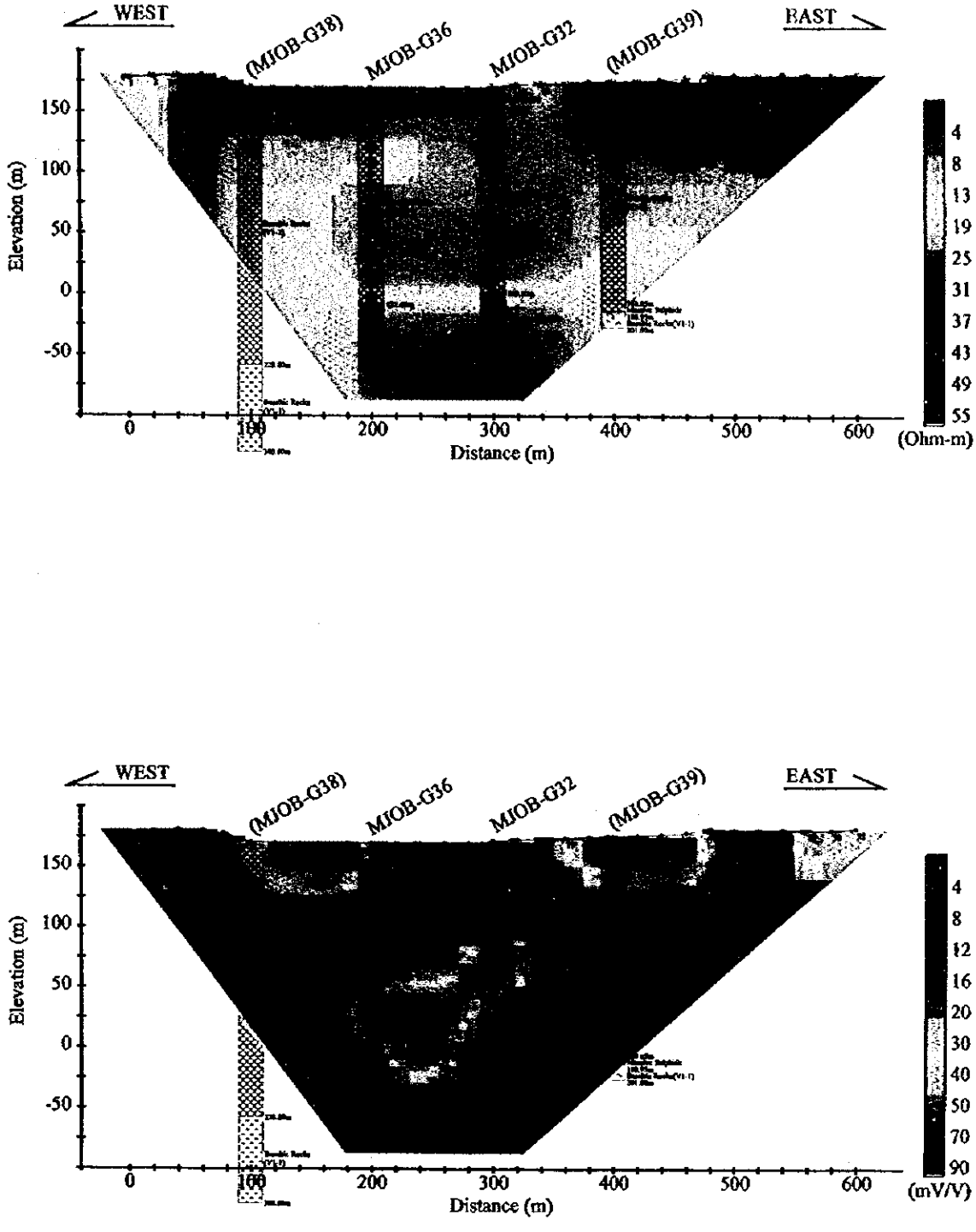

Fig.7 Analyzed resistivity section (upper) and chargeability section (lower) along No.3 ore body EW line, Ghuzayn area

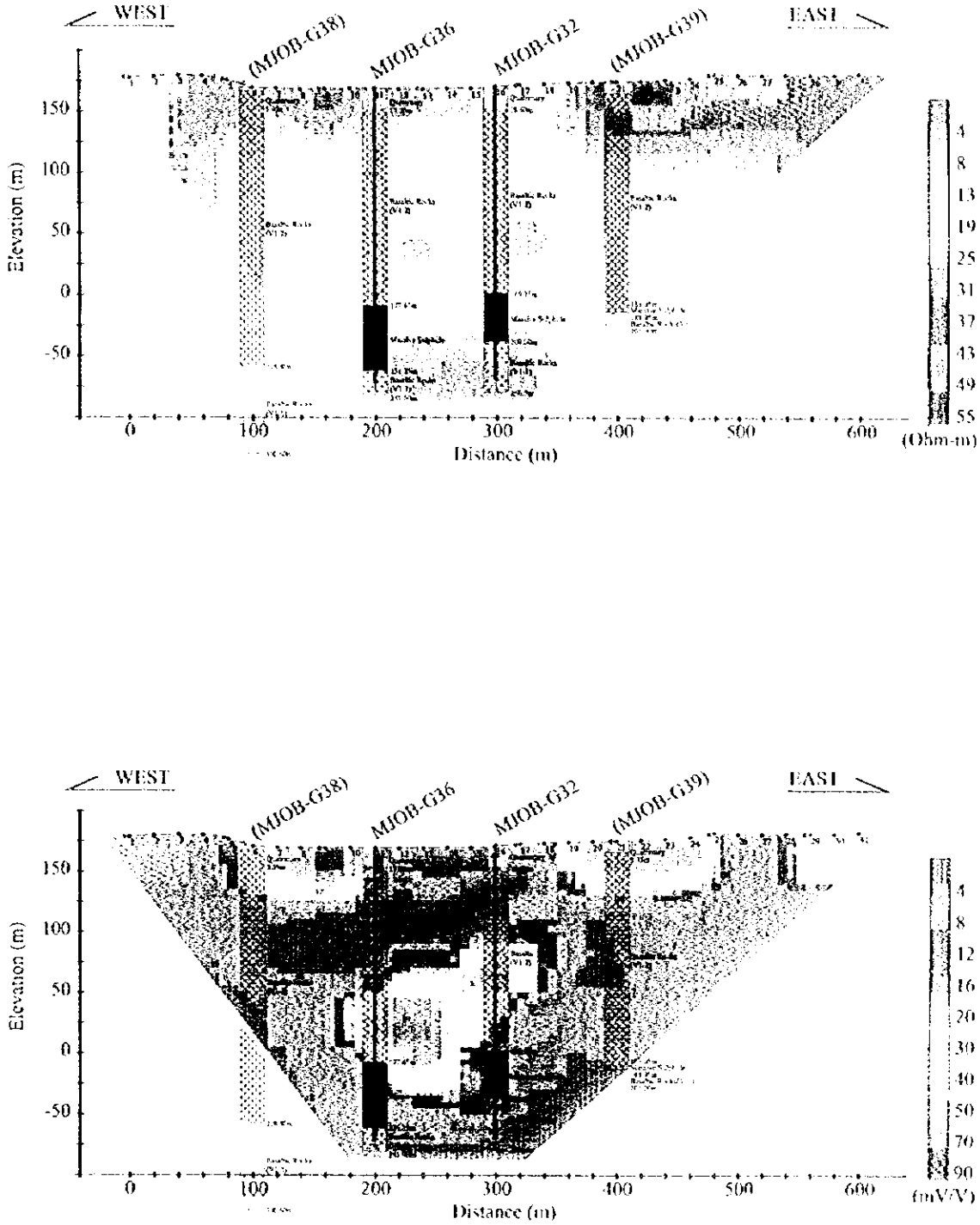

Fig.7 Analyzed resistivity section (upper) and chargeability section (lower) along No.3 ore body EW line, Ghuzayn area

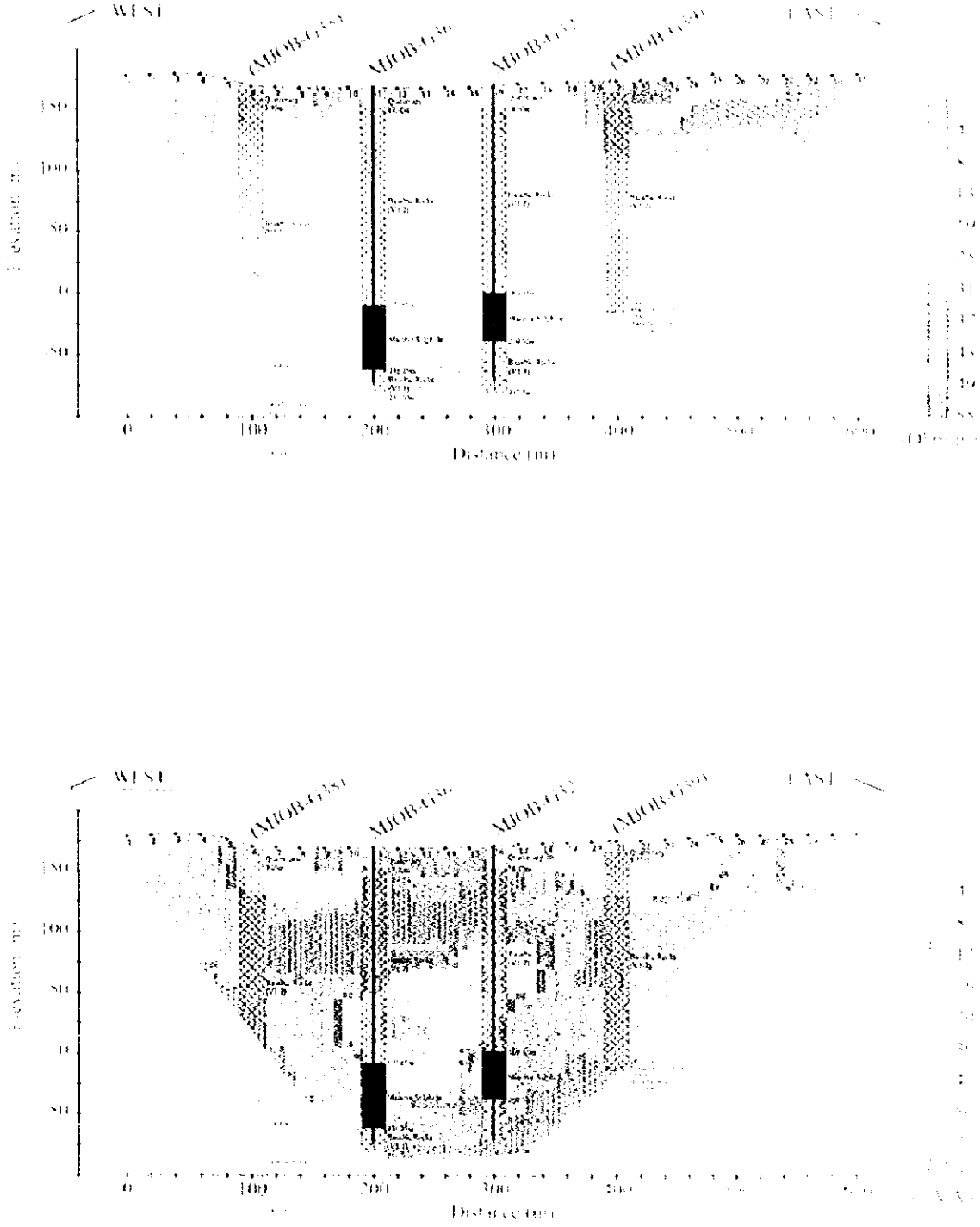

Fig. 7 Analyzed resistivity section (upper) and chargeability section (lower) along No.3 ore body E-W line, Ghuzayn area

5-2 N-S line over ore body No. 3

5-2-1 Survey line

This survey line was designed for delineating the extension of the No.3 ore body which was discovered in 1997. Electrodes were deployed in the boreholes MJOB-G32 and MJOB-G33 that penetrated the ore body No. 3. Surface line was 400m long (Fig. 8). The potential electrode spacing was 20m on the surface and 10m in the boreholes. The current electrode spacing was 80m both on the surface and in the boreholes.

5-2-2 Result of measurement

Almost every data was good, because distance between current source and potential dipole was shorter than the E-W line. The line measured on the surface was 400m in length and the distance between potential and current electrode was less than 417m. The ore body, however, affected remarkably the data, just as the data taken on the E-W line. When the potential dipole was located near the ore body, the potential difference could not be acquired effectively, and a result, some of the apparent resistivity values became negative depending on the specific potential-current electrode configuration. To overcome this problem during analysis, negative apparent resistivity values were replaced with 0.0001 Ω·m in order to add the information of low resistivity environment to the data.

5-2-3 Results of analysis

The inverted resistivity is shown in Fig.9 (upper part) and the inverted chargeability is shown in Fig.9 (lower part).

In resistivity section, relatively resistive zone of about 80Ω·m is shown around southernmost surface line and low resistivity zone is analyzed around 190m depth (-20m level) in the hole MJOB-G32 and from 200m depth (-30m level) to 240m depth (-70m level) in the hole MJOB-G33. Low resistivity zone at the bottom of the boreholes corresponds to the location of the massive sulphide ore body. This low resistivity zone does not extend northward from MJOB-G33 and becomes shallower and wider in the southern side of MJOB-G32. In MJOB-G31 located at 100m south of MJOB-G32, a thick ore body is intersected at shallow depth. But the low resistivity occurs at deeper levels and more southward than the ore body location. The resistivity contrast between bedrock and the ore body is small as well as in the other line. One of the reasons is the influence of pyrite dissemination around the ore body. Another reason is that efficient data could not be acquired due to the fact that S/N ratio decreases because the ore body shows extremely low resistivity.

High resistivity at the southern end of the surface line is considered to be caused by a fault because the resistivity suddenly changes at 320m from northern end of the surface line. Its shape is not clear because of the edge of analyzed area.

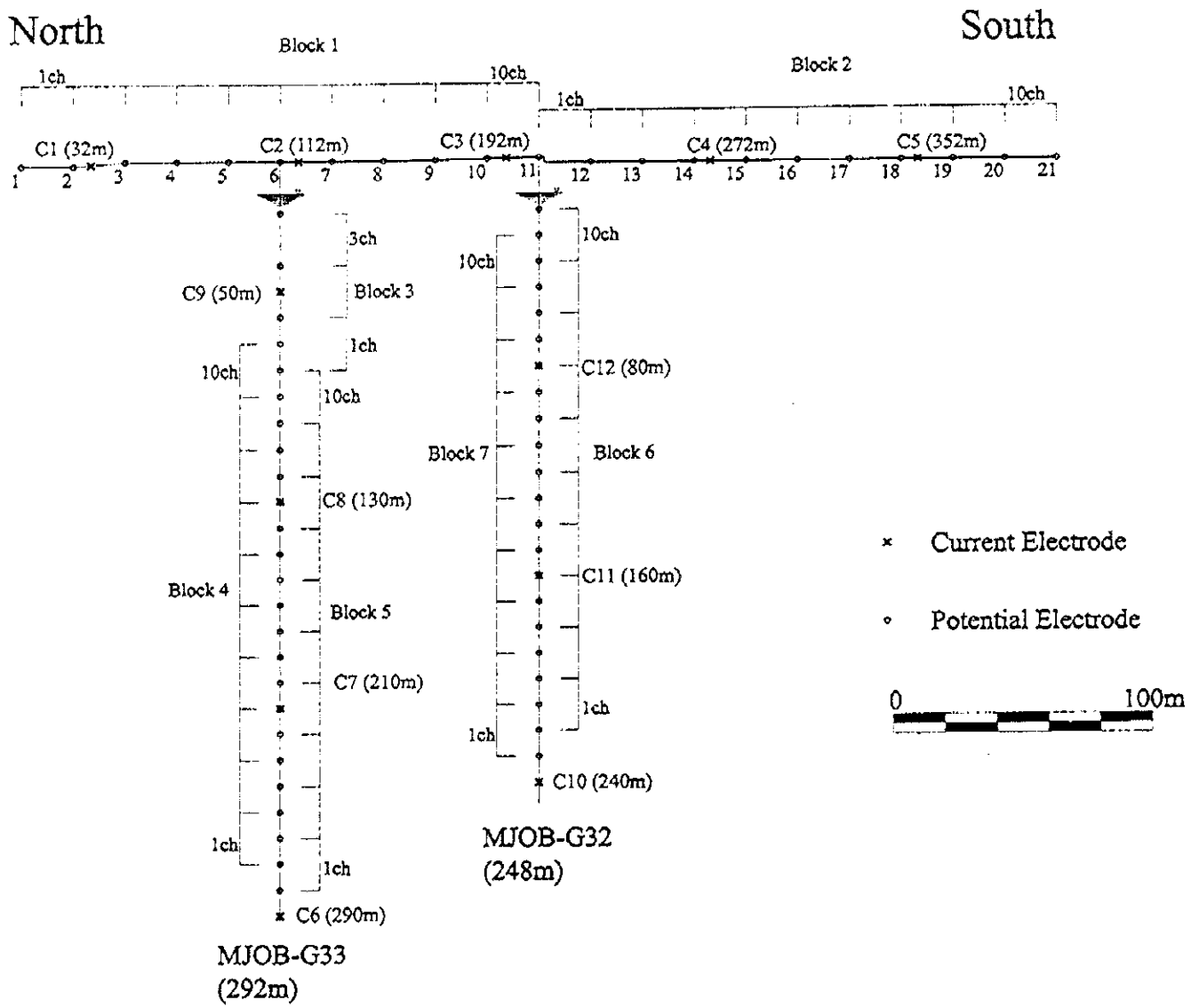

Fig.8 Profile of the IP tomography configuration along No.3 ore body NS line, Ghuzayn area

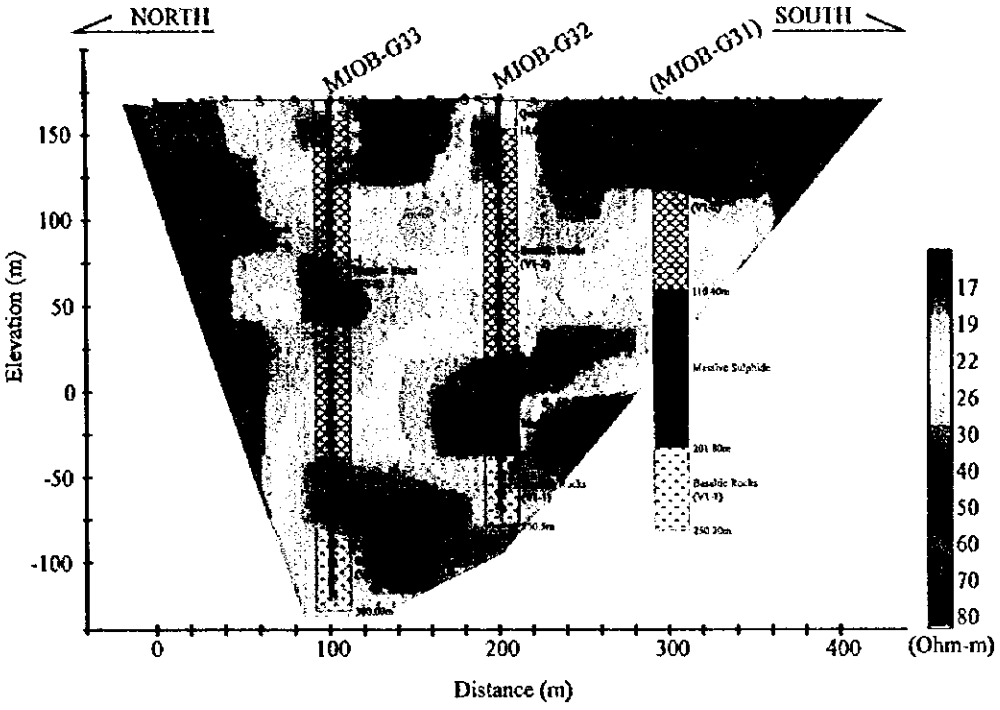

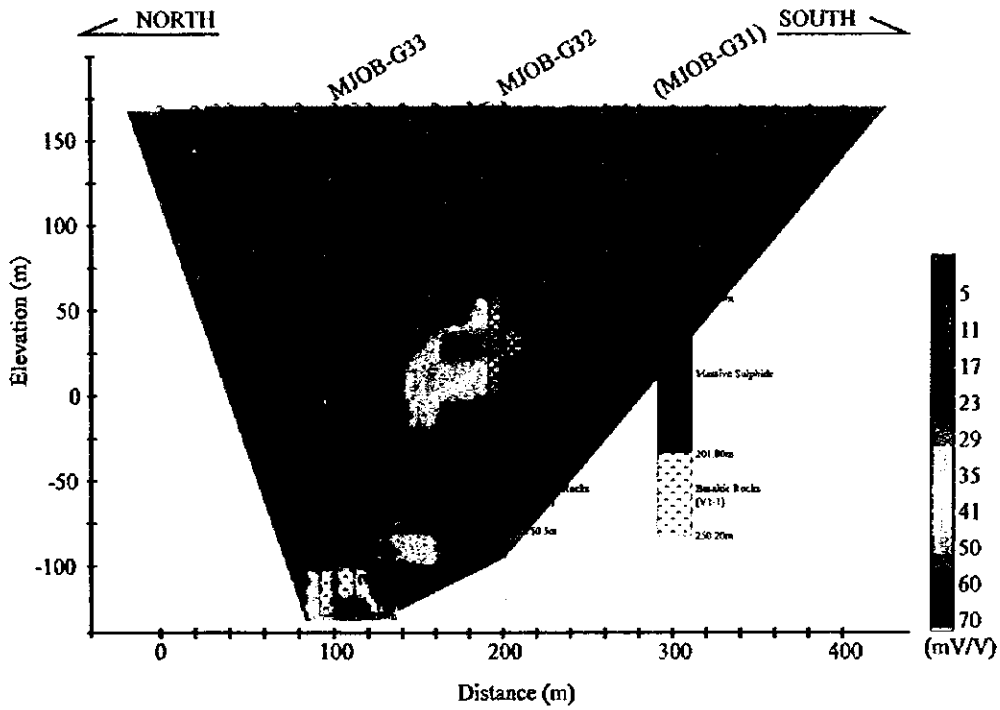

Fig.9 Analyzed resistivity section (upper) and chargeability section (lower) along No.3 ore body NS line, Ghuzayn area

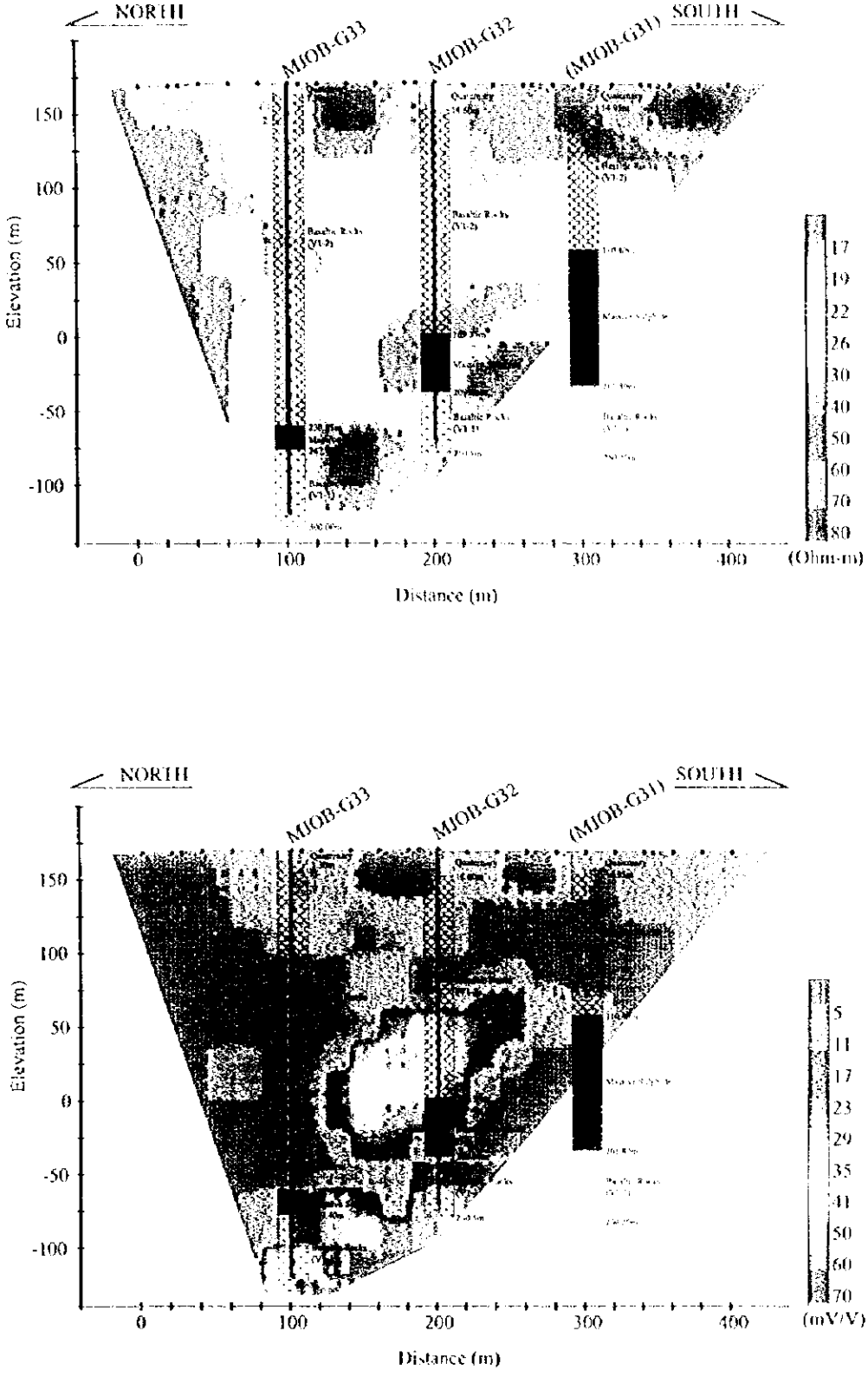

Fig.9 Analyzed resistivity section (upper) and chargeability section (lower) along No.3 ore body NS line, Ghuzayn area

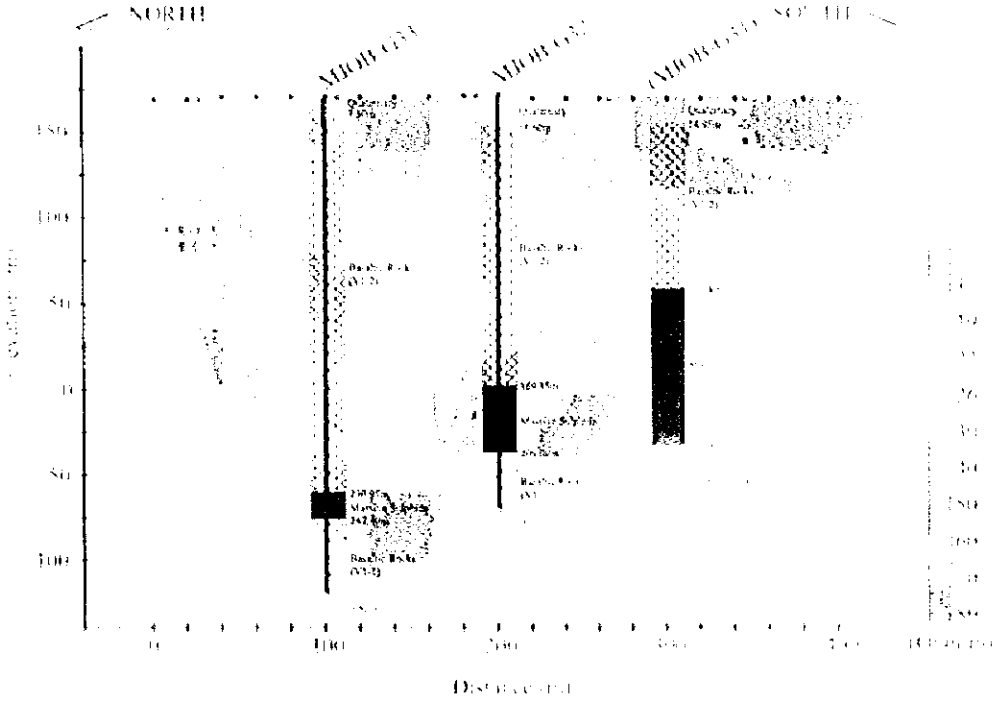

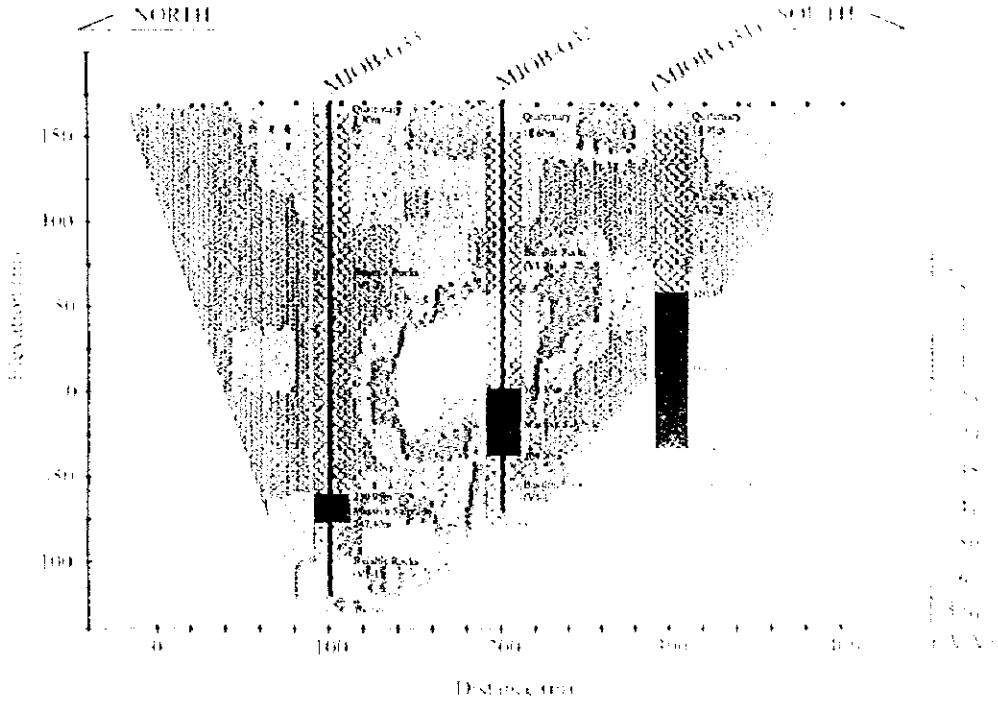

Fig.9 Analyzed resistivity section (upper) and chargeability section (lower) along No.3 ore body NS line, Ghuzayn area

In chargeability section, high chargeability zone of over 30mV/V occurs at the center and bottom of analyzed section. High chargeability zone at the bottom is affected by the ore body because it corresponds to the low resistivity zone. But high chargeability zone at the center of the section is supposed to be affected by pyrite dissemination over above ore body because the resistivity is not so high. Although the ore body was intersected by MJOB-G31 from 110.40m depth (60m level) to 201.80m depth (-32m level), the influence of this ore body is not observed. Actual analyzed area will be smaller than the assumed analysis area due to low resistivity

5-3 N-S line over ore body No.2

5-3-1 Survey line

This survey line was designed for delineating the extension of the ore body No. 2 that was discovered in 1996. Electrodes were deployed in the borehole MJOB-G20 and MJOB-G5 that penetrated ore body No.2. But in MJOB-G20, borehole cable could not be inserted to the depth of intersection of the ore body because this borehole was obstructed at a depth of 190m. Therefore electrodes in MJOB-G20 were deployed down to 180m depth. MJOB-G5 is located about 30m west from the surface line. MJOB-G5 is assumed to be projected onto the section composed of surface line and MJOB-G20 in analysis procedure. As shown in Fig. 10, this line had a surface length of 400m.

5-3-2 Result of measurement

The data was affected by the ore body remarkably as well as other lines. S/N ratio decreases and signal was shaded by the ore body, when the current electrode was located below the ore body and potential dipole on the surface. Some of apparent resistivity values became negative in a certain potential-current electrode configuration.

5-3-3 Results of analysis

The inverted resistivity is shown in Fig.11 (upper part) and the inverted chargeability is shown in Fig.11 (lower part).

In resistivity section, high resistivity is analyzed at the southern side of the surface line and low resistivity at the northern side of the surface line. Resistivity along MJOB-G20 is low. Resistivity tends to become low toward north and at depth. Although the ore body was intersected from 136.90m depth (53m level) to 170.60m depth (19m level) in MJOB-G5, its influence cannot be recognized in the analyzed section. It is impossible to evaluate the continuity of the ore body because the low resistivity cannot be recognized between MJOB-G5 and MJOB-G20. Low resistivity zone is interpreted from 30m depth (160m level) to 40m depth (150m level) in MJOB-G20. Pillow lava in this section shows no alteration because there is no factor that shows low resistivity. High resistivity zone at the southern side of the surface line continues to high resistivity zone over 100 ohm-m which is represented around gossan in the results of the ground IP survey in 1996 and similar high resistivity

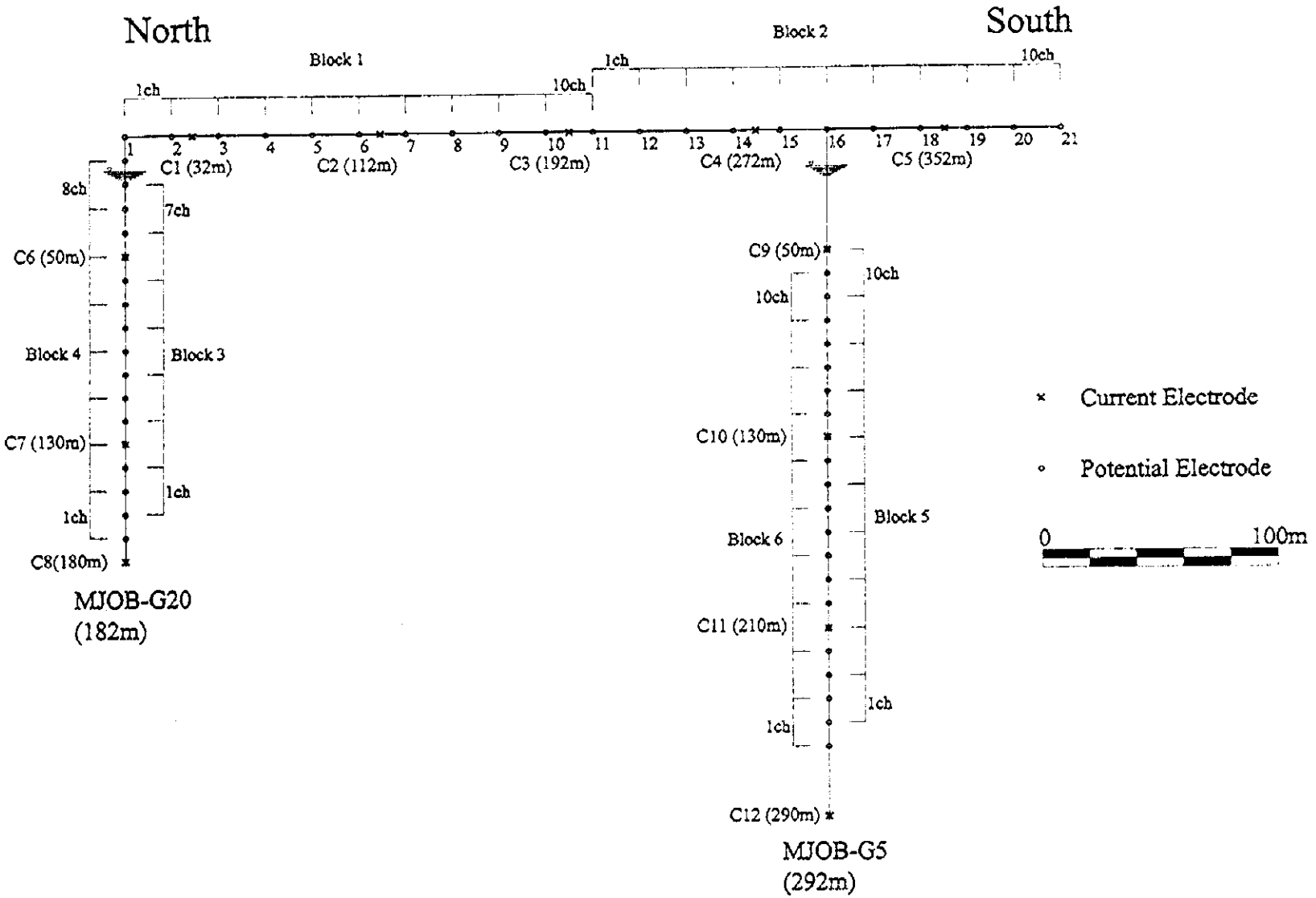

Fig.10 Profile of the IP tomography configuration along No.2 ore body NS line, Ghuzayn area

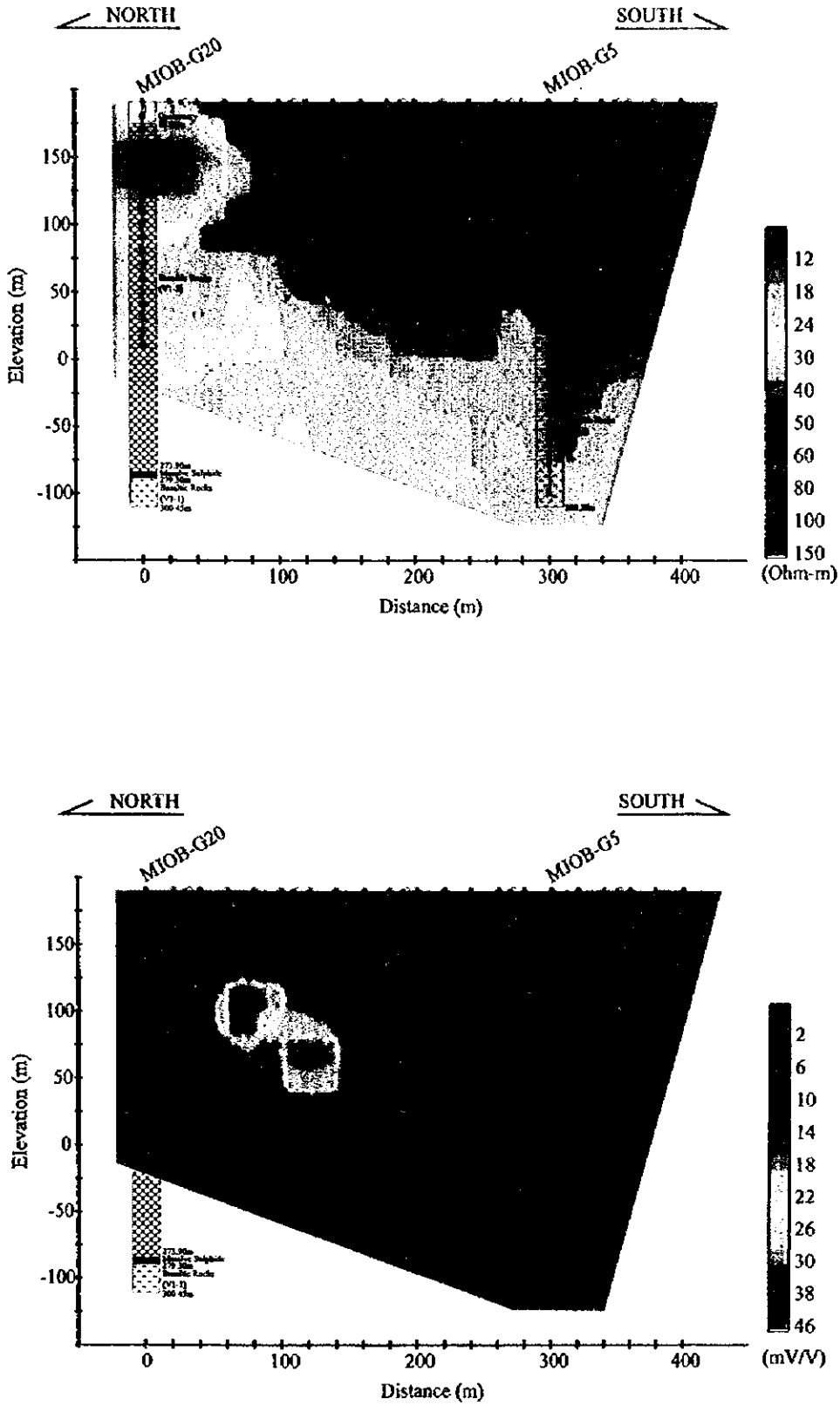

Fig.11 Analyzed resistivity section (upper) and chargeability section (lower) along No.2 ore body NS line, Ghuzayn area

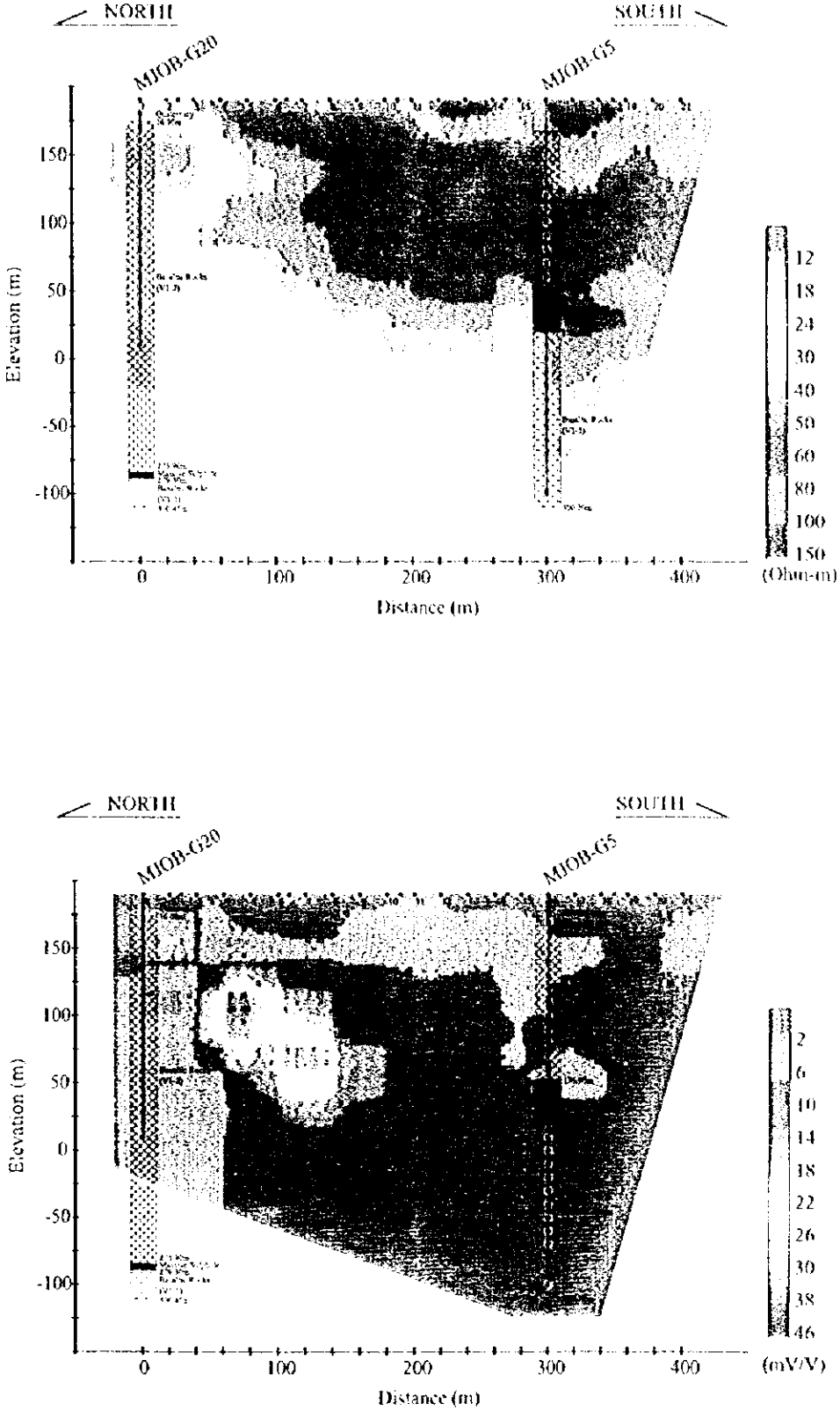

Fig.11 Analyzed resistivity section (upper) and chargeability section (lower) along No.2 ore body NS line, Ghuzayn area

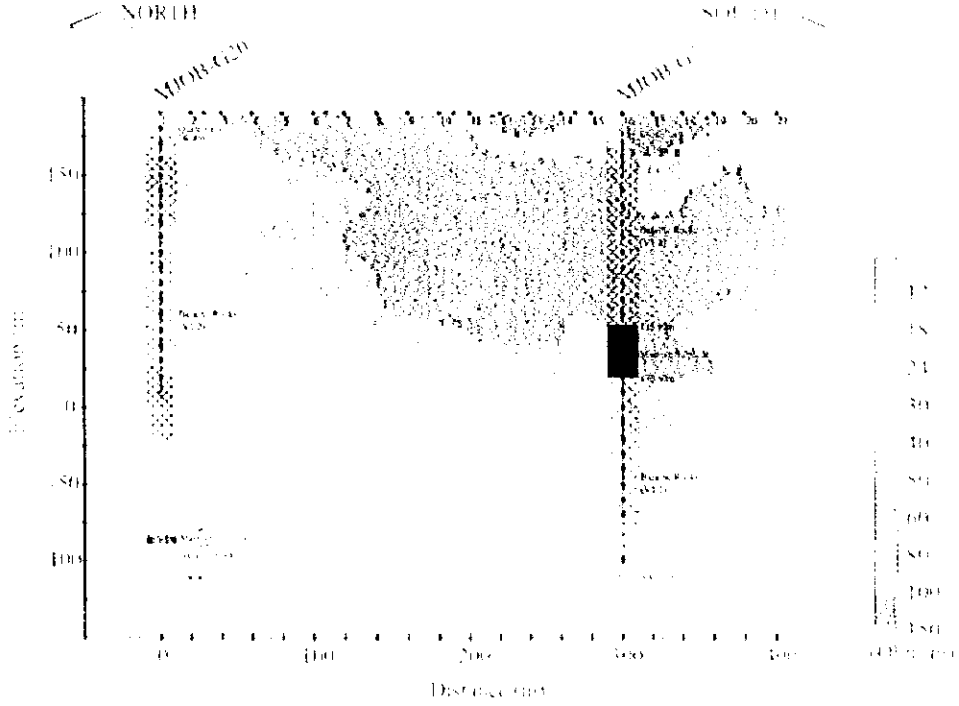

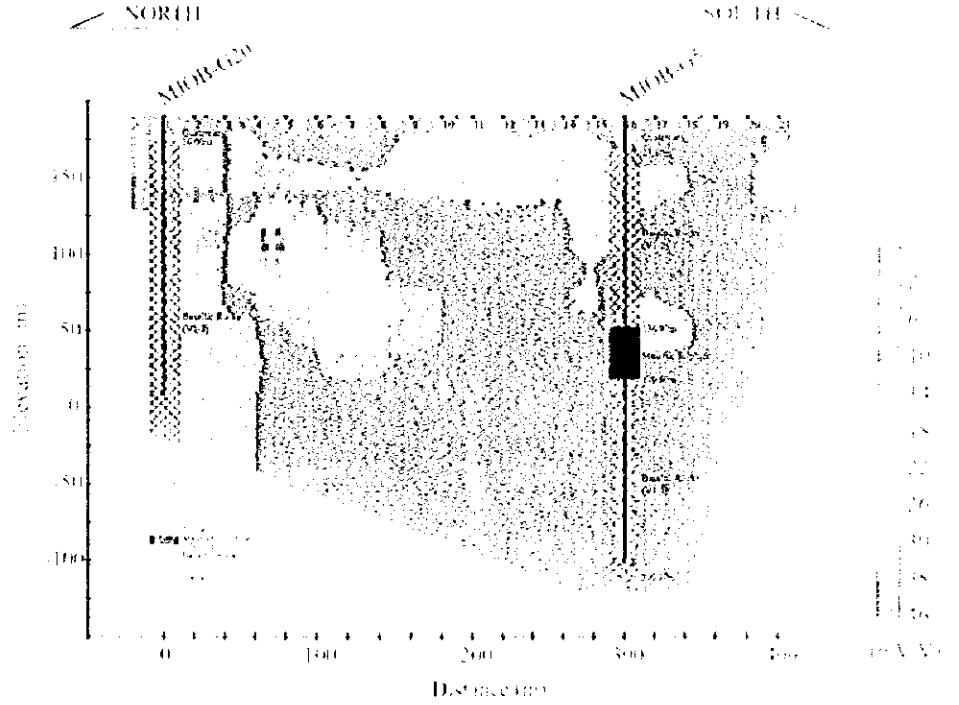

Fig.11 Analyzed resistivity section (upper) and chargeability section (lower) along No.2 ore body NS line, Ghuzayn area

zone was represented in the results of the ground IP survey in 1998.

In chargeability section, almost every data shows low chargeability. The data around the ore body does not show high chargeability. But high chargeability zone over 50mV/V exists 50m south from MJOB-G20 and about 80m below the surface (110m level). The raw data affected by this area shows high chargeability, so this chargeability zone will not be false image. The reason is not clear because pyrite dissemination is unexpected around here.

6 Conclusions

As it is case for these analyzed ore bodies, it is difficult to accurately delineate the ore body in the case of extremely low resistivity environments, although the ore body can be roughly extracted as having a low resistivity and high chargeability. The accuracy and resolution of IP tomography are improved as compared to the results with ground IP survey. However, in order to delineate accurately the shape and extension of the ore body, the following problems related to the IP tomography system must be solved:

1) Analysis program can not treat negative apparent resistivity.
   Negative apparent resistivity value is not wrong as far as the system adopts pole-dipole electrode array. Negative value often appears in contrasts with low resistivity or strong resistivity environments. Negative apparent resistivity means that the low resistive body exists nearby. Therefore this analysis program deletes important data with useful information.
2) Signal and S/N ratio decreases near the ore body when pole-dipole array is used.
   Efficient potential differences can not be generated if the potential dipole contacts with the ore body and S/N ratio become worse. During data processing and analysis, these data should be deleted.
3) Analysis program cannot utilize resistivity and chargeability of drill cores or surface rock samples.

To solve the above problems, it is necessary that the acquisition system can select variable electrode spacing and acquire efficient data near the ore body. In order to improve the accuracy, it is also necessary to utilize the data including negative apparent resistivity.